72-3442

TINER, Robert Leo, 1944-
A STUDY OF THE AMMONIA COMPLEXES OF COBALT(II) CHLORIDE AND THE CRYSTAL FIELD TREATMENT OF COPPER(I) CHLORIDE.

The University of Oklahoma, Ph.D., 1971
Chemistry, inorganic

University Microfilms, A XEROX Company, Ann Arbor, Michigan

THIS DISSERTATION HAS BEEN MICROFILMED EXACTLY AS RECEIVED

Downloaded from SHAREOK. Persistent Handle URL: https://hdl.handle.net/11244/3154

THE UNIVERSITY OF OKLAHOMA

GRADUATE COLLEGE

A STUDY OF THE AMMONIA COMPLEXES OF COBALT(II) CHLORIDE AND THE CRYSTAL FIELD TREATMENT OF COPPER(I) CHLORIDE

A DISSERTATION

SUBMITTED TO THE GRADUATE FACULTY

in partial fulfillment of the requirements for the

degree of

DOCTOR OF PHILOSOPHY

BY

ROBERT LEO TINER

Norman, Oklahoma

1971

A STUDY OF THE AMMONIA COMPLEXES OF COBALT(II)
CHLORIDE AND THE CRYSTAL FIELD TREATMENT
OF COPPER(I) CHLORIDE

APPROVED BY

Norman Fogel

Bernard O. Heaton

Robert L. Mazzarin

Stanley C. Nicky

Francis J. Schmitz

DISSERTATION COMMITTEE

PLEASE NOTE:

Some Pages have indistinct print. Filmed as received.

UNIVERSITY MICROFILMS

To Jo Dean

ACKNOWLEDGEMENT

The author wishes to express his appreciation to Dr. Norman Fogel for the suggestion of this research topic and for his valuable assistance throughout the course of this study.

The author also gratefully acknowledges the aid of Dr. B. O. Heston, Dr. A. P. Hagen, Dr. A. L. Lott, and fellow graduate students who provided helpful suggestions.

The author wishes to thank Mrs. Nancy Heinicke for typing this manuscript.

The author is also indebted to his parents for their love and assistance throughout his college years.

The author most of all wishes to thank his loving wife for her understanding, patience, assistance, and encouragement for the past three years.

TABLE OF CONTENTS

Page

LIST OF TABLES vi

LIST OF FIGURES viii

PART I, A STUDY OF THE AMMINE COMPLEXES OF COBALT(II) CHLORIDE 1

Chapter

1. INTRODUCTION 2

2. COMPOUND PREPARATION AND ANALYSIS 8

3. DISSOCIATION VAPOR PRESSURE 18

4. SPECTRA 48

5. MAGNETIC MOMENTS 95

6. CONCLUSIONS AND DISCUSSIONS 121

PART II, CRYSTAL FIELD TREATMENT OF COPPER(I) CHLORIDE 128

1. CRYSTAL FIELD TREATMENT OF COPPER(I) CHLORIDE 129

REFERENCES 139

LIST OF TABLES

Table		Page
1.	Compound Analysis	12
2.	f Values of Stable Cobalt(II) Ammine Chloride Complexes	23
3.	Vapor Pressure Data; $Co(NH_3)_6Cl_2(s) = Co(NH_3)_4Cl_2(s) + 2NH_3(g)$	29
4.	Vapor Pressure Data; $Co(NH_3)_4Cl_2(s) = \beta\text{-}Co(NH_3)_2Cl_2(s) + 2NH_3(g)$	30
5.	Vapor Pressure Data; $\alpha\text{-}Co(NH_3)_2Cl_2(s) = Co(NH_3)Cl_2(s) + NH_3(g)$	31
6.	Vapor Pressure Data; $Co(NH_3)Cl_2(s) = CoCl_2(s) + NH_3(g)$	31
7.	Pressure-Temperature Data for Log P vs. 1/T $Co(NH_3)_6Cl_2(s) = Co(NH_3)_4Cl_2(s) + 2NH_3(g)$	33
8.	Pressure-Temperature Data for Log P vs. 1/T $[Co(NH_3)_4Cl_2](NH_3)_2(s) = Co(NH_3)_4Cl_2(s) + 2NH_3(g)$	34
9.	Pressure-Temperature Data for Log P vs. 1/T $Co(NH_3)_4Cl_2(s) = \beta\text{-}Co(NH_3)_2Cl_2(s) + 2NH_3(g)$	35
10.	Pressure-Temperature Data for Log P vs. 1/T $Co(NH_3)_4Cl_2(s) = \alpha\text{-}Co(NH_3)_2Cl_2(s) + 2NH_3(g)$	36
11.	Pressure-Temperature Data for Log P vs. 1/T $\alpha\text{-}Co(NH_3)_2Cl_2(s) = Co(NH_3)Cl_2(s) + NH_3(g)$	37
12.	Pressure-Temperature Data for Log P vs. 1/T $Co(NH_3)Cl_2(s) = CoCl_2(s) + NH_3(g)$	38
13.	Thermodynamic Constants From Equilibrium Data at 25°C	43

Table		Page
14.	Calculated Standard Enthalpies and Entropies of Formation	47
15.	Term Energies for d^7 Electronic Configuration	52
16.	Energy Difference Between d^7 Free Ion Terms	52
17.	Crystal Field Splitting of Free Ion States	54
18.	Effect of $\hat{V}_o$ Upon the "d" Orbitals	54
19.	Spin Allowed d^7 States and Crystal Field Energies In Weak Octahedral Field	55
20.	Correlation: O_h-Lower Symmetry	56
21.	Effect of $\hat{V}_t$ Upon the "d" Orbitals	58
22.	Ground State Dependence Upon Ds and Dt	58
23.	Non Zero Elements for the Secular Determinant in Figure 14	63
24.	Infrared Assignments	67
25.	Near Infrared Overtones	67
26.	Ammonia Overtone Band Assignments and Descriptions	78
27.	Collected Spectral Data	79
28.	Spectral Fitting Parameters	88
29.	Magnetic Susceptibility Data	106
30.	Magnetic Data Summary	120
31.	State Energies in Terms of Dq, Ds, and Dt	136
32.	Spectral Data	137

LIST OF FIGURES

Figure		Page
1.	Infrared Spectrum of $Co(NH_3)_6Cl_2$	14
2.	Infrared Spectrum of $Co(NH_3)_4Cl_2$	15
3.	Infrared Spectra of α and β-$Co(NH_3)_2Cl_2$	16
4.	Infrared Spectrum of $Co(NH_3)Cl_2$	17
5.	Vapor Pressure Apparatus	20
6.	Thermogravimetric Analysis of $Co(NH_3)_6Cl_2$	24
7.	Vapor Pressure vs. f; $Co(NH_3)_6Cl_2(s) = Co(NH_3)_4Cl_2(s) + 2NH_3(g)$	26
8.	Vapor Pressure vs. f; $Co(NH_3)_4Cl_2(s) = \beta\text{-}Co(NH_3)_2Cl_2(s) + 2NH_3(g)$	27
9.	Vapor Pressure vs. f; $\alpha\text{-}Co(NH_3)_2Cl_2(s) = Co(NH_3)Cl_2(s) + NH_3(g)$; $Co(NH_3)Cl_2(s) = CoCl_2 + NH_3(g)$	28
10.	Log P vs 1/T; $[Co(NH_3)_4Cl_2](NH_3)_2(s) = Co(NH_3)_4Cl_2(s) + 2NH_3(g)$; $Co(NH_3)_6Cl_2(s) = Co(NH_3)_4Cl_2(s) + 2NH_3(g)$	39
11.	Log P vs. 1/T; $Co(NH_3)_4Cl_2(s) = \beta\text{-}Co(NH_3)_2Cl_2(s) + 2NH_3(g)$; $Co(NH_3)_4Cl_2(s) = \alpha\text{-}Co(NH_3)_2Cl_2(s) + 2NH_3(g)$	40
12.	Log P vs. 1/T; $Co(NH_3)Cl_2(s) = CoCl_2(s) + NH_3(g)$	41
13.	Log P vs. 1/T; $\alpha\text{-}Co(NH_3)_2Cl_2(s) = Co(NH_3)Cl_2(s) + NH_3(g)$	42
14.	Secular Determinant for High Spin States	62

Figure Page

15. Energy Level Diagram for Spin Allowed States Showing Effect of Considered Pertubations 69

16. Energy Level Diagram for Spin Forbidden States of Lowest Energy 70

17. Attachment to DK-1Spectrophotometer for Obtaining Low Temperature Crystal Spectra 73

18. Tanabe-Sugano Diagram for Co(II) 76

19. Solution Spectra of $Co(NH_3)_6^{++}$ 88

20. $Co(NH_3)_6Cl_2$ Spectrum 89

21. $Co(NH_3)_4Cl_2$ Spectrum 90

22. β-$Co(NH_3)_2Cl_2$ Spectrum 91

23. α-$Co(NH_3)_2Cl_2$ Spectrum 92

24. $Co(NH_3)Cl_2$ Spectrum 93

25. $CoCl_2$ Spectrum 94

26. Faraday Magnetic Balance 98

27. d vs. m for $HgCo(SCN)_4$ 101

28. T vs. $1/X_m^c$ for $CoCl_2$ 107

29. T vs. $1/X_m^c$ for $Co(NH_3)Cl_2$ 108

30. T vs. $1/X_m^c$ for α-$Co(NH_3)_2Cl_2$ 109

31. T vs. $1/X_m^c$ for β-$Co(NH_3)_2Cl_2$ 110

32. T vs. $1/X_m^c$ for $Co(NH_3)_4Cl_2$ 111

33. T vs. $1/X_m^c$ for $Co(NH_3)_6Cl_2$ 112

34. X_m^c vs. $1/T-\theta$ for $CoCl_2$ 114

35. X_m^c vs. $1/T-\theta$ for $Co(NH_3)Cl_2$ 115

36. X_m^c vs. $1/T-\theta$ for α-$Co(NH_3)_2Cl_2$ 116

37. X_m^c vs. $1/T-\theta$ for β-$Co(NH_3)_2Cl_2$ 117

Figure Page

38. X_m^c vs. 1/T-θ for $Co(NH_3)_4Cl_2$ 118

39. X_m^c vs. 1/T-θ for $Co(NH_3)_6Cl_2$ 119

40. Apparatus for Preparing CuCl 131

41. Visible and Ultraviolet Spectra of CuCl 133

42. Energy Level Diagram for CuCl 135

PART I

A STUDY OF THE AMMONIA COMPLEXES OF COBALT(II) CHLORIDE

A STUDY OF AMMONIA COMPLEXES OF COBALT (II) CHLORIDE AND A CRYSTAL FIELD TREATMENT OF COPPER(I) CHLORIDE

CHAPTER I

INTRODUCTION

Purpose

The primary objective of this study is to elucidate the structural rearrangements connected with displacing ammonia molecules with chloride ions as inner coordination sphere ligands in a series of ammonia-cobalt(II) chloride complex compounds. To accomplish this study, three separate investigations were completed.

To determine the number, composition, and stability of the various complexes formed with the general formula, $Co(NH_3)_nCl_2$, equilibrium, dissociation vapor pressure of the stepwise deammination of the complex containing the highest percentage of ammonia was studied at constant temperature and as a function of temperature. From this study, the thermodynamic functions for the reaction and the formation of the complexes were determined. This was related to the structural change which occurs as each compound is formed from the preceeding complex.

The second investigation was a fitting of the reflectance spectra of the stable ammine complexes. These spectra were interpreted using ligand field pertubation techniques. A computer program written by Joy[1] was utilized in the interpretations. Pertubations considered were electronic interaction, crystal field, distortion, and spin-orbit coupling. The corresponding parameters varied were B and C, Dq, Ds and Dt, and λ. Configuration interaction was also taken into account, except for spin-orbit coupling, which appears only on the diagonal. The validity of this approximation will be discussed later in Chapter 4.

The third study was a measurement of the magnetic moments of each of the stable species. The magnetic moments are related to the environment of the central metal ion, i.e., the symmetry of the inner coordination sphere ligands.

All of these investigations are useful in deducing the structural rearrangements accompanying deammination.

Another objective of this study is to gain some insight into the behavior of cobalt(II) chloride complexes possessing other simple ligands such as water and pyridine. Both of these systems have been thoroughly investigated,[2,3,4,5] however, some controversy exists as to the spectral ground state of the tetragonally distorted octahedral complexes. For a complex possessing D_{4h} symmetry and elongated along the z axis, the ground state symmetry should be $^4A_{2g}$. For compression along this axis, a ^4E_g ground state is predicted.[6]

Both water and pyridine are capable of π bonding with the transition metal. Two of the sp^3 hybridized oxygen orbitals of the water molecule contain nonbonded pairs of electrons. One of these orbitals can form a coordinate covalent σ bond with a metal orbital of appropriate symmetry. The other nonbonded orbital of the oxygen atom could interact with metal orbitals of appropriate symmetry thus forming a coordinate covalent π bond between the metal and ligand. The sp^2 hybridized nitrogen of the pyridine ligand cannot itself form π bonds with the metal since none of the nitrogen orbitals are available for bonding, however, the conjugated π system of the ring can interact with orbitals of appropriate symmetry belonging to the cobalt(II) ion. Evidence of π bonding is taken from infrared spectra which changes the electron density of the ring.[7]

The π bonding could possibly cause an inversion of the terms arising from the tetragonal splitting of the octahedral ground state, $^4T_{1g}(F)$, instead of the order otherwise expected. This inversion has been proposed by Yatsumirskii and Volchenskova[8] in fitting the spectra of $Co(NH_3)_4(H_2O)_2Cl_2$ and by Fogel, et al.,[5] in fitting the spectra of $Co(H_2O)_4Cl_2$.

Contrary to water and pyridine, ammonia is incapable of π bonding with the cobalt(II) ion, since three of the sp^3 hybridized orbitals are instrumental in forming covalent σ bonds with the hydrogens and the other forms a coordinate covalent σ bond with a metal orbital of appropriate symmetry. The third shell orbitals of nitrogen are high enough in energy that they should not take part in the bonding

scheme. Therefore, it is felt that the interpretation of the ammonia cobalt(II) chloride system will assist in elucidating the water and pyridine systems.

Survey of Previous Work

From the vapor pressure study it was found that cobalt(II) chloride reacts with excess ammonia to produce pink, flesh-colored $Co(NH_3)_6Cl_2$. Stepwise thermal decomposition of this compound with the evolution of ammonia vapor yields a series of intermediate complexes which is accompanied by a change in color from pink through various shades of red and blue to the light blue color of the final product, $CoCl_2$. These compounds have the general formula, $Co(NH_3)_nCl_2$ with n = 6, 4, β-2, α-2, 1, and 0.

Clark, et al.,[9] reported the formation of $Co(NH_3)_{10}Cl_2$ with specially prepared $CoCl_2$. This compound was not prepared in this study.

Rose[10] reported the formation of blue tetramminecobalt(II)* chloride from direct ammination of the anhydrous salt. Bersch[11] later showed that direct ammination led to the hexammine* complex instead. Since that time several different preparations of the hexammine have been reported.[8,12,13,14,15] A detailed study of this compound has been reported, but the various data have not been collated.

The crystal structure is reported by Ibers, et al.,[16] with a Co-N bond length of 2.114 ± 0.009 A° and a Co-Cl bond length of 4.37 A°. The crystal belongs to the Fm3m space group and the complex

* I.U.P.A.C. spelling is tetraammine and hexaammine.

possesses O_h symmetry. Structures of the lower ammines have not been determined.

The visible solution spectrum of $Co(NH_3)_6^{++}$ in water has been reported by Roberts and Field,[17] and the complete crystal field spectrum of this ion in solution has been reported by numerous authors.[8,18,19] Yatsumirskii, and Volchenskova[8] fitted the solution spectra using a ligand field treatment, and assuming an octrahedral field. Neglecting configuration interaction, they obtained a B value of 880 cm^{-1} and a Dq value of 1200 cm^{-1}. Cotton and Haas[18] treated the spectra using the L. C. A. O. - M. O. method but were unable to obtain an accurate fit.

The magnetic moment of $Co(NH_3)_6Cl_2$ was determined at room temperature by Mellor and Goldacre.[20]

The heat of formation of the hexammine was determined calorimetrically.[21]

The reflectance spectrum of the hexammine (Figure 20) is almost identical to that of the solution spectra (Figure 19). The difference is a broadening of the absorbance bands which is to be expected.

Tetramminecobalt(II) chloride cannot be obtained from thermogravimetric analysis data,[22] and is apparently formed only by the slow decomposition of the higher ammine. Clark, et al.,[9] prepared the complex by continuous deammination of the hexammine over acid. German and Jamsett[23] reported the formation of the complex from a solution of ethyl or methyl acetate. Both of these preparations

yielded a dirty white compound. German[24] also reported other lower ammines which were dirty white in color.

Curtis and Burns[25] reported the preparation of $Co(NH_3)_3Cl_2$ from a solution of amyl alcohol. This was later proven to be a mixture of the diammine and higher ammines. Pentamminecobalt(II) chloride was reported by Clark, et al.,[9] but this was also shown to be a mixture of higher and lower ammines.

Two forms of the diammine complex have been isolated. Rose[26] reported the preparation of the low temperature, blue isomer in 1871, and Biltz and Fetkenheuer[27] prepared the high temperature, red isomer and a purple monoammine complex in 1914. All three of these compounds have remained essentially uncharacterized.

The crystal structure of $CoCl_2$ has been reported,[28] and the magnetic moment[29] and spectra[30,31] have been studied extensively.

Ferguson, et al.,[31] have studied the cold temperature spectra (25°A) of cobalt(II) chloride. A constant value of B = 780 cm^{-1} or 80% of the free ion value was assumed in the calculations. Other parameters calculated from a best fit of the spectrum were C/B = 4.40, λ = 140 cm^{-1}, and Dq = 690 cm^{-1}.

CHAPTER 2

COMPOUND PREPARATION AND ANALYSIS

Preparation

Hexamminecobalt(II) chloride has been prepared by several methods. Ephraim[12] prepared the compound by passing dry ammonia over anhydrous cobalt(II) chloride. This method was easiest and best suited for this study.

Hexaquocobalt(II) chloride (Mallinckrodt's Analytical Grade) was carefully dehydrated at 120°C under vacuum. It has been shown previously[32] that the cobalt(II) chloride does not decompose at this temperature if the system is kept under vacuum. Anhydrous ammonia (Matheson) was slowly added to the evacuated reaction vessel which contained the anhydrous cobalt(II) chloride. The controlled addition was necessary since the heat of reaction is large enough to cause the lower ammine complexes to melt.[9,33] Continued ammination changes the light blue of the anhydrous compound to various colors of purple, red, and blue, and finally to the pink, flesh color of the hexammine.

The hexammine could also be prepared by bubbling the ammonia through solutions of the cobalt(II) chloride in different solvents

such as water, methanol, ethanol, acetone, ether, chloroform, amyl alcohol, ethyl acetate, and methyl acetate. This method of preparation yielded the hexammine complex as the ultimate product if the temperature of the solvent was kept below 30°C. By raising the temperature of the solvent, the lower ammines were prepared. This is a temperature effect, and is not due to solvent properties.[9]

Preparing the complexes by the wet method meant washing and drying the product, greatly increasing the possibility of contamination with impurities, especially oxygen. Upon drying, ammonia is lost by the complex, since the hexammine has an appreciable vapor pressure at room temperature. The dry method got rid of these problems and was therefore the best choice for this work.

The hexammine compound when dry is stable in air, but will react slowly with atmospheric oxygen to form the peroxide, $[(NH_3)_5Co(O_2)Co(NH_3)_5]Cl_4$.[34] This reaction is accompanied by a change in color from pink to brown. The wet hexammine compound reacts rapidly to form this species.

The hexammine reacts slowly with atmospheric water vapor which displaces the ammonia. The compound can be stored indefinitely in a closed tube with an ammonia atmosphere.

Tetramminecobalt(II) chloride was prepared by the slow decomposition of the hexammine under partial vacuum at -10°C. The compound formed is blue in color, in agreement with the results of Rose.[10] The dry tetrammine is stable in an inert atmosphere, but reacts rapidly with atmospheric moisture to form the mixed ligand

complex, $Co(NH_3)_4(H_2O)_2Cl_2$. Compounds with mixed ammonia-water ligands have been characterized by Yatsumirskii[8] and Jorgensen.[19] The color of this mixed complex is similar to that of the hexammine. The tetrammine can be stored indefinitely in a closed tube.

The deep blue β-diamminecobalt(II) chloride was formed by decomposition of the hexammine under vacuum at room temperature. The complex reacts readily with atmospheric water to form a pink complex, slightly deeper in color than the hexammine. This isomer can be stored indefinitely in a closed tube.

The reddish α-diamminecobalt(II) chloride was formed by heating the β isomer at 67°C.[9] The isomer is stable at room temperature for long periods of time in the absence of ammonia and water vapor. In the presence of either of these, the transition to the β form is rapid. The transition to the β form is also rapid at liquid nitrogen temperature.

It should be noted that even though the β to α transition temperature is 67°C, the α form can be prepared by deammination of the higher ammines at temperatures above 37°C. A similar effect has been observed in the dipyridinates.[3]

$Co(NH_3)Cl_2$ can be prepared by the deammination of the higher ammines at 150°C. The deep purple compound can be stored indefinitely in a closed tube. It reacts readily with atmospheric water to form a reddish complex similar in color to the hexaquo compound.

By bubbling ammonia through an aqueous solution of $CoCl_2$, rose red octahedral crystals were formed. These crystals analyzed

to the same composition as the hexammine powder. The magnetic moment and the spectra of the crystals are equivalent to those of the powder. Therefore, the molecular structure of the hexammine powder is taken to be the same as that of the crystals.

Crystals of the other ammine complexes could not be grown.

Analysis

Since all of the compounds were prepared from anhydrous cobalt(II) chloride, the analysis of this compound for the chloride is satisfactory. Also since anhydrous cobalt(II) chloride is the final product of the deammination process, an analysis of this product for the chloride ion will determine if any other reaction other than deammination occured, i.e., decomposition of $CoCl_2$. Analysis of both the beginning compound and the end product for the chloride ion yielded the same results within experimental error.

Deammination of the complexes contaminated with trace amounts of water yielded a white salt which sublimed to the upper part of the sample chamber at temperatures above 150°C. The infrared spectrum of this sublimed compound is identical to that of ammonium chloride.[35] In addition, the product obtained upon complete deammination contained a dark black solid. The analysis of this mixture yielded a lower chloride content than does pure $CoCl_2$.

This hydrolysis reaction accompanying the deammination process is represented by:

$$Co(NH_3)_nCl_2(s) + H_2O(g) = CoO(s) + 2NH_4Cl(g) + (n - 2)NH_3(g).$$

Therefore, if any of the complexes contained traces of water, the contamination was detected by the formation of the white salt and the low percentage of chloride in the analysis of the final deammination product.

The method used for the analysis of the chloride ion was that of Volhard.[36] Gravimetric methods yielded similar results.

The analysis of each of the ammine complexes for ammonia was accomplished by measuring the mass of the complex formed and subtracting the origional mass of the anhydrous cobalt(II) chloride.

Since all complexes contain only Co, NH_3, and Cl, the difference in the total mass of the compound and the ammonia plus chloride is an analysis for the amount of Co present.

The results obtained from at least three analysis of each complex are given in Table 1. All of the results fall within the range given.

TABLE 1

COMPOUND ANALYSIS

Compound	Percentages Co		Cl		NH_3	
	Theo.	Exper.	Theo.	Exper.	Theo.	Exper.
$CoCl_2$	45.39	45.5 ± .6	54.61	54.4 ± .6		
$Co(NH_3)Cl_2$	40.13	40.1 ± .6	48.29	48.1 ± .6	11.60	11.78 ± .4
$\alpha Co(NH_3)_2Cl_2$	35.96	36.5 ± .6	43.26	43.1 ± .6	20.78	20.38 ± .6
$\beta Co(NH_3)_2Cl_2$	35.96	36.2 ± .6	43.26	43.3 ± .6	20.78	20.46 ± .4
$Co(NH_3)_4Cl_2$	29.77	29.5 ± .6	35.82	36.0 ± .6	34.41	34.52 ± .3
$Co(NH_3)_6Cl_2$	25.40	25.7 ± .6	30.56	30.4 ± .6	44.04	43.89 ± .3

The absence of water can be demonstrated by the far infrared spectra from 300 cm^{-1} - 4000 cm^{-1}. These spectra are presented in Figs. 1-4. The spectra indicate that within their reliability no water is present since this would appear as a high energy shoulder on the $\nu(NH_3)$ peak, 3400 cm^{-1}.[37] The discussion and further use of these spectra will be presented in Chapter 4.

FIGURE 1

INFRARED SPECTRUM OF $Co(NH_3)_6Cl_2$

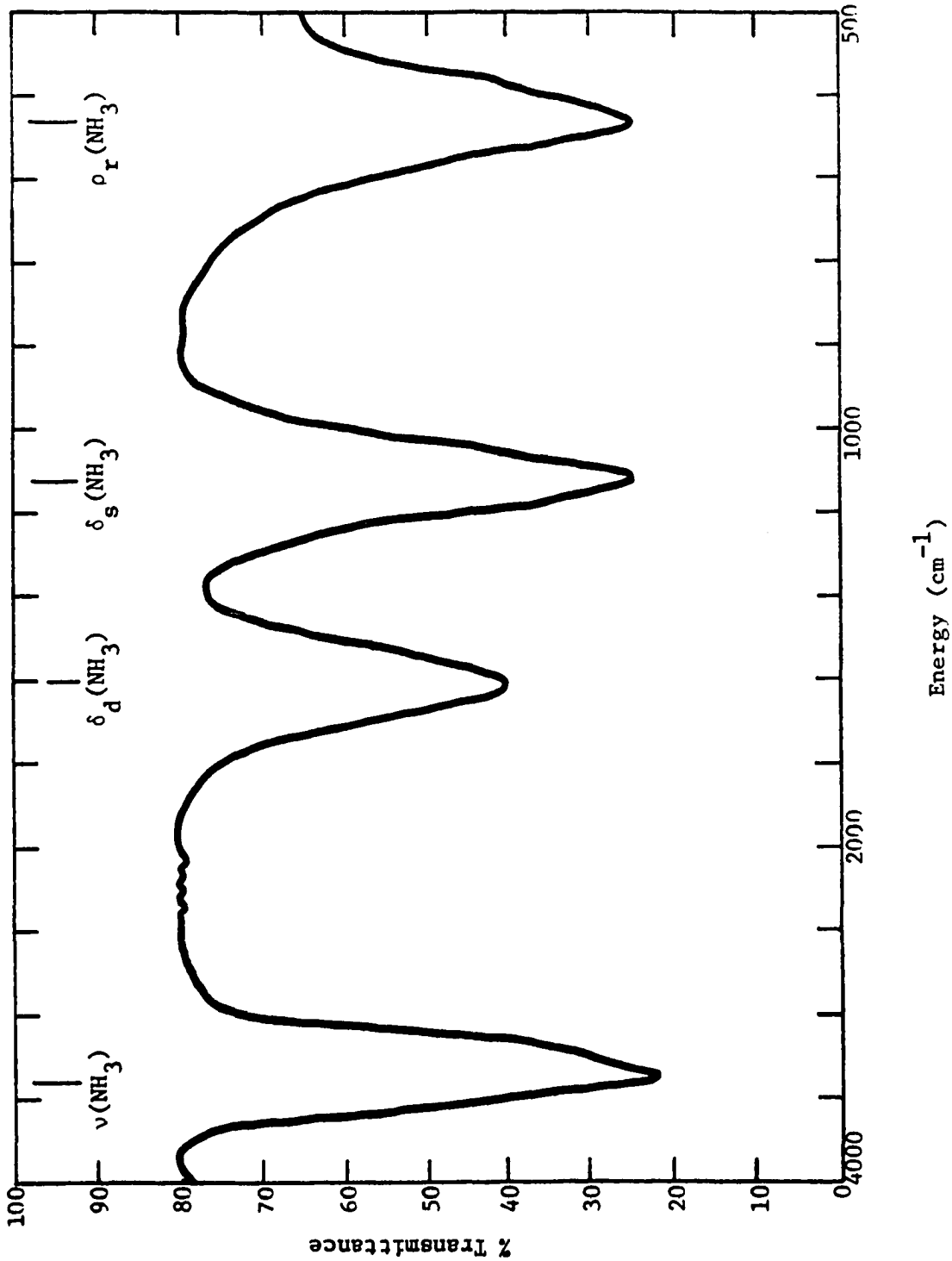

FIGURE 2

INFRARED SPECTRUM OF $Co(NH_3)_4Cl_2$

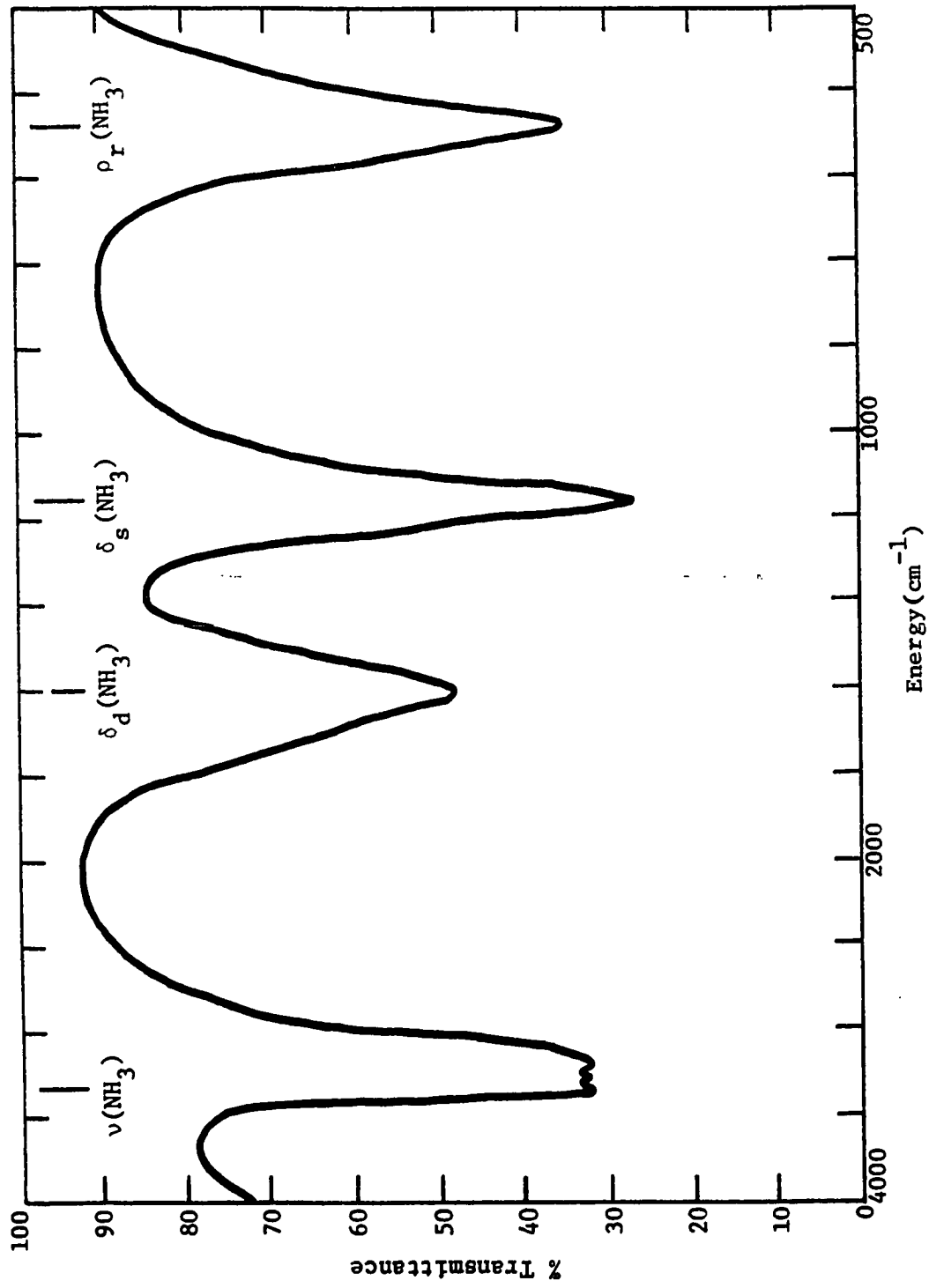

FIGURE 3

INFRARED SPECTRA OF α-$Co(NH_3)_2Cl_2$ and β-$Co(NH_3)_2Cl_2$

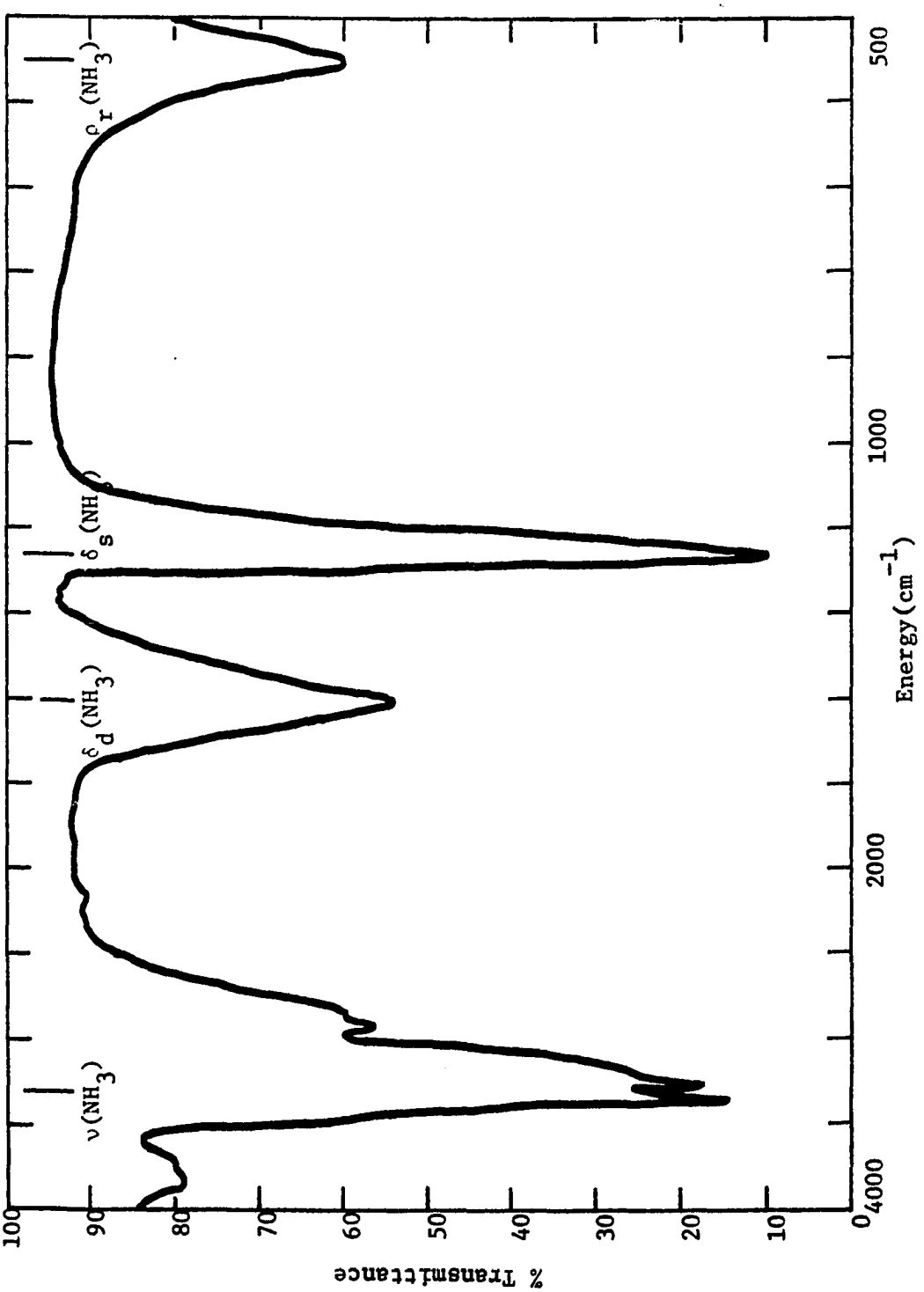

FIGURE 4

INFRARED SPECTRUM OF $Co(NH_3)Cl_2$

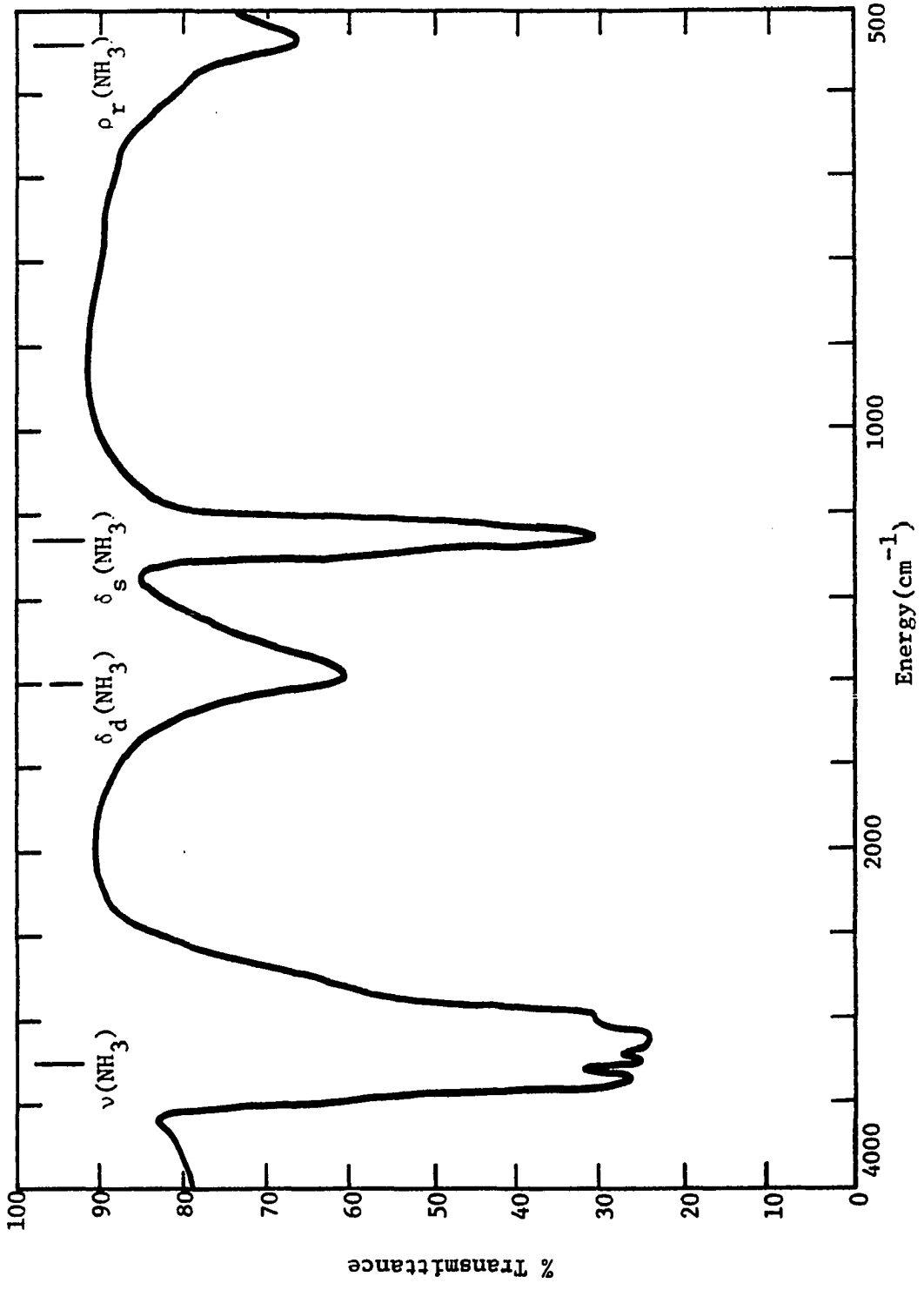

CHAPTER 3

DISSOCIATION VAPOR PRESSURE

Anhydrous cobalt(II) chloride when exposed to anhydrous ammonia gas forms a complex with six ammonia molecules for each metal atom at room temperature.

The deammination of $Co(NH_3)_6Cl_2$ is accomplished by the removal of ammonia by evacuation. The final product is cobalt(II) chloride.

The number and composition of the stable cobalt(II) chloride ammine complexes is determined from a plot of the equilibrium vapor pressure of the system as a function of the mass. Applying the phase rule, a sharp decrease in the equilibrium vapor pressure should occur whenever the mass corresponds to that of a stable complex. This process is generalized by the deammination reaction,

$$Co(NH_3)_nCl_2(s) = Co(NH_3)_{n-m}Cl_2(s) + mNH_3(v),$$

where n = 6, 4, 2, and 1, and the corresponding m values are m = 2, 2, 1, and 1.

The equilibrium constant for the general reaction is

$$K_{eq} = \frac{[Co(NH_3)_{n-m}Cl_2]P^m_{NH_3}}{[Co(NH_3)_nCl_2]}$$

and since the complexes are present in their standard states, their activities will be one, and the equilibrium constant is a function of the equilibrium vapor pressure only. Thus

$$K_{eq} = P^{m}_{NH_3}$$

where P is the pressure in atmospheres.

From the temperature dependence of the equilibrium constants, thermodynamic data is obtained.

Experimental Procedure

The apparatus used is shown in Figure 5.

A quartz fibre spring (A) with a total mass capacity of one gram and a maximum extension of approximately 10 cm was utilized to measure the sample mass. The spring extension is linear within this mass limit and can be readily calibrated with known weights in units of grams per centimeter extension. With the use of a cathetometer (B), the mass of the sample can be measured by the extension of the spring in the closed system.

The two springs employed had force constants of 0.09928 g./cm. and 0.09919 g./cm.

Ammonia reacted with all available stopcock greases upon standing for long periods of time. For this reason Teflon® stopcocks (C) were used in the experiments. The ground glass joints (D) were sealed with black wax to prevent leakage.

The mercury in the manometer (E) was carefully degassed and the capillary trap in the manometer allowed for the trapping of any gas present in the manometer when filling. No reaction

FIGURE 5

VAPOR PRESSURE APPARATUS

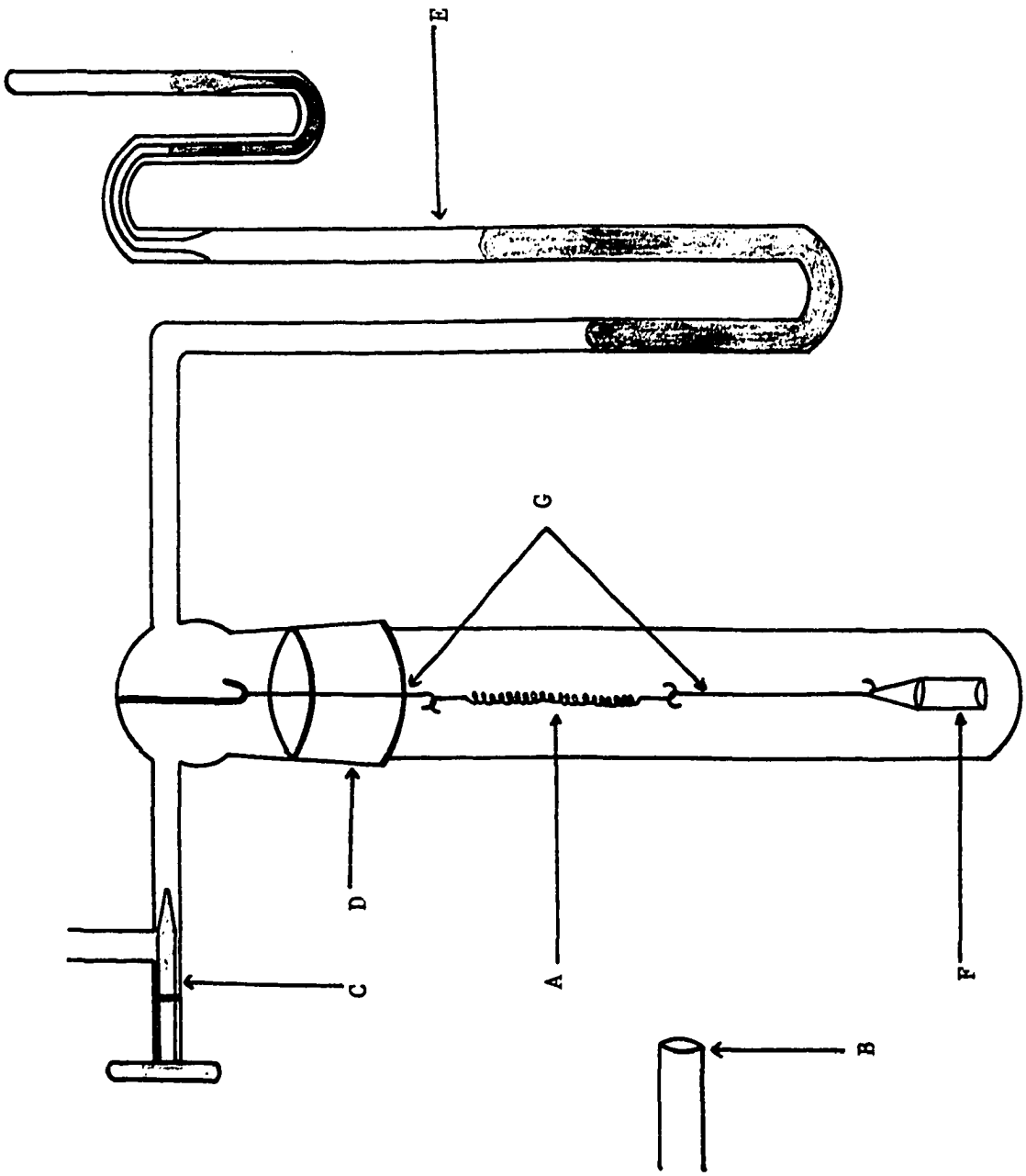

occured between the ammonia and mercury. This was checked by placing an amount of ammonia in the apparatus and allowing it to stand for several days. No apparent change in pressure was observed.

A sample of anhydrous cobalt(II) chloride was suspended from the spring in a glass bucket (F). Quartz fibres (G) were connected to both ends of the spring between the suspension hook and bucket. The reason for this will be given later. The sample was heated and all atmospheric water which was absorbed during transfer was carefully removed under vacuum. The cobalt chloride was then weighed. Anhydrous ammonia was added to the system and allowed to react until the reaction was complete. Weighing indicated that $Co(NH_3)_6Cl_2$ was obtained.

The sample chamber was submerged in a constant temperature bath. The apparatus is built in such a way that the sample could be submerged without placing the manometer into the bath. As long as the bath temperature is close to or above room temperature, no mercury will be transfered to the sample chamber.

The quartz fibre allowed the spring to remain above the bath so that the spring extension could be determined easily.

Water baths were used below 50°C and oil baths from 50 to 100°C. The temperature regulation system for the water bath consisted of a bimetallic temperature sensor and an electric resistance heater working through an electronic relay (Precision Scientific 62690). The water was circulated by means of small circulating pumps. The water level was maintained constant by the use of a siphon system.

This was necessary since only part of the apparatus was submerged. Above 30°C the temperature was controlled by loss of heat to the surroundings. Below 30°C, cold water was circulated through a copper tubing coil submerged in the bath. The temperature was maintained within ± 0.05°C.

The regulation system for the oil bath consisted of a mercury capillary sensor, with a mechanical stirrer for circulation. The temperature was maintained within ± 0.10°C.

Above 100°C the sample chamber was inserted into a solid aluminum cylinder into which holes were drilled for the sample tube, temperature regulator, and thermometer. The block was wrapped with heating tape and insulated on all sides. Silicone oil was used to insure contact between the aluminum cylinder and the thermometer, regulator, and sample chamber. The temperature was maintained within ± 1.0°C.

With these apparatus the temperature and composition could be controlled. By evacuating the system, ammonia could be removed and at equilibrium, vapor pressure-composition curves were obtained. By maintaining constant composition, and varying the temperature, pressure-temperature curves were obtained.

Experimental Results and Calculations

A thermogravimetric analysis was obtained by placing the sample under vacuum until no mass loss was detected at a particular temperature. This indicated that a stable species was formed. Previous work[28,27,26] published on the system indicated only four

stable species, $Co(NH_3)_6Cl_2$, α and β-$Co(NH_3)_2Cl_2$, and $CO(NH_3)Cl_2$. This previous work was verified. However, by applying a partial vacuum at -10°C, a compound of composition $Co(NH_3)_4Cl_2$ was isolated. This compound has been reported previously by Clark.[9]

The thermogravimetric analysis is shown in Figure 6. The plot is of temperature versus composition where the composition is expressed in terms of the weight fraction, f, the weight of the compound divided by the initial mass of $CoCl_2$. The value of f for each of the ammoniates is given in Table 2.

TABLE 2

f VALUES OF STABLE COBALT(II) AMMINE CHLORIDE COMPLEXES

Compound	f Value
$Co(NH_3)_6Cl_2$	1.787
$Co(NH_3)_4Cl_2$	1.525
$Co(NH_3)_2Cl_2$	1.262
$Co(NH_3)Cl_2$	1.131
$CoCl_2$	1.000

Equilibrium vapor pressure versus f curves were obtained for each stepwise loss of ammonia. These curves are given in Figures 7-9, with the data presented in Tables 3-6. The phase rule, F = C - P + 2, where C is the number of components and P is the number of phases of the system, is the basis for the explanation of the shape of these curves.

FIGURE 6

THERMOGRAVIMETRIC ANALYSIS OF $Co(NH_3)_6Cl_2$

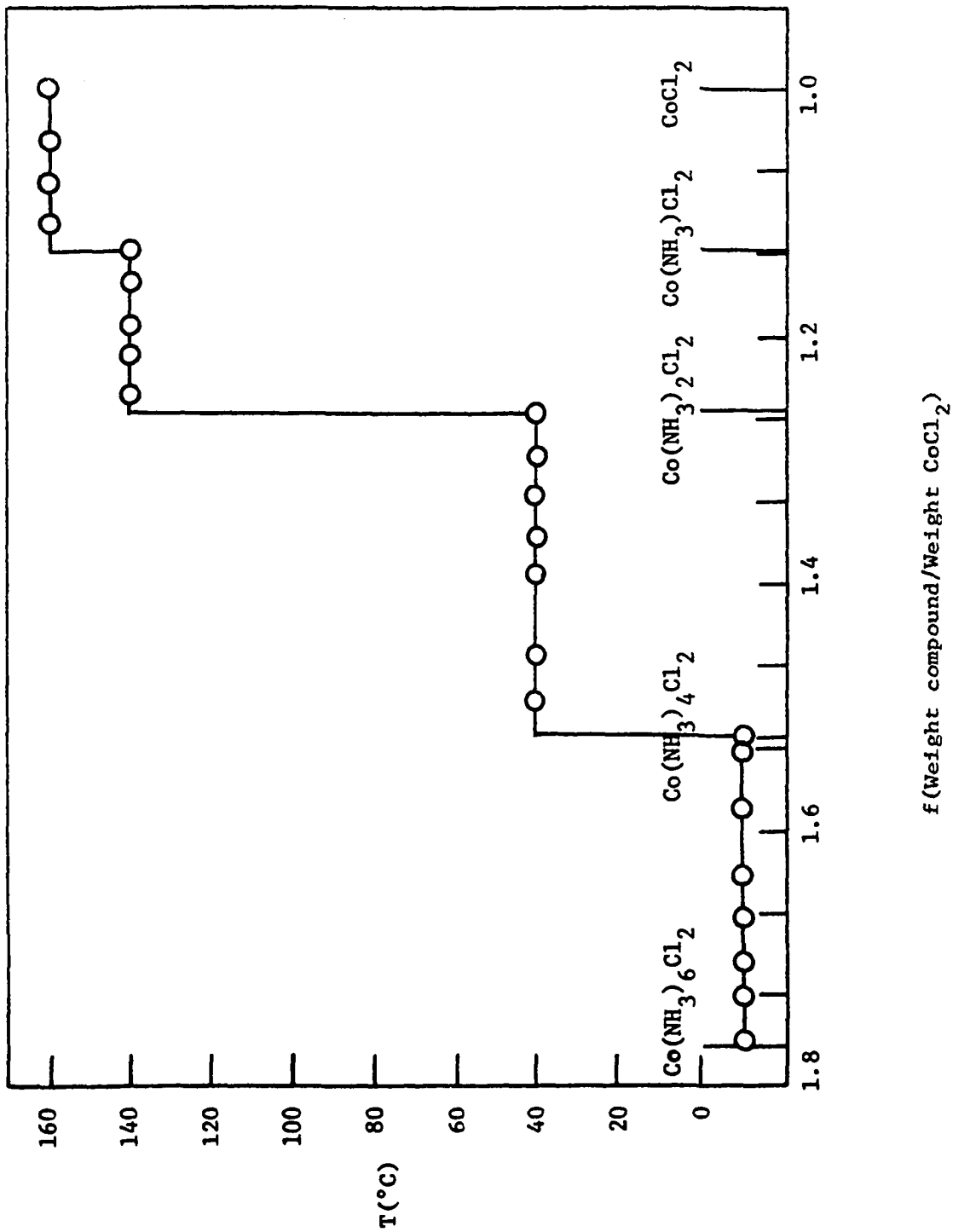

On the plateau there is an equilibrium between two solid compounds, i.e., $Co(NH_3)_nCl_2$ and $Co(NH_3)_{n-m}Cl_2$. The ammonia gas represents another phase, making a total of three. The number of components is two, $CoCl_2$ and NH_3. Thus the phase rule yields F = 2 - 3 + 2 = 1 degree of freedom, and since the temperature representing the one degree of freedom is held constant, the pressure of the system should remain constant. This condition will exist whenever there are two solid phases in equilibrium with the ammonia gas.

Whenever the value of f corresponds to a pure compound, only one solid component is present. At this composition an additional degree of freedom exists, and even though the temperature is held constant the pressure is free to change.

The equilibrium constants were evaluated by taking the pressure-temperature data at the midpoint of the plateau, that is at a composition such that

$$\frac{[Co(NH_3)_{n-m}Cl_2](s)}{[Co(NH_3)_nCl_2](s)} = 1.$$

The pressure-temperature data was taken by heating one sample to a temperature where the vapor pressure was higher than the equilibrium pressure at the temperature under consideration. Another sample with the same composition was kept at a lower temperature and pressure. The two samples were placed in the thermostated bath until the pressures became equal. The equilibrium was thus approached from both sides, and the attainment of the same pressure showed that equilibrium had been reached.

The thermodynamic relationship at constant temperature is

FIGURE 7

$Co(NH_3)_6Cl_2(s) = Co(NH_3)_4Cl_2(s) + 2NH_3(g)$

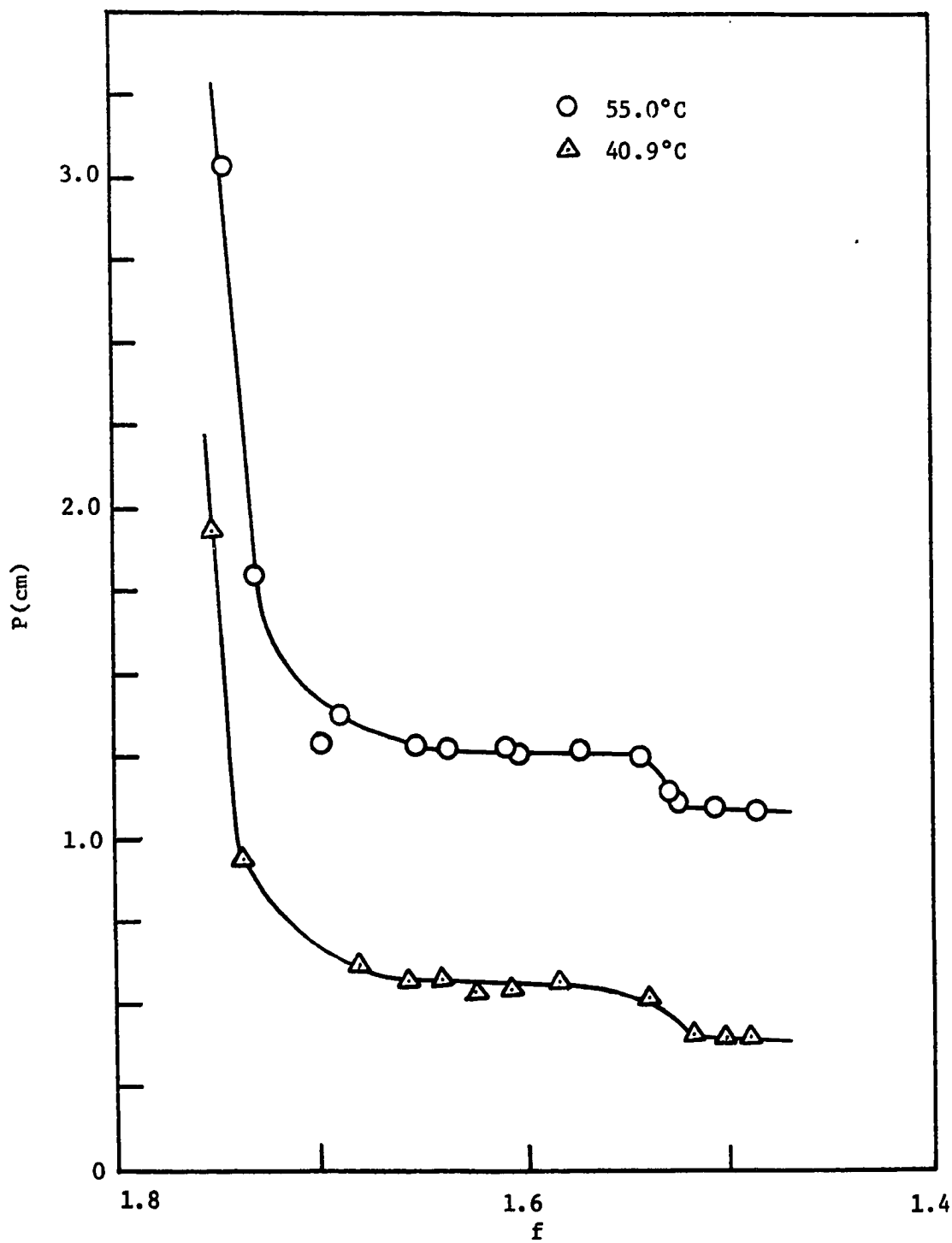

FIGURE 8

$Co(NH_3)_4Cl_2(s) = \beta\text{-}Co(NH_3)_2Cl_2(s) + 2NH_3(g)$

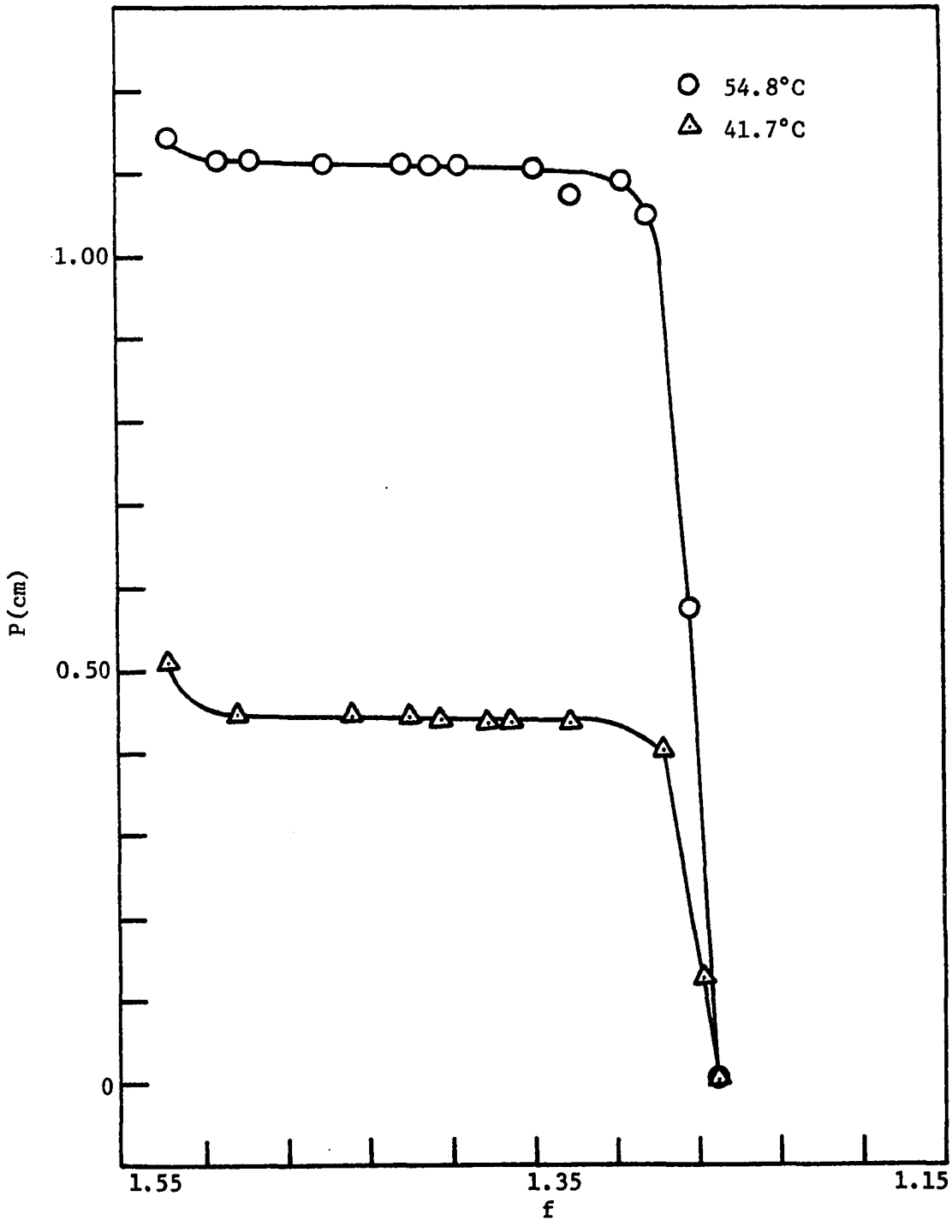

FIGURE 9

(A) α-$Co(NH_3)_2(s) = Co(NH_3)Cl_2(s) + NH_3(g)$

(B) $Co(NH_3)Cl_2(s) = CoCl_2(s) + NH_3(g)$

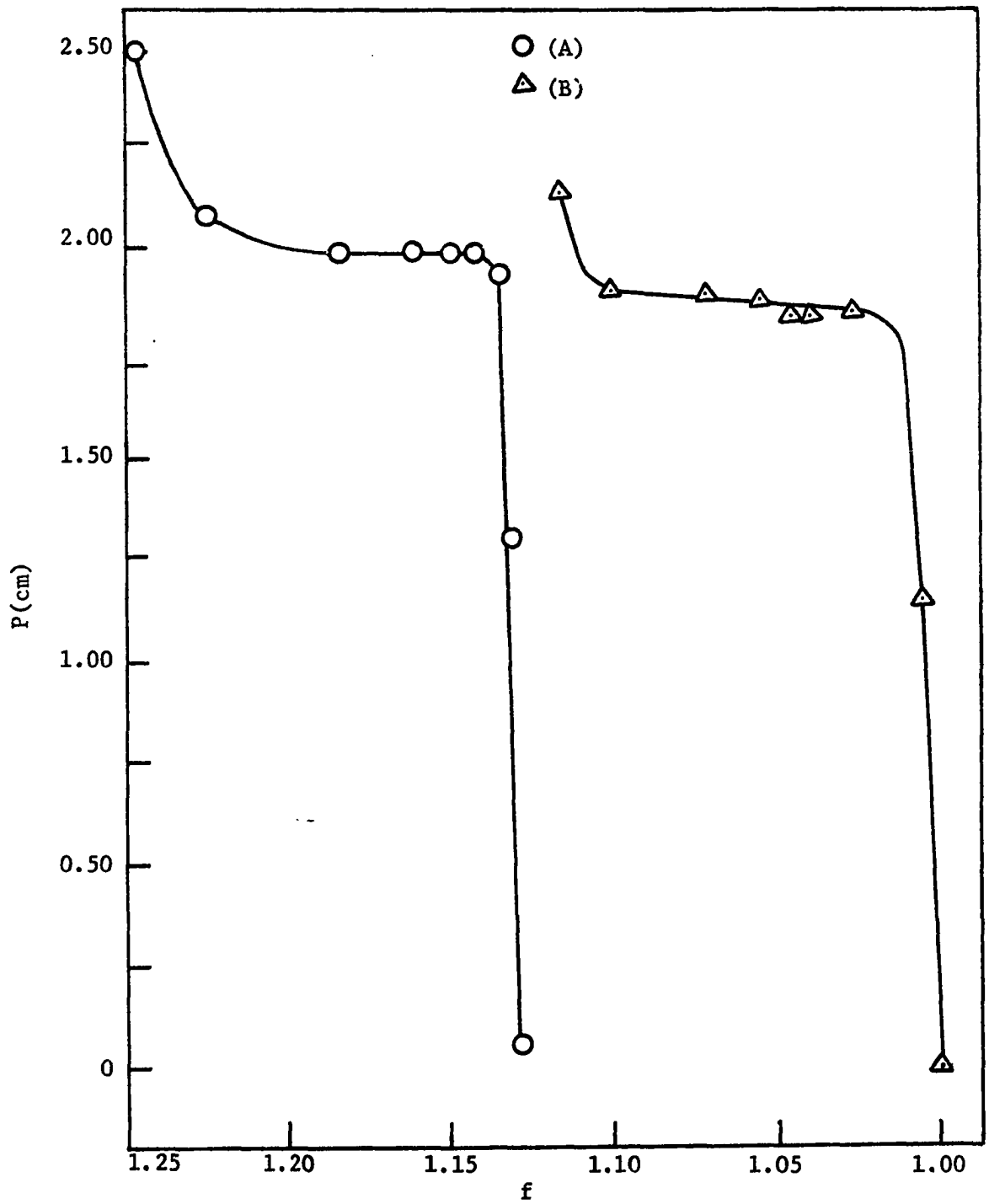

TABLE 3

VAPOR PRESSURE DATA
$Co(NH_3)_6Cl_2(s) = Co(NH_3)_4Cl_2(s) + 2NH_3(v)$

T°C	f	P(cm)	T°C	f	P(cm)
55.0	1.744	3.025	40.9	1.749	1.925
	1.730	1.800		1.736	0.940
	1.698	1.285		1.680	0.600
	1.688	1.375		1.655	0.570
	1.649	1.280		1.640	0.585
	1.635	1.270		1.623	0.560
	1.608	1.275		1.607	0.550
	1.602	1.265		1.584	0.560
	1.579	1.265		1.538	0.530
	1.545	1.250		1.518	0.405
	1.539	1.260			
	1.534	1.180			
	1.528	1.140			
	1.520	1.110			

TABLE 4

VAPOR PRESSURE DATA
$Co(NH_3)_4Cl_2(s) = \beta\text{-}Co(NH_3)_2Cl_2(s) + 2NH_3(v)$

T°C	f	P(cm)	T°C	f	P(cm)
54.8	1.528	1.140	41.7	1.526	0.510
	1.500	1.115		1.493	0.450
	1.485	1.115		1.437	0.440
	1.450	1.110		1.410	0.445
	1.413	1.110		1.393	0.440
	1.397	1.110		1.372	0.430
	1.385	1.105		1.346	0.435
	1.331	1.070		1.317	0.435
	1.306	1.090		1.284	0.400
	1.293	1.045		1.267	0.120
	1.271	0.570		1.257	0.000
	1.260	0.000			

TABLE 5

VAPOR PRESSURE DATA
α-$Co(NH_3)_2Cl_2(s) = Co(NH_3)Cl_2(s) + NH_3(v)$

T°C	f	P(cm)	T°C	f	P(cm)
150.0	1.268	1.540	150.0	1.150	0.200
	1.255	0.825		1.142	0.200
	1.248	0.250		1.135	0.195
	1.225	0.210		1.132	0.195
	1.183	0.200		1.128	0.005
	1.162	0.200			

TABLE 6

VAPOR PRESSURE DATA
$Co(NH_3)Cl_2(s) = CoCl_2(s) + NH_3(v)$

T°C	f	P(cm)	T°C	f	P(cm)
202.0	1.116	0.215	202.0	1.039	0.185
	1.099	0.190		1.011	0.185
	1.072	0.190		1.005	0.095
	1.054	0.190		1.002	0.000
	1.045	0.185			

$$\Delta F^\circ = -RT \ln K = \Delta H^\circ - T\Delta S^\circ.$$

The equilibrium vapor pressure, $P^m_{NH_3}$, for the cobalt(II) chloride ammine system is equal to the equilibrium constant and by rearranging the above equation becomes

$$-\log P_{NH_3} = \frac{\Delta H^\circ}{2.303mRT} - \frac{\Delta S^\circ}{2.303mR}.$$

From the above equation it is seen that a plot of -log P versus 1/T will yield a straight line with a slope equal to $\Delta H^\circ/2.303mR$ and an intercept on the -log P axis of $-\Delta S^\circ/2.303R$. This plot will yield a straight line only if ΔH° is independent of temperature over the range studied, i.e., ΔC_p is approximately constant for this range. Otherwise a nonlinear curve can exist.

Pressure-temperature data were measured and treated with a least squares analysis.[39] The data are given in Tables 7-12 and the graphs are shown in Figures 10-13.

The values of the thermodynamic constants calculated for the individual reactions are given in Table 13.

The data for the equilibrium between the hexammine and the tetrammine yield two straight lines with different slopes intersecting at approximately 38°C (Figure 10). This change in slope must be due to a change in solid phase. This phase change could be caused by either the $Co(NH_3)_6Cl_2$ or the $Co(NH_3)_4Cl_2$ changing to a different structural isomer, or by the appearance of an entirely new species of different composition.

There is a possibility that an equilibrium of the type

TABLE 7

PRESSURE-TEMPERATURE DATA FOR LOG P VS 1/T
$[Co(NH_3)_6]Cl_2(s) = [Co(NH_3)_4Cl_2](s) + 2NH_3(v)$

P(cm)	P x 10^3(atm)	-Log P(atm)	T(°A)	(1/T) x 10^3(°A)
0.585	7.697	2.114	314.0	3.185
0.570	7.500	2.125	314.0	3.185
0.695	9.145	2.039	317.6	3.148
0.700	9.211	2.036	317.6	3.148
0.855	11.250	1.949	321.2	3.113
0.865	11.382	1.944	321.2	3.113
1.030	13.553	1.868	324.7	3.080
1.040	13.684	1.864	324.7	3.080
1.275	16.776	1.775	328.1	3.047
1.285	16.908	1.772	328.1	3.047

Least Squares Analysis

Slope = 2508 ± 40

Intercept = -5.863 ± 0.126

Root Mean Square Deviation = 0.0062

TABLE 8

PRESSURE-TEMPERATURE DATA FOR LOG P VS 1/T
$[Co(NH_3)_4Cl_2]\cdot 2NH_3(s) = [Co(NH_3)_4Cl_2](s) + 2NH_3(g)$

P(cm)	P x 10^3(atm)	-Log P(atm)	T(°A)	(1/T) x 10^3(°A)
0.335	4.408	2.354	293.4	3.408
0.335	4.408	2.354	293.4	3.408
0.385	5.066	2.295	299.1	3.343
0.385	5.066	2.295	299.1	3.343
0.430	5.658	2.247	303.4	3.296
0.445	5.855	2.232	303.4	3.296
0.470	6.184	2.209	307.5	3.252
0.470	6.184	2.209	307.5	3.252
0.510	6.711	2.173	311.0	3.215
0.510	6.711	2.173	311.0	3.215

Least Squares Analysis

Slope = 950.3 ± 28.4

Intercept = -0.8842 ± 0.0937

Root Mean Square Deviation = 0.0061

TABLE 9

PRESSURE-TEMPERATURE DATA FOR LOG P VS 1/T
$Co(NH_3)_4Cl_2(s) = \beta\text{-}Co(NH_3)_2Cl_2(s) + 2NH_3(g)$

P(cm)	P x 10^3(atm)	-Log P(atm)	T(°A)	(1/T) x 10^3(°A)
0.130	1.711	2.767	293.1	3.411
0.155	2.039	2.691	297.0	3.367
0.190	2.500	2.602	300.9	3.323
0.220	2.895	2.538	303.9	3.291
0.220	2.895	2.538	304.0	3.289
0.255	3.355	2.474	307.0	3.257

Least Squares Analysis

Slope = 1918 ± 26

Intercept = -3.773 ± 0.088

Root Mean Square Deviation = 0.0036

TABLE 10

PRESSURE-TEMPERATURE DATA FOR LOG P VS 1/T
$Co(NH_3)_4Cl_2(s) = \alpha\text{-}Co(NH_3)_2Cl_2(s) + 2NH_3(v)$

P(cm)	P x 10^3(atm)	-Log P(atm)	T(°A)	(1/T) x 10^3(°A)
0.340	4.474	2.349	311.6	3.209
0.405	5.329	2.273	313.9	3.186
0.420	5.526	2.258	313.9	3.186
0.440	5.789	2.237	314.8	3.177
0.550	7.237	2.140	318.2	3.143
0.545	7.171	2.144	318.2	3.143
0.770	10.130	1.994	322.7	3.099
0.770	10.130	1.994	322.7	3.099
1.110	14.610	1.835	327.9	3.050
1.105	14.540	1.837	327.9	3.050

Least Squares Analysis

Slope = 3185 ± 39

Intercept = -7.876 ± 0.123

Root Mean Square Deviation = 0.0068

TABLE 11

PRESSURE-TEMPERATURE DATA FOR LOG P VS 1/T
α-$Co(NH_3)_2Cl_2(s) = Co(NH_3)Cl_2(s) + NH_3(v)$

P(cm)	P x 10^3(atm)	-Log P(atm)	T(°A)	(1/T) x 10^3(°A)
0.200	2.632	2.580	422.1	2.370
0.200	2.632	2.580	422.1	2.370
0.260	3.421	2.466	426.1	2.347
0.260	3.421	2.466	426.1	2.347
0.350	4.605	2.337	432.1	2.315
0.350	4.605	2.337	432.1	2.315
0.520	6.842	2.165	439.1	2.278
0.500	6.579	2.182	439.1	2.278
0.700	9.211	2.036	446.1	2.242
0.710	9.342	2.030	446.1	2.242
0.910	11.974	1.922	451.1	2.217
0.870	11.447	1.941	451.1	2.217
1.450	19.079	1.719	461.1	2.169
1.355	17.749	1.749	461.1	2.169

Least Squares Analysis

Slope = 4174 ± 44

Intercept = -7.324 ± 0.099

Root Mean Square Deviation = 0.0109

TABLE 12

PRESSURE-TEMPERATURE DATA FOR LOG P VS 1/T
$Co(NH_3)Cl_2(s) = CoCl_2(s) + NH_3(v)$

P(cm)	P x 10^3(atm)	-Log P(atm)	T(°A)	(1/T) x 10^3(°A)
0.105	1.382	2.859	461.6	2.167
0.105	1.382	2.859	461.6	2.167
0.185	2.434	2.614	473.1	2.114
0.185	2.434	2.614	473.1	2.114
0.250	3.289	2.483	480.1	2.083
0.250	3.289	2.483	490.1	2.083
0.385	5.066	2.295	488.9	2.046
0.385	5.066	2.295	488.9	2.046
0.530	6.974	2.157	496.6	2.014
0.545	7.171	2.144	496.6	2.014
0.680	8.947	2.048	501.8	1.993
0.690	9.079	2.042	501.8	1.993
0.875	11.513	1.939	507.6	1.970
0.845	11.118	1.945	507.6	1.970

Least Squares Analysis

Slope = 4663 ± 30

Intercept = -7242 ± 0.062

Root Mean Square Deviation = 0.0074

FIGURE 10

(a) $[Co(NH_3)_4Cl_2](NH_3)_2(s) = Co(NH_3)_4Cl_2(s) + 2NH_3(g)$

(b) $Co(NH_3)_6Cl_2(s) = Co(NH_3)_4Cl_2(s) + 2NH_3(g)$

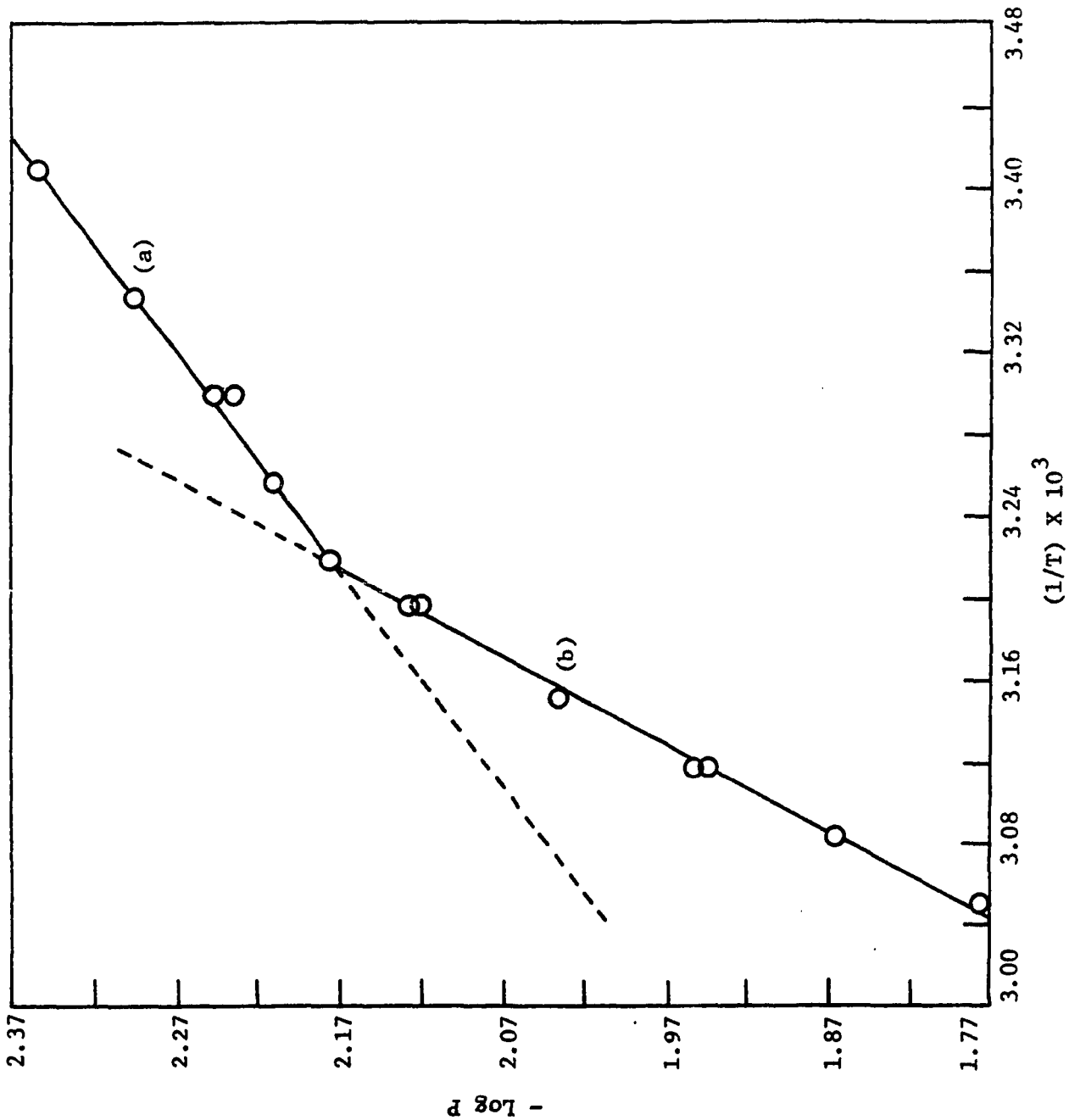

FIGURE 11. Log P(atm.) vs. 1/T(°A)

(a) $Co(NH_3)_4Cl_2(s) = \beta\text{-}Co(NH_3)_2Cl_2 + 2NH_3(g)$

(b) $Co(NH_3)_4Cl_2(s) = \alpha\text{-}Co(NH_3)_2Cl_2 + 2NH_3(g)$

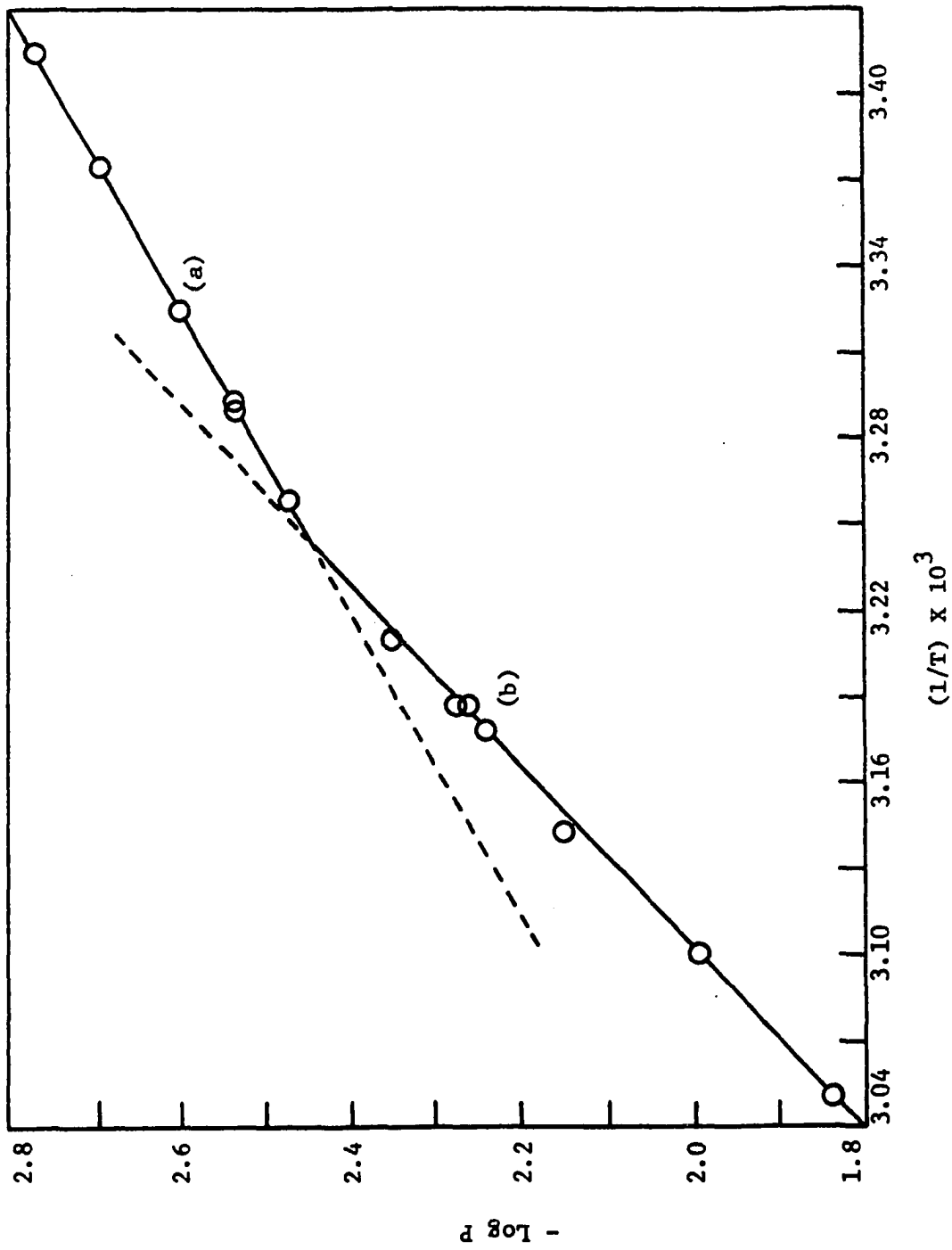

FIGURE 12

Log P(atm.) vs. 1/T(° A)

$Co(NH_3)Cl_2(s) = CoCl_2(s) + NH_3(g)$

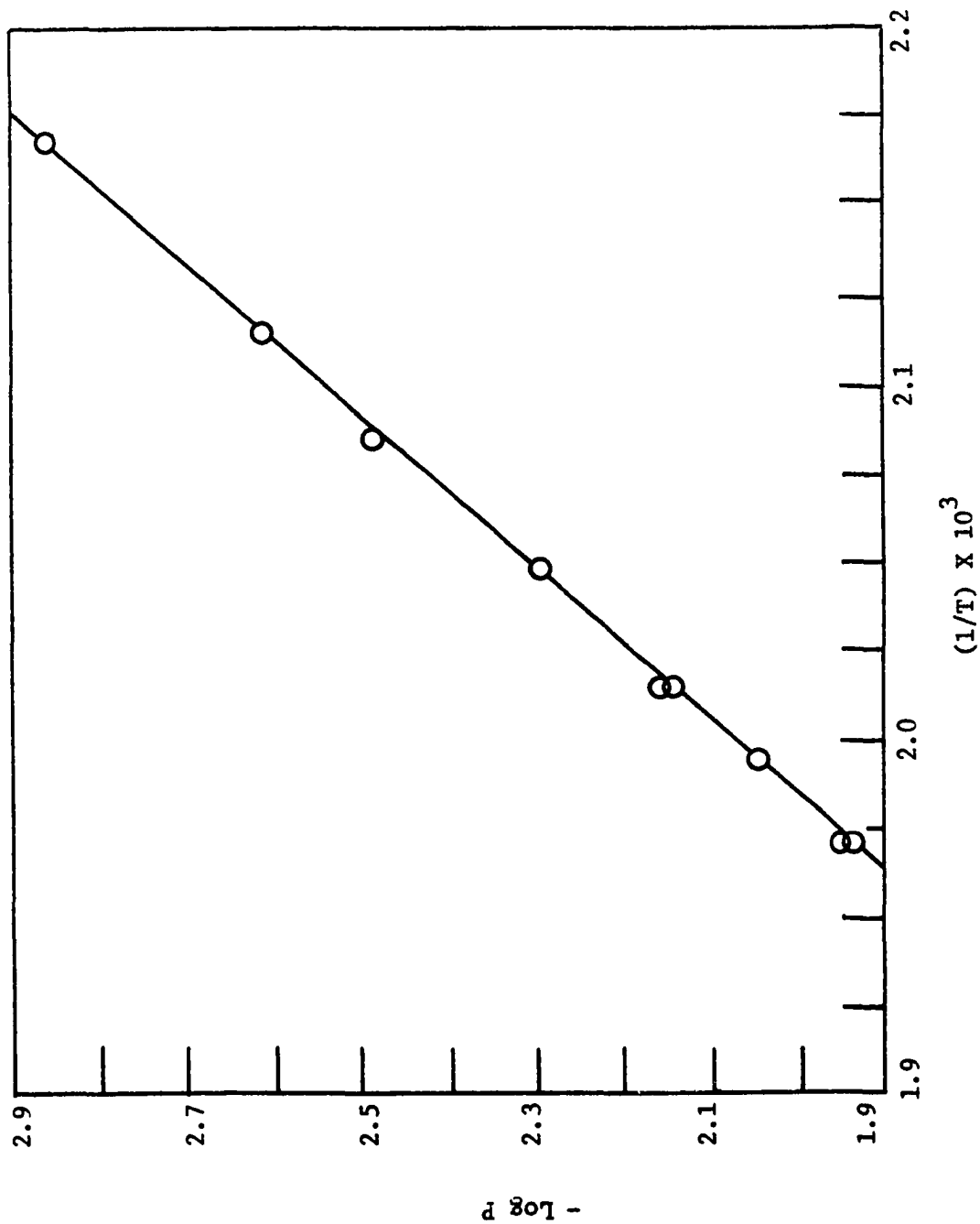

FIGURE 13

Log P(atm.) vs. 1/T(°A) for

α-$Co(NH_3)_2Cl_2(s) = Co(NH_3)Cl_2(s) + NH_3(g)$

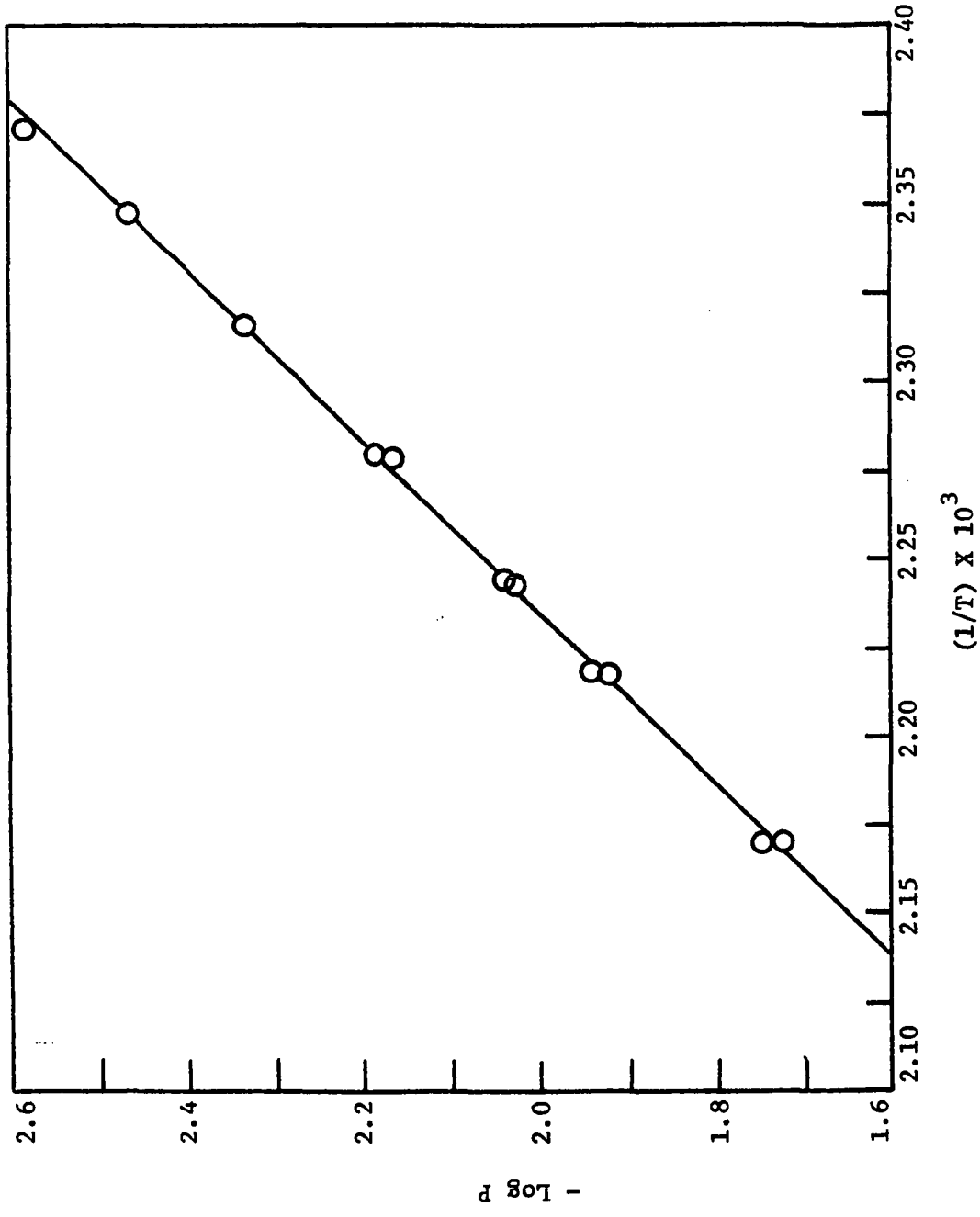

TABLE 13

THERMODYNAMIC CONSTANTS FROM EQUILIBRIUM DATA AT 25°C

	ΔH° (Kcal/mole)	ΔS° (eu/mole)	ΔF° (Kcal/mole)
$Co(NH_3)_6Cl_2 = Co(NH_3)_4Cl_2 + 2NH_3$	22.95 *(25.8)(40)	53.65	6.95
$Co(NH_3)_4Cl_2 \cdot 2NH_3 = Co(NH_3)_4Cl_2 + 2NH_3$	8.69	8.09	6.28
$Co(NH_3)_4Cl_2 = \beta\text{-}Co(NH_3)_2Cl_2 + 2NH_3$	17.55	34.53	7.26
$Co(NH_3)_4Cl_2 = \alpha\text{-}Co(NH_3)_2Cl_2 + 2NH_3$	29.15 *(25.8)(40)	72.08	7.67
$\beta\text{-}CO(NH_3)_2Cl_2 = \alpha\text{-}Co(NH_3)_2Cl_2$	11.60	38.45	0.41
$\alpha\text{-}Co(NH_3)_2Cl_2 = Co(NH_3)Cl_2 + NH_3$	19.10 (19.77)(7)	33.51	9.19
$Co(NH_3)Cl_2 = CoCl_2 + NH_3$	21.34 (21.10)(21)	33.14	11.46
$Co(NH_3)_6Cl_2 = CoCl_2 + 6NH_3$	92.54 (93.6)(41)	192.38	35.27

* Value given is twice the average ΔH° for each mole of ammonia lost in the reaction $Co(NH_3)_6Cl_2 = Co(NH_3)_2Cl_2 + 4NH_3$. The experimental value obtained for this reaction is ΔH° = 52.1 Kcal/mole while the reported value from reference (40) is ΔH° = 51.6 Kcal/mole.

$Co(NH_3)_6Cl_2 = Co(NH_3)_2Cl_2 + 4NH_3$ could exist. However, the curves for $Co(NH_3)_4Cl_2 = Co(NH_3)_2Cl_2 + 2NH_3$ and $Co(NH_3)_6Cl_2 = Co(NH_3)_4Cl_2 + 2NH_3$ should converge at this temperature and become one line since the tetrammine would no longer be stable. This is not observed for the phase change noted above.

Another possibility for a phase change would be to have an isomer of $Co(NH_3)_4Cl_2$. Two octahedral configurations, one cis the other trans, are possible. If this were the case a similar result would be indicated in the curve for the equilibrium between $Co(NH_3)_4Cl_2$ and $Co(NH_3)_2Cl_2$. There is a break in this curve at approximately the same temperature, but there is sufficient evidence to assign this break to an isomeric change in the diammine complex. This will be discussed later.

From Table 13 it is noted that the enthalpy of reaction, 8.69 Kcal/mole, is much smaller than those obtained for all of the other reactions of this study (20 Kcal/mole). This reduction in the enthalpy is compatible with two of the ammonia molecules of the hexammine complex having moved to the outer coordination sphere and are thus more easily removed.

This change in structure would cause the $Co(NH_3)_6Cl_2$ complex to appear similar in nature to the tetrammine species. The complex could be more correctly written as $[Co(NH_3)_4Cl_2]\cdot 2NH_3$. The color of the equilibrium mixture changed to the blue color attributed to the tetrammine.

It should be noted that this was the only data obtained

indicating the existence of this species. This species was observed only when an equilibrium pressure of ammonia was present. All attempts to obtain a spectra of this equilibrium state failed due to the highly reactive nature of the species. In an atmosphere of ammonia other than the equilibrium condition, ammonia was either added or lost by the complex. In an inert atmosphere ammonia was readily lost. In addition the complex also had a very strong affinity for atmospheric water.

The existence of a species of this type can be expected since this type of stable complex is present in both the water[2] and pyridine[3] systems. No mention of the existence of this compound could be found in the literature.

As previously mentioned, the pressure-temperature plot for the equilibrium of the tetrammine and the diammine (Figure 11) also exhibits a change in slope at approximately 36°C. This change in slope is attributed to a change in the phase of $Co(NH_3)_2Cl_2$. The deammination of $Co(NH_3)_4Cl_2$ below 36°C yields a blue powder while the deammination above this temperature yields a red powder. The composition of both was determined to be the same, therefore, the change must be in the structure. Previous studies indicate the existence of two isomers of the diammine with the colors reported above. F. Rose[26] reported the transition temperature as 67°C. This reported temperature is the point at which an immediate change in color is noted. The transition temperature of 36°C was determined from equilibrium data.

The blue color belongs to the β isomer of the complex while the red color comes from the α complex.[27] The diammine is unlike the hydrate[2] and pyridinate[3] complexes in that only one species is present for the hydrate and the two forms of the pyridinate are due to a change from octahedral to tetrahedral symmetry. The spectra and magnetic moments confirm that both diammine species are octahedral (Tables 27 and 30).

The difference in heats of reaction between the tetrammine and the two diammines is the energy of transition from one species to the other. This energy of transition from the β isomer to the α isomer was found to be 11.60 Kcal/mole.

The thermodynamic constants determined agree reasonably well with literature values where available. Most of these values were determined calorimetrically.

Once the thermodynamic constants for each deammination step are obtained the standard enthalpies of formation of each of the ammines can be calculated by using the standard enthalpies of formation for solid cobalt(II) chloride, -77.8 Kcal/mole,[42] and gaseous ammonia, -11.04 Kcal/mole.[42] This calculation is made by use of the equation

$$\Delta H_f^\circ \ Co(NH_3)_n Cl_2(s) = \Delta H_f^\circ \ Co(NH_3)_{n-m} Cl_2(s) + m\Delta H_f^\circ \ NH_3(v) - \Delta H_R^\circ.$$

The entropies of formation can be calculated in the same manner, with the standard entropy of formation of cobalt(II) chloride, 25.4 eu/mole,[42] and of ammonia, 46.01 eu/mole.[42]

The calculated standard enthalpies and entropies of formation are given in Table 14.

The values agree within one percent of the literature values.

TABLE 14

CALCULATED STANDARD ENTHALPIES AND ENTROPIES OF FORMATION

Compound	ΔH_f°(Kcal/mole)	S_f°(eu/mole)	$S^\circ_{f(n-m)} - S^\circ_{f(n)}$
$CoCl_2$	-77.8(42)	25.4	
			- 7.7
$Co(NH_3)Cl_2$	-110.2 (-109.2)(43) (-110.3)(42)	38.3	
			-12.5
α-$Co(NH_3)_2Cl_2$	-140.3 (-140.2)(42) (-138.7)(41)	50.8	
			24.5
β-$Co(NH_3)_2Cl_2$	-151.9	26.2	
			-44.5
$Co(NH_3)_4Cl_2$	-191.6	70.7	
			-38.4
$[Co(NH_3)_6]Cl_2$	-236.6 (-236.5)(21) (-239.0)(43) (-240.2)(42)	109.1	
			-55.5
$[Co(NH_3)_4Cl_2]\cdot 2NH_3$	-222.3	164.6	

CHAPTER 4

SPECTRA

Preliminary Discussion

The absorption spectra of the series of cobalt(II) chloride ammines exhibit a series of bands between 2400 mu and 300 mu. These absorptions correspond to d→d electronic transitions of Co(II), and to overtones of the ammonia stretching and bending modes.[44]

The number, shape, energy, and intensity of the d→d absorption bands are dependent upon the energy of the "d" orbitals, their degeneracy, the number and kind of ligands, and the geometry of the complex. The free ion of a transition metal has five degenerate "d" orbitals. Transitions can occur because of a loss of degeneracy of these "d" orbitals under the influence of the electric field produced by the ligands.

This change of degeneracy of the "d" orbitals was first proposed by Bethe.[45] He considered the ligands as point charges, and the interaction between the central ion and the ligands to be purely electrostatic in nature. This interpretation is the basis for crystal field theory.

Later a modification of this approach was developed,

accounting for covalent bonding which occurs between the metal and its ligands. This modified approach is known as ligand field theory and is the basis for explaining the spectra.

Since the structure[28] and spectra[31] of $CoCl_2$ and the structure of $Co(NH_3)_6Cl_2$ [16] are known, both having a symmetric octahedral ligand symmetry (O_h), the spectra will be discussed using these for a comparative basis.

Assuming a symmetric octahedron there is a possibility of two different ground state configurations, i.e., $^4T_{1g}(t_{2g}^5 e_g^2)$ for weak field and $^2E_g(t_{2g}^6 e_g^1)$ strong field. With ammonia and/or chloride as ligands, octahedral cobalt(II) is weak field.[6]

Theory

The energy of any electronic state can be determined in theory from an integral of the form

$$E = \int \psi^* H \psi d\tau$$

where ψ is the normalized wave function and $\hat{H}$ is the Hamiltonian operator.

The approach used will be to add pertubations to the free ion Hamiltonian, $\hat{H}_f$ [12] which has the form:

$$\hat{H}_f = (-h^2/2m)\sum_i \nabla_i^2 - \sum_i (Ze^2/r_i) + (1/2) \sum_{\substack{i \\ i \neq j}} \sum_j (Ze^2/r_{ij}) + \sum_i \xi_i(r) l_i \cdot s_i$$

where the first term is the kinetic energy, the second term is the potential energy due to the interaction of the electrons with the nucleus, the third is the potential energy due to the interaction of electrons with one another, and the fourth is the potential due

to spin-orbit coupling. The Hamiltonian to be considered for this system is:

$$\hat{H}_o = \hat{H}'_f + \hat{V} + \hat{V}_t.$$

$\hat{H}'_f$ is no longer the free ion Hamiltonian even though it contains the same terms, since in a ligand field the electron interaction[46] and the spin-orbit coupling[47] are decreased in magnitude.

The second term of $\hat{H}_o$ is the octahedral operator which accounts for the splitting of the free ion terms due to the crystal field. This splitting is measured in terms of the spectral parameter, D_q.

The third term considers that the ligand field is not a totally symmetric octahedron, but of a somewhat lower symmetry, i.e., D_{4h} or C_{2v}.

Using Russel-Saunders coupling the terms of the free ion of a particular d^n configuration can be derived. These terms arise due to the interaction of the electrons, i.e., the third term of $\hat{H}_f$. These states are designated by term symbols, using Mulliken's notation[48] of ^{2S+1}L, where S is the total spin quantum number of the system, 2S + 1 is the multiplicity, and L is the total angular momentum quantum number. The states arising from d^7 are given in Table 15.

To calculate the energy of each of the states arising from L-S coupling, appropriate wave functions must be found, by making use of lowering and raising operators[6] or by the method devised by Slater.[49] Utilizing the coulomb integral and the exchange integral one can determine the energy of the free ion terms as functions of

three parameters, F_o, F_2, and F_4. F_o accounts for the symmetrical part of the electron repulsions involving only the radial functions of the electrons, and F_2 and F_4 are functions of the angular dependent electron repulsions.

The values of the term energies for a d^7 configuration are given in Table 15.[6] It is readily seen from Table 16 that the difference in the energy of any two states is a function of F_2 and F_4 only. The energies are simplified by using Racah's parameters,[50] B and C, with $B = F_2 - 5F_4$ and $C = 35F_4$. The energy difference between the ground term and other terms with the same multiplicity is a function of B only. The energy difference in terms of Racah's formalism is also given in Table 16.

The actual values of B and C are determined from experimental data and are thus semi-empirical quantities. B and C can be determined for the free ion from the spectra of gaseous atoms and ions. These parameters when determined experimentally for a complex ion are usually found to be less than the values for the free ion. This change in term separation is attributed to several factors, the most important is the migration of charge from the ligands to the central ion.[51] Another reason is that in determining the wave functions only d^n configurations have been considered, and it is quite possible that excited configurations of the type $d^{n-1}s^1$ could exist.

The octahedral operator $\hat{V}$ may be expanded in a series of normalized spherical harmonics:

$$\hat{V} = \sum_i \sum_l \sum_m Y_l^m (\theta_i \phi_i) R_{nl}(r_i).$$

TABLE 15

TERM ENERGIES FOR d^7 ELECTRONIC CONFIGURATION

Term	Energy
^4F	$3F_0 - 15F_2 - 72F_4$
^4P	$3F_0 - 147F_4$
^2H	$3F_0 - 6F_2 - 12F_4$
^2G	$3F_0 - 11F_2 + 13F_4$
^2F	$3F_0 + 9F_2 - 87F_4$
a^2D	$3F_0 + 5F_2 + 3F_4$
	$-\sqrt{193F_2^2 - 1650F_2F_4 + 8325F_4^2}$
b^2D	$3F_0 + 5F_2 - 3F_4$
	$+\sqrt{193F_2^2 - 1650F_2F_4 + 8325F_4^2}$
^2P	$3F_0 - 6F_2 - 12F_4$

TABLE 16

ENERGY DIFFERENCE BETWEEN d^7 FREE ION TERMS

Term Interval	Energy Gap F Parameters	Racah Parameters
$^4P \leftarrow {}^4F$	$15F_2 - 75F_4$	15B
$^2H \leftarrow {}^4F$	$9F_2 + 60F_4$	9B + 3C
$^2G \leftarrow {}^4F$	$4F_2 + 85F_4$	4B + 3C
$^2F \leftarrow {}^4F$	$24F_2 - 15F_4$	24B + 3C
$^{a}_{b}2D \leftarrow {}^4F$	$20F_2 + 75F_4$	20B + 5C
	$\mp\sqrt{193F_2^2 - 1650F_2F_4 + 8325F_4^2}$	$\mp\sqrt{193\ B^2 + 8BC + 4C^2}$
$^2P \leftarrow {}^4F$	$9F_2 + 60F_4$	9B + 3C

It can be shown that $\hat{V}$ has the form:[6]

$$\hat{V} = \sum_i \frac{1}{4\pi} R_o(r_i) + Y_4^o + \sqrt{5/14}(Y_4^4 + y_4^{-4}).$$

As a first approximation, the first term gives rise to a uniform shift in energy of the five "d" orbitals. As a second approximation, the influence of this term would result from the interactions of highly excited configurations of the type already considered by the Racah parameters. Since only an energy difference between levels is being considered this term may be ignored.

The crystal field splitting of the free ion states due to a cubic field is obtained by using group theory.[52] These splittings are listed in Table 17.

In the following discussion $\hat{V}_0$ will be called the octahedral operator and have the form:

$$\hat{V}_0 = Y_4^0 + \sqrt{5/14}(Y_4^4 + Y_4^{-4}).$$

The octahedral operator has the effect of coupling together all spherical harmonics which have M_L different by four or $M_L = 0$, i.e., Y_L^2 and Y_L^{-2}, Y_L^1 and Y_L^{-3}, Y_L^{-1} and Y_L^3, and Y_L^0. Thus eigenstates to $\hat{V}_0$ can be obtained by forming the proper linear combinations of the various states.

The nonvanishing matrix elements of the "d" electrons quantized along the fourfold z axis and operated upon by $\hat{V}_0$ give the results listed in Table 18.

The energies of the term states are obtained by applying the octahedral operator to the proper eigenfunctions which are given by Fieschi and Löwdin.[53] These energies for the spin allowed states

TABLE 17

CRYSTAL FIELD SPLITTING OF FREE ION STATES

Free Ion State	Crystal Field State(s)
S	A_1
P	T_1
D	$E + T_2$
F	$A_2 + T_1 + T_2$
G	$A_1 + E + T_1 + T_2$
H	$E + 2T_1 + T_2$

TABLE 18

EFFECT OF $\hat{V}_0$ UPON THE "d" ORBITALS

Operation	Energy
$(d_{\pm2}\|\hat{V}_0\|d_{\pm2})$	Dq
$(d_{\pm2}\|\hat{V}_0\|d_{\mp2})$	5Dq
$(d_{\pm1}\|\hat{V}_0\|d_{\pm1})$	-4Dq
$(d_0\|\hat{V}_0\|d_0)$	6Dq

are listed in Table 19.

TABLE 19

SPIN ALLOWED d^7 STATES AND CRYSTAL FIELD ENERGIES IN WEAK OCTAHEDRAL FIELD

Free Ion Term	Crystal Field State	Energy
^4F	$^4T_{1g}$	- 6Dq
	$^4T_{2g}$	2Dq
	$^4A_{2g}$	12Dq
^4P	$^4T_{1g}$	15B

The ligand field is very seldom of true octahedral symmetry. The third term of $\hat{H}_0$, $\hat{V}_t$, becomes an effective pertubation whenever the symmetry is lowered to D_{4h}. The $\hat{V}_t$ operator has the form

$$\hat{V}_t = AR_2(r)Y_2^0 + BR_4'(r)Y_4^0,$$

where $\hat{V}_t$ is a pertubation which accounts for the tetragonal distortion present in a trans-MX_4Y_2 complex with the two ligands on the z axis different to those in the xy plane, or in a MX_6 complex possessing Jahn-Teller distortion.[54] The splitting of the octahedral levels due to a descent in symmetry from O_h to D_{4h} is presented in Table 20.[55]

Under D_{4h} symmetry the crystal field ground state depends upon whether the ligands are compressed (E_g) or elongated (A_{2g}) along the z axis as compared to the metal-ligand distance in the xy plane.

The terms Y_4^4 and Y_4^{-4} do not occur in the tetragonal operator

TABLE 20

CORRELATION O_h - LOWER SYMMETRY

O_h	D_{4h}	D_{2h}	C_{2v}
T_{1g}	$A_{2g} + E_g$	$B_{1g} + B_{2g} + B_{3g}$	$A_2 + B_1 + B_2$
T_{2g}	$B_{2g} + E_g$	$B_{1g} + B_{2g} + B_{3g}$	$A_1 + B_1 + B_2$
A_{2g}	B_{1g}	A_{1g}	A_2
A_{1g}	A_{1g}	A_{1g}	A_1
E_g	$A_{1g} + B_{1g}$	$A_{1g} + A_{1g}$	$A_1 + A_2$

since the four ligands in the xy plane are left unaltered by a substitution of two ligands on the z axis. The overall effect on these orbitals having no z component is that they are not distorted, but their energies change.

The spherical harmonics of Y_2^0 and Y_4^0 in terms of rectangular coordinates normalized to one are:

$$Y_2^0 = \sqrt{\frac{5}{4\pi}\frac{1}{4}}\,\frac{3z^2 - r^2}{r^2}$$

and

$$Y_4^0 = \sqrt{\frac{9}{4\pi}\frac{1}{64}}\,\frac{35z^4 - 30z^2r^2 + 3r^4}{r^4}$$

Using the operator equivalent method[56] of substituting $\hat{l}_z$ for z, it can be shown that $\hat{V}_t$ becomes:

$$\hat{V}_t = Ds(\hat{l}_z^2 - 2) - Dt[(35/12)\hat{l}_z^4 - (155/12)\hat{l}_z^2 + 6]$$

where Ds and Dt are splitting parameters of Y_2^0 and Y_4^0. The effect

of $\hat{V}_t$ on the "d" orbitals is shown in Table 21.[6]

The sign and magnitude of Ds and Dt determines the ground state symmetry as shown in Table 22. With a positive Ds and a negative Dt the ground state is A_{2g} while reversing the signs yields an E_g ground state, however, if Ds and Dt have the same sign, the ground state can be either A_{2g} or E_g.

The ordering of the excited states also depends upon the sign and magnitude of Ds and Dt. This order can change even though the ground state does not.

The effect of $\hat{V}_t$ on the overall pertubation matrix must be determined by operating with $\hat{V}_t$ on the appropriate wave functions obtained by the use of raising and lowering operators.

The overall energy of the system is preserved by the action of $\hat{V}_t$, however, the energy of the orbitals containing a z component is lowered when there is elongation along the z axis, stabilizing these orbitals. For compression these orbitals are destabilized.

The spin-orbit contribution to the splitting is often neglected in studying the crystal field spectra for first row transition elements. This is because the spin-orbit splitting is small in comparison to the other pertubations considered.

The multiplet structure of the S-O bands is usually poorly resolved, and it has been determined in only a few cases for $3d^n$ complexes.

The spin-orbit operator, $\hat{H}_{so}$ has the form:

$$\hat{H}_{so} = \xi \hat{l} \cdot \hat{s}$$

TABLE 21

EFFECT OF $\hat{V}_t$ UPON THE "d" ORBITALS[6]

Operator	Result	
$(\hat{l}_z^2 - 2)$	d_0	$-2d_0$
	$d_{\pm1}$	$-d_{\pm1}$
	$d_{\pm2}$	$2d_{\pm2}$
$[(35/12)\hat{l}_z^4 - (155/12)\hat{l}_z^2 + 6]$	d_0	$6d_0$
	$d_{\pm1}$	$-4d_{\pm1}$
	$d_{\pm2}$	$d_{\pm2}$

TABLE 22

GROUND STATE DEPENDENCE UPON Ds AND Dt

Sign Ds	Sign Dt	Magnitude Limits	Z axis Effect	Ground State
+	+	Ds > (75/24)Dt	Elongation	$^4A_{2g}$
+	+	Ds < (75/24)Dt	Compression	^4E_g
+	-	None	Elongation	$^4A_{2g}$
-	+	None	Compression	^4E_g
-	-	Ds < (75/24)Dt	Elongation	$^4A_{2g}$
-	-	Ds > (75/24)Dt	Compression	^4E_g

which treats the interaction of the spin of the electrons with their own orbital motion. ξ is the one-electron spin-orbit coupling parameter, and $\hat{l}$ and $\hat{s}$ are the orbital angular momentum and spin operators. The spin-orbit coupling constant, λ, is used in considering the splitting of terms and is related to ξ by

$$\lambda = \pm \frac{\xi}{2S}$$

where λ is positive for a subshell less than half filled and negative for a subshell more than half filled. Thus for a d^7 configuration, λ is negative.

The spin-orbit coupling operator can be expanded to give:

$$\hat{l}\cdot\hat{s} = (\hat{l}_z\hat{s}_z + \tfrac{1}{2}\hat{l}_+\hat{s}_- + \tfrac{1}{2}\hat{l}_-\hat{s}_+)$$

where $\hat{l}_\pm$ and $\hat{s}_\pm$ are raising and lowering operators with $\hat{l}_\pm = \hat{l}_x \pm i\hat{l}_y$ and $\hat{s}_\pm = \hat{s}_x \pm i\hat{s}_y$.

Applying these operations to the appropriate wave functions, a further pertubation is made to the Hamiltonian.

For a first order approximation only the T states are split by spin-orbit coupling in an octahedral field.[57]

The method used to determine the pertubation due to spin-orbit coupling was somewhat simplified. Roots of the high spin states were determined and are:

$$E = 3/2\ \alpha\lambda \qquad (1)$$

$$= -\alpha\lambda \qquad (2)$$

$$= -5/2\ \alpha\lambda \qquad (3)$$

and for low spin:

$$E = 1/2\ \alpha\lambda \qquad (4)$$

$$= -\alpha\lambda \qquad (5)$$

where α is a constant and can be evaluated by applying the $\hat{l}_z$ operator. This method was developed by Abragam and Pryce[58,59]. Low[60] has also calculated the spin-orbit coupling of the ground state of Co^{++} using this method.

In the D_{4h} point group, roots (1) and (3) belong to E_g states and root (2) belongs to the singlet states, A_{2g} from T_{1g} and B_{2g} from T_{2g}. For low spin root (4) belongs to E_g and root (5) to the singlet B_{2g} and A_{2g} states.

These roots were added to the appropriate diagonal elements of the matrices. All off diagonal elements of spin-orbit coupling were ignored.

The assignment of only two roots to the ^4E_g states which are actually eight fold degenerate with respect to spin-orbit coupling, and only one root to the two fold degenerate singlet states greatly simplifies the spin-orbit coupling.

The overall effect of S-O coupling as treated here is to decrease the degeneracy of the states having E symmetry under D_{4h}. The notation used to designate these two states is E(1) and E(3), with the one and three arising from the previously discussed roots. The usual method used to designate the states is the double group notation as described by Bethe.[45]

One last pertubation to be considered is the interaction of terms of like symmetry. This is a second order pertubation and results in terms of like symmetry and multiplicity having a greater

energy separation than otherwise expected.

For a d^7 configuration under D_{4h} symmetry there exists three ^4E_g states and two $^4A_{2g}$ states.

Configuration interactions occur due to $\langle\psi T_{1g}(F)|V_0|\psi T_{1g}(P)\rangle$, $\langle\psi E_g(T_{1g})|V_t|\psi E_g(T_{2g})\rangle$, and others of similar nature having non-zero values. These non-zero values are off diagonal elements of the pertubation matrices. For this reason and since the pertubation is small compared to first order pertubations, the effect is often ignored, however, it must be considered to obtain a precise fit of the spectra.

Interaction of terms of the low spin states of like symmetry is also included in the calculations. Mixing of the low spin states with the high spin states by spin-orbit coupling is ignored, therefore, the matrix for the high spin states is considered separately from the low spin matrices.

To determine the pertubation parameters, Dq, B, C, Ds, Dt, and λ, one must evaluate the secular determinant obtained from performing the operations upon the wave functions.

The secular determinant shown in Figure 14 corresponds to the determinant used in calculating the energies related to the spin allowed transitions under D_{4h} symmetry. A similar determinant exists for the low spin states. The energies of the non-zero elements of the determinant are given in Table 23 as functions of the pertubation parameters.

FIGURE 14

SECULAR DETERMINANT FOR HIGH SPIN STATES

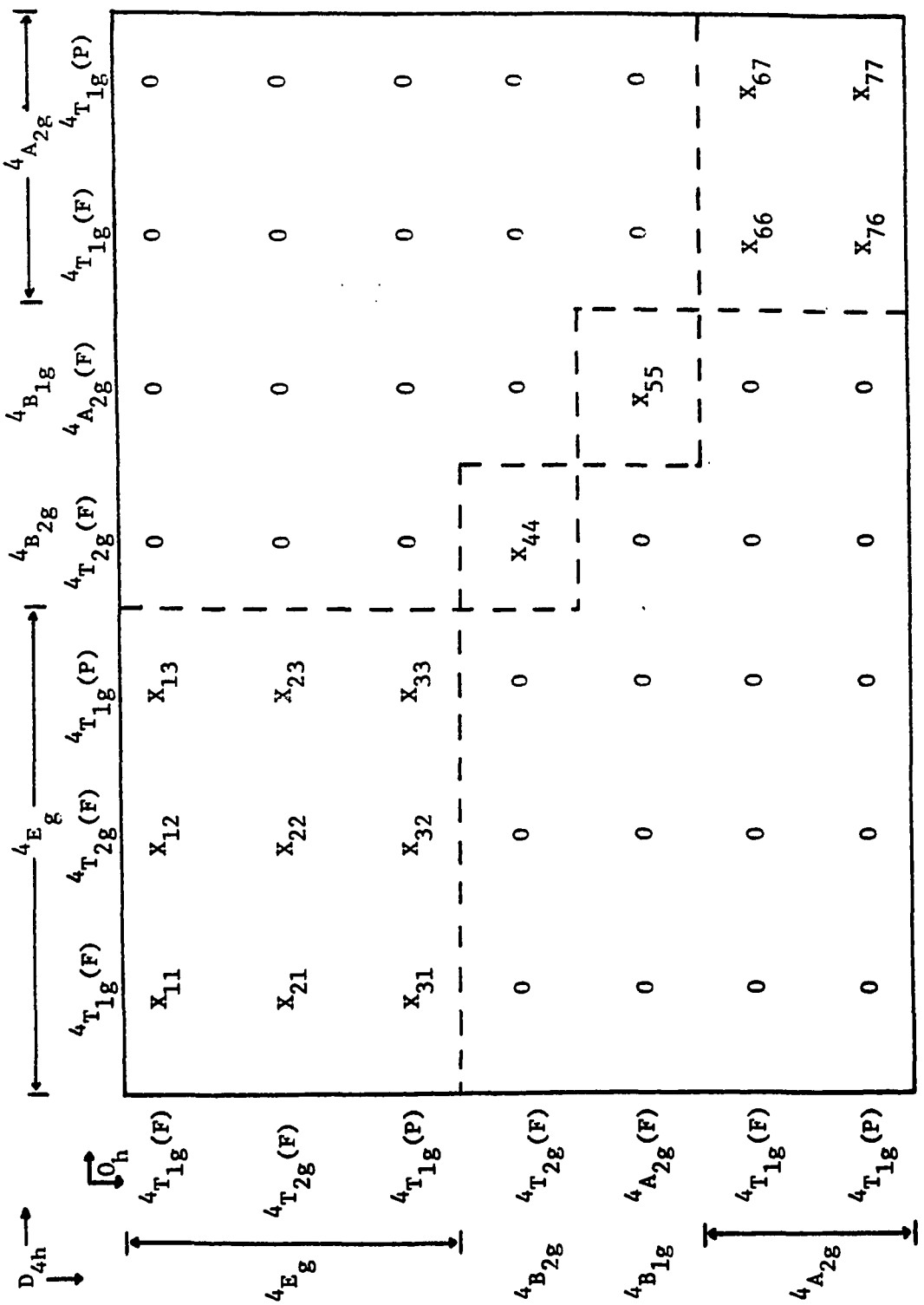

TABLE 23

NON ZERO ELEMENTS FOR THE SECULAR DETERMINANT IN FIGURE 14

Element	Energy
X_{11}	$-6Dq + 2/5Ds + 9/4Dt$
$X_{12} = X_{21}$	$+\sqrt{15/5}Ds - \sqrt{15/4}Dt$
$X_{13} = X_{31}$	$+4Dq - 6/5Ds - 3/2Dt$
X_{22}	$+2Dq + 7/4Dt$
$X_{23} = X_{32}$	$+\sqrt{12/5}Ds + \sqrt{15/4}Dt$
X_{33}	$15B - 7/5Ds$
X_{44}	$2Dq - 7Dt$
X_{55}	$12Dq - 7Dt$
X_{66}	$-6Dq - 4/5Ds + 6Dt$
$X_{67} = X_{76}$	$+4Dq + 12/5Ds - 4Dt$
X_{77}	$15B + 14/5Ds$

Band Intensities and Half Widths

The d→d transitions of interest are electric dipole transitions. To be allowed the intensity integral,

$$I \propto \int \psi' \mu \psi d\tau,$$

must be non-zero, i.e., the total integral must contain an A_{1g} component. I is the intensity of the transition, ψ' is the wave function of the excited state, ψ is the wave function of the ground state, and μ is the electric dipole operator.

Complexes with O_h or D_{4h} symmetry have a center of symmetry. Thus all of the "d" orbitals will be symmetric with the center of inversion as will the corresponding symmetry states of the "d" orbital transformations, i.e., the "d" orbitals transform as g states. The electric dipole operator when decomposed into its x, y, and z components is found to transform as μ states. The direct product of two g states and one μ state must lead to a μ state. Thus it becomes obvious that the intensity integral is zero. Therefore, the d→d transitions are electronically forbidden.

If, however, the complete wave function is taken as a product of the electronic wave function and a vibronic wave function, the intensity integral is of the form:

$$I \propto \int (\psi_v' \psi_e) \mu (\psi_v \psi_e) d\tau$$

and it can be shown that in most cases the intensity integrals will be non-zero.

From group theory it can be determined that the vibrational symmetry modes are:

$$A_{1g},\ E_g,\ 2T_{1u},\ T_{2g},\ \text{and}\ T_{2u}$$

under O_h symmetry, and

$$2A_{1g},\ B_{1g},\ B_{2g},\ E_g,\ 2A_{2u},\ B_{2u},\ \text{and}\ 3E_u$$

under D_{4h} symmetry.

The ground vibrational state always has A_{1g} symmetry and does not change the intensity integral, therefore, ψ_v is ignored. The intensity integral will be non-zero if there exists a normal mode of vibration which has the same symmetry as one of the representations spanned by $\psi_e'\mu\psi_e'$.

For a d^7 configuration under O_h or D_{4h} symmetry, all of the transitions are allowed due to one or more vibrational symmetry modes.

Since the transitions are taken to be from the lowest vibronic level of the ground state to the vibronic ground state of the excited states, an error is encountered in using the same parameter values to fit all of the transitions. However, this method is good for a first order approximation, and the energy of the observed transitions can be calculated within $\pm$ 100 cm^{-1}.

It should also be noted that certain hot band transitions may be observed. This is the case where the transition from the ground state does not occur from the lowest energy vibrational state but from one of higher energy. The peaks due to these transitions cause some difficulty in making the assignments of the spin forbidden transitions since they will appear as shoulders on the intense bands.

Infrared Overtones

In considering the crystal field spectra of the ammine complexes, it is noted that some of the bands located in the near I-R region of the spectrum cannot be assigned to crystal field transitions. These peaks arise due to overtones of the infrared active stretching, rocking, and bending modes.[61,62,63]

From the I-R spectra in Figures 1-4 various combinations of the bands are made such that their energies are located in the near infrared region.

The assignments of the infrared active bands in Table 24 were made according to Nakamoto.[22]

The more intense combination bands and their calculated energies as obtained from the infrared spectra are presented in Table 25. Other bands of lower intensity exist in the intermediate ammine complexes due to the splitting of the symmetric stretching mode of the ammonia molecules which are under different environments in the same complex.

The half-width of the absorption bands is informative in making the spectral assignments. Some of the bands are relatively sharp while others are rather broad.

A plot of the term energy as a function of the field strength for the d^7 electronic configuration is presented in the Tanabe-Sugano diagram[64] of Figure 18. The slope of the curve belonging to each of the states is a function of the population of the two levels, t_{2g} and e_g, arising from the "d" orbitals in an octahedral

TABLE 24

INFRARED ASSIGNMENTS

Compound	Assignment $\nu(NH_3)$	$\delta_d(NH_3)$	$\delta s(NH_3)$
$Co(NH_3)_6Cl_2$	3280 cm^{-1}	1605 cm^{-1}	1155 cm^{-1}
$Co(NH_3)_4Cl_2$	3280	1595	1155
β-$Co(NH_3)_2Cl_2$	3290	1600	1230
α-$Co(NH_3)_2Cl_2$	3280	1595	1230
$Co(NH_3)Cl_2$	3280	1605	1260

TABLE 25

NEAR INFRARED OVERTONES

Compound	$2\nu(NH_3)$	$\nu(NH_3)+\delta d(NH_3)$	$\nu(NH_3)+\delta s(NH_3)$	$\nu(NH_3)+\delta d(NH_3)+\delta s(NH_3)$
$Co(NH_3)_6Cl_2$	6560 cm^{-1}	4885 cm^{-1}	4435 cm^{-1}	6040 cm^{-1}
$Co(NH_3)_4Cl_2$	6560	4875	4435	6030
β-$Co(NH_3)_2Cl_2$	6580	4890	4520	6120
α-$Co(NH_3)_2Cl_2$	6560	4875	4510	6105
$Co(NH_3)Cl_2$	6560	4885	4540	6145

field. For an electron transition between two states of different slope the electronic distribution between the t_{2g} and e_g states is changed. This means that the equilibrium distance between the metal and ligand is changed due to the transition. The greater the difference is between the two slopes, the broader is the band for the transition in question. For a transition occuring between states of the complex which have the same electronic distribution, the peak will be very sharp. Such a transition occurs when the excited state has the same electronic configuration as the ground state.

The weak field spin allowed energy level diagram for the cobalt(II) chloride ammine complexes considering all of the pertubations is given in Figure 15, and the spin forbidden diagram for the lower energy states is given in Figure 16. The b^2D and ^2F states lie at higher energies than those investigated. The ordering of the excited states can vary depending upon the sign and magnitude of Ds and Dt as was shown in Table 22.

Experimental

The absorption spectra were all obtained from powder samples. The instrument used was a Beckman DK-1 recording spectrophotometer fitted with a Beckman reflectance attachment, and a modified Brown potentiometric strip recorder. The diffusion sphere was recoated several times with fresh magnesium oxide.

The samples were finely powdered and placed in 15mm. microscope well slides. The slide was filled, and covered with a very thin glass cover slide, held in place with cellophane tape. Since

FIGURE 15

ENERGY LEVEL DIAGRAM FOR SPIN ALLOWED STATES SHOWING EFFECT OF CONSIDERED PERTUBATIONS

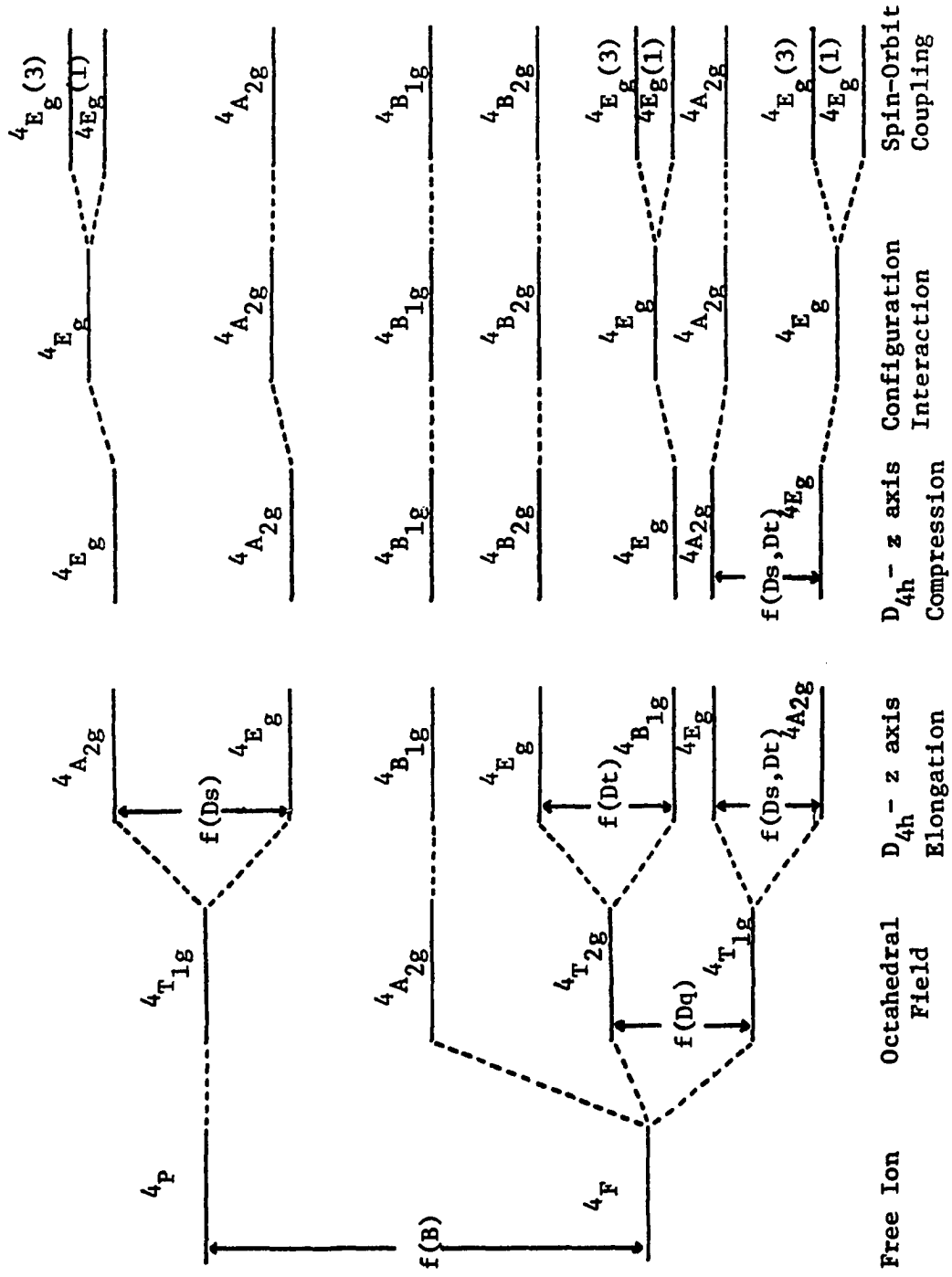

FIGURE 16

ENERGY LEVEL DIAGRAM FOR SPIN FORBIDDEN STATES OF LOWEST ENERGY

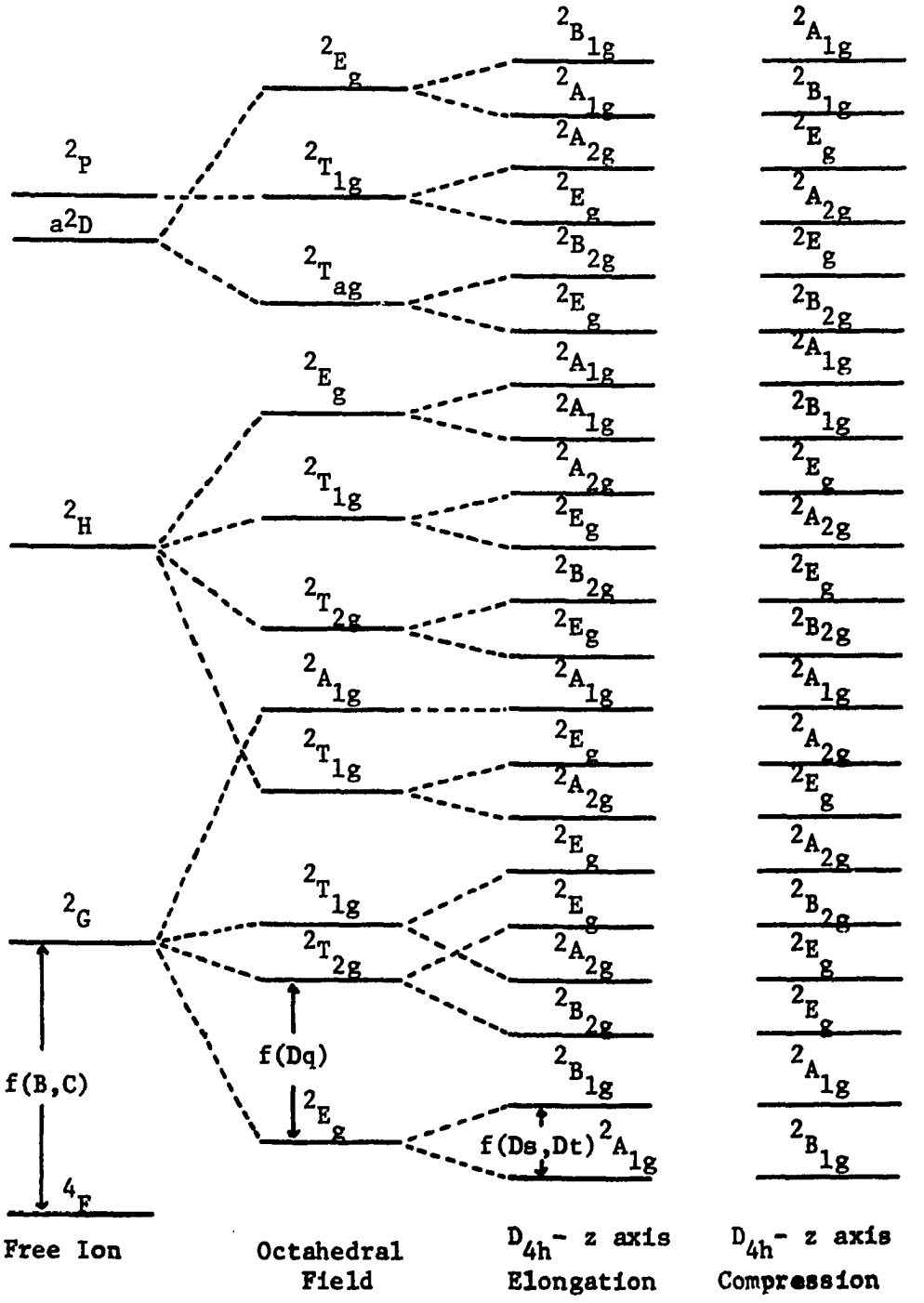

the samples are all oxygen and water sensitive, a dry bag was used in preparing the slides. The tape effectively sealed the samples and prevented decomposition or reaction with the atmosphere for the time necessary to record the spectra. After standing for a time exposed to the atmosphere, the samples did undergo a reaction and were thus discarded after each spectral recording.

The reference port was covered by a slide prepared from freshly ignited MgO and covered in the same manner as the sample slides. Two such slides were prepared and a spectra of the two was obtained to determine that the reference slide and the glass covers would show no absorption peaks in the region of interest.

All of the spectra were obtained under approximately the same conditions. The conditions of the recorder were: sensitivity, 3.0; time constant, 0.1; intensity range, 0-1 volts; and scan time, 3 minutes.

A PbS detector was used in the region from 2400-700 mμ and a photomultiplier tube was employed in the region from 700-300 mμ. The source was a 6V incadescent tungsten lamp for the near I-R and visible regions and a hydrogen lamp for the near UV.

The samples were prepared as previously stated in Chapter 2.

Attempts to prepare stable complexes of the type $[Co(NH_3)_4Cl_2](NH_3)_2$ with ammonia in the outer coordination sphere were not successful, even though thermodynamic data from Chapter 3 indicated that the above complex is stable under certain equilibrium conditions.

Since the shape and intensity of the absorption peaks of

reflectance spectra are a function of particle size and packing of the sample, no absolute absorbance can be determined, and only relative intensities are measured. The 100% and zero controls were varied until the full range of the instrument was used. This allowed for a better resolution of the peaks.

The reflectance spectra thus obtained are presented in Figures 20-25.

The actual peak positions are sometimes difficult to determine. The major peaks seen in the spectra are composed of two or more absorptions.

Three techniques are discussed in the literature for obtaining better spectral resolution in the solid phase. These consist of obtaining transmittance spectra of very thin crystals,[5] of cooling the sample to quench the vibration of the electrons, thus causing a sharpening of the peaks,[31] and of employing polarized light.[65,66,67]

All of these methods require crystals of the sample.

In order to obtain crystal spectra an apparatus for mounting and cooling of the crystal was developed to modify the Beckman DK-1 spectrophotometer. This apparatus is shown in Figure 17, and it has proven to be very useful if crystals of the sample can be grown.

The crystal is planed down to where the thickness is such that light is transmitted through it. The crystal (A) is then mounted over hole (B) in the aluminum plate (C). The appropriate mask is placed in the reference port (D) so that the recorder can

FIGURE 17

ATTACHMENT TO DK-1 SPECTROPHOTOMETER FOR OBTAINING

LOW TEMPERATURE CRYSTAL SPECTRA

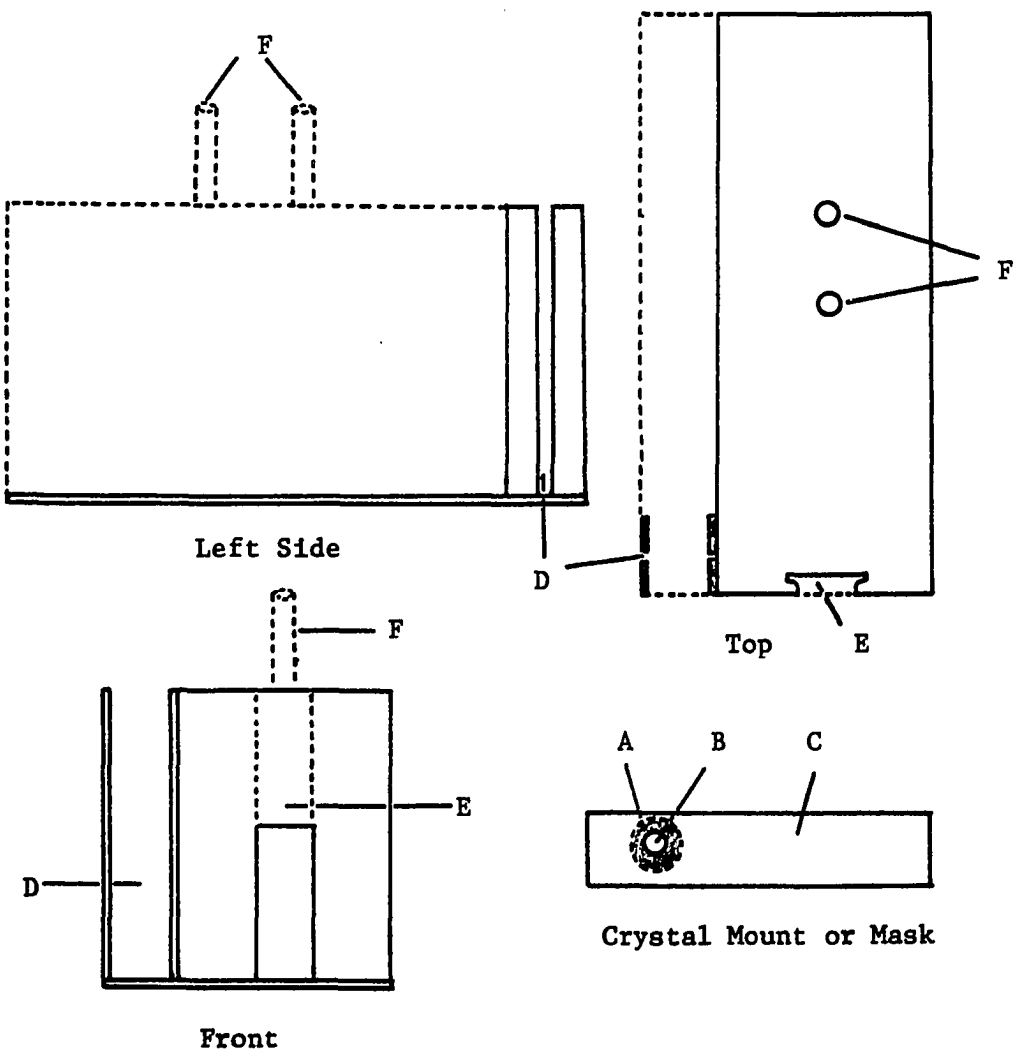

be scaled to obtain both the maximum and minimum of the absorbance bands. The crystal slide is inserted into slit (E) and the apparatus which is thoroughly insulated on all sides is placed into the cell compartment of the spectrophotometer. The compartment is flushed with dry nitrogen and liquid nitrogen is forced into the hollow block through one of the inlet tubes (F), while continuously flushing the cell compartment. The crystal is cooled by convection through the metal.

Small, red, octahedral crystals were obtained for $Co(NH_3)_6Cl_2$. After the crystals were planed down, the crystals were approximately 0.1-0.2 cm. in diameter. The spectra thus obtained for these crystals were very intense.

Attempts at growing crystals of the lower ammines failed. Thus since the calculations of the spectral fitting of the lower ammines must be based upon a reflectance spectra, the spectra in Figure 20 of $Co(NH_3)_6Cl_2$ is also a reflectance spectra.

Spectra Fitting

The Fortran program written by H. Joy[1] iterates the spectral parameters until the best fit of the assigned transitions is obtained.

Assuming octahedral symmetry, the ground state for $Co(NH_3)_6Cl_2$ and $CoCl_2$ is $^4T_{1g}$. Assignments were made for the two one electron transitions to the $^4T_{2g}$ and $^4T_{1g}(P)$. The transition to the $^4A_{2g}$ state is a two electron transition, and is thus of lower intensity than the other two spin allowed transitions.[68] Ds and Dt were set at zero, as they must be for octahedral symmetry. The spin allowed

transitions are independent of C, thus the parameter C/B was set at 4.0. Spin-orbit coupling was ignored for the first calculation. B was assigned the free ion value of 971 cm^{-1} for the hexammine complex and 800 cm^{-1} for the anhydrous complex since chloride lies below ammonia in the nephelauxetic series.[69] The program was then allowed to iterate to get the best fit. The splitting of the two bands by spin-orbit coupling was next taken into consideration. The fit of the spin allowed bands was then obtained.

From the Tanabe-Subano diagram (Figure 18) it was observed that the ^2E_g state of lowest energy was at a slightly lower energy than the $^4T_{2g}$ state for the determined Dq and B. In the experimental spectra, a shoulder was observed on the low energy side of the band assigned to the spin allowed transition. This shoulder was assigned to the ^2E_g transition. Setting all of the parameters except C/B, a fit of the spin forbidden transitions was obtained.

The spectral fitting obtained in this manner and the assignments of the absorption bands is given in Table 27. The parameters for these fittings are given in Table 28. The values of B'/B are obtained by dividing the calculated value of B by the free ion values.

All of the spectra of the intermediate ammine complexes were fit assuming D_{4h} or pseudo D_{4h} symmetry.[70] Fitting of these spectra was obtained in relatively the same manner as the fitting of the symmetric octahedral species above, except that Ds and Dt were also iterated.

FIGURE 18

TANABE-SUGANO DIAGRAM FOR Co(II)d^7

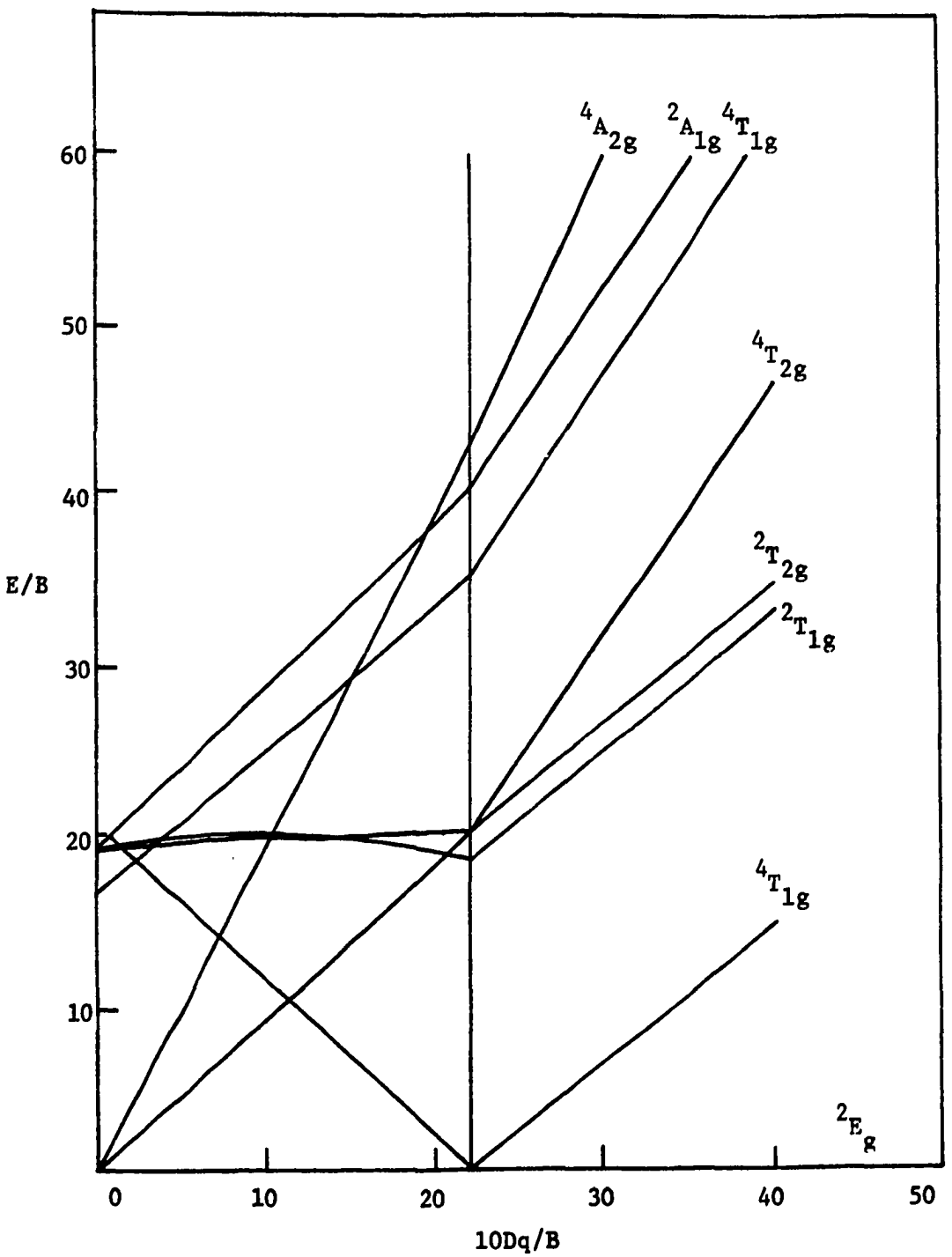

Assignment of the peaks belonging to the transitions to the $^4T_{2g}$ state is very difficult for the intermediate ammines since the ammonia overtones in the near infrared occur in approximately the same region. Before making these assignments, the peaks belonging, to these overtones were located. These assignments and their description and energy are listed in Table 26.

Attempts to fit the spectra assuming both a $^4A_{2g}$ and a ^4E_g ground state were made. All possible signs and magnitudes of Ds and Dt consistent with the type of distortion as discussed in the theory section were also considered.

In some cases a small error fitting parameter was obtained indicating a good fit of the assigned transitions, however, upon investigating the values obtained for the parameters one or more of them was found to be totally unreasonable, and it was therefore assumed that an incorrect assignment had been made. For the intermediate ammines, reasonable values of Dq lie between the values obtained for the hexammine (1030 cm^{-1}) and $CoCl_2$ (660 cm^{-1}). B should also have a value located between these two species and is expected to decrease in magnitude as ammonia molecules are displaced by the chlorides. The spin-orbit coupling parameter was held within 70% of the free ion value of -177 cm^{-1} and C/B is expected to possess a value between 4.0 and 5.0.[71]

TABLE 26

AMMONIA OVERTONE BAND ASSIGNMENTS AND DESCRIPTIONS

Compound	Peak Position mu	Peak Position cm^{-1}	Peak Description	Assignment
$Co(NH_3)_6Cl_2$	1525	6557	M-Sharp	2ν
	2020	4950	VS-Sharp	$\nu + \delta_d$
	2205	4535	VS-Sharp	$\nu + \delta_s$
	1640	6073	W-Broad	$\nu + \delta_d + \delta_s$
$Co(NH_3)_4Cl_2$	1535	6536	M-Broad	2ν
	2020	4950	MS-Sharp	$\nu + \delta_d$
	2205	4535	MS-Sharp	$\nu + \delta_s$
	1625	6154	W-Broad	$\nu + \delta_d + \delta_s$
β-$Co(NH_3)_2Cl_2$	1530	6536	W-Broad	2ν
	2025	4938	MS-Sharp	$\nu + \delta_d$
	2165	4619	M-Sharp	$\nu + \delta_s$
	1740	5747	W-Broad	$\nu + \delta_d + \delta_s$
α-$Co(NH_3)_2Cl_2$	1540	6495	M-Broad	2ν
	2025	4938	S-Sharp	$\nu + \delta_d$
	2160	4630	M-Sharp	$\nu + \delta_s$
	1700	5882	W-Broad	$\nu + \delta_d + \delta_s$
$Co(NH_3)Cl_2$	1540	6495	W-Broad	2ν
	2015	4963	W-Broad	$\nu + \delta_d$
	2160	4630	MW-Sharp	$\nu + \delta_s$
	1715	5831	W-Broad	$\nu + \delta_d + \delta_s$

TABLE 27

COLLECTED SPECTRAL DATA

	Transition	Calculated cm^{-1}	Calculated mu	Observed cm^{-1}	Peak Description
		I. $Co(NH_3)_6Cl_2$			
1.	$^4T_{1g}(F) \rightarrow {}^4T_{1g}(F)$	336		Not in region investigated	
		892			
2.	$\rightarrow {}^4T_{2g}(F)$	9,562	1046	9,524	MS-Broad
		9,762	1024	9,756	
		9,882	1012	9,901	
3.	$\rightarrow {}^4A_{2g}(F)$	19,990	500	20,000	MS-Shoulder
4.	$\rightarrow {}^4T_{1g}(P)$	20,613	485	20,916	VS-Sharp
		20,969	477	20,964	
		21,185	472	20,186	
5.	$\rightarrow {}^2E_g(G)$	8,267	1210	8,264	Shoulder of $^4T_{2g}(F)$
6.	$\rightarrow {}^2T_{1g}(G)$	16,584	603	16,529	Shoulder of $^4T_{1g}(P)$
		16,614	602	16,529	
7.	$\rightarrow {}^2T_{2g}(G)$	17,025	587	16,980	" " "
		17,345	577	17,280	
8.	$\rightarrow {}^2T_{1g}(H)$	21,046	475	21,055	" " "
		21,415	567	21,370	
9.	$\rightarrow {}^2A_{1g}(G)$	24,748	404	24,770	Shoulder of CT
10.	$\rightarrow {}^2T_{2g}(H)$	26,383	379	26,290	" " "
		26,466	378	26,440	
11.	$\rightarrow {}^2T_{1g}(H)$	27,843	359	27,870	" " "
		27,948	358	27,870	

TABLE 27 - Continued

	Transition	Calculated cm^{-1}	Calculated mu	Observed cm^{-1}	Peak Description
		II. $Co(NH_3)_4Cl_2$			
1.	$^4E_g(1) \rightarrow {}^4E_g(3)$	942		Not in region investigated	
2.	$\rightarrow {}^4A_{2g}$	3,278			
3.	$\rightarrow {}^4B_{2g}$	5,977	1673	6,000	Mixed with NH_3 overtones
4.	$\rightarrow {}^4E_g(1)$	8,860	1129	8,889	M-Broad
5.	$\rightarrow {}^4E_g(3)$	9,200	1087	9,302	M-Broad
6.	$\rightarrow {}^4B_{1g}$	15,200	658	15,152	S-Doublet
7.	$\rightarrow {}^4A_{2g}$	16,010	625	16,000	S-Doublet
8.	$\rightarrow {}^4E_g(1)$	19,181	521	19,120	VS-Sharp
9.	$\rightarrow {}^4E_g(3)$	19,783	505	19,802	VS-Sharp
10.	$\rightarrow {}^2A_{1g}$	9,403	1063	9,370	Shoulder on $^4T_{2g}$ band
11.	$\rightarrow {}^2B_{1g}$	10,000	1000	10,040	"
12.	$\rightarrow {}^2E_g$	14,255	701	14,340	Shoulder on 6.
13.	$\rightarrow {}^2E_g$	14,866	673	14,920	Shoulder on 6.
14.	$\rightarrow {}^2B_{2g}$	17,348	576	17,310	Shoulder on 8.
15.	$\rightarrow {}^2A_{2g}$	17,647	567	17,560	"
16.	$\rightarrow {}^2E_g$	18,282	547	18,310	"
17.	$\rightarrow {}^2A_{1g}$	19,710	507	19,800	Shoulder on 9.
18.	$\rightarrow {}^2A_{2g}$	20,778	481	20,768	"
19.	$\rightarrow {}^2B_{2g}$	21,488	465	21,490	"
20.	$\rightarrow {}^2A_{2g}$	21,786	459	21,750	"
21.	$\rightarrow {}^2B_{1g}$	23,477	426	23,410	"

TABLE 27 - Continued

	Transition	Calculated cm^{-1}	Calculated mu	Observed cm^{-1}	Peak Description
22.	$^4E_g(1) \rightarrow {}^2E_g$	24,568	407	24,560	Shoulder on CT
23.	$\rightarrow {}^2B_{2g}$	26,019	384	25,920	"
24.	$\rightarrow {}^2E_g$	26,874	372	26,920	"
25.	$\rightarrow {}^2A_{1g}$	27,096	369	27,110	"
26.	$\rightarrow {}^2A_{2g}$	27,795	360	27,700	"
	III. α-$Co(NH_3)_2Cl_2$				
1.	$^4E_g(1) \rightarrow {}^4E_g(3)$	738		Not in region investigated	
2.	$\rightarrow {}^4A_{2g}$	1,842			
3.	$\rightarrow {}^4B_{2g}$	6,738	1484	6,760	Mixed with NH_3 overtones
4.	$\rightarrow {}^4E_g(1)$	8,530	1174	8,600	M-Broad
5.	$\rightarrow {}^4E_g(3)$	8,790	1135	8,825	M-Broad
6.	$\rightarrow {}^4B_{1g}$	15,547	643	15,504	MS-Broad
7.	$\rightarrow {}^4A_{2g}$	18,230	549	18,190	MS-Broad
8.	$\rightarrow {}^4E_g(1)$	19,085	524	19,048	S-Sharp
9.	$\rightarrow {}^4E_g(3)$	19,562	511	19,608	S-Sharp
10.	$\rightarrow {}^2B_{1g}$	9,121	1096	9,090	Shoulder on 5.
11.	$\rightarrow {}^2A_{1g}$	9,488	1055	9,500	"
12.	$\rightarrow {}^2E_g$	14,214	704	14,280	Shoulder on 6.
13.	$\rightarrow {}^2E_g$	14,629	684	14,610	"
14.	$\rightarrow {}^2A_{2g}$	16,137	620	16,040	"
15.	$\rightarrow {}^2B_{2g}$	16,217	617	16,130	"

TABLE 27 - Continued

	Transition	Calculated cm^{-1}	Calculated mu	Observed cm^{-1}	Peak Description
16.	$^4E_g(1) \rightarrow {}^2E_g$	18,359	545	18,360	Shoulder on 8.
17.	$\rightarrow {}^2A_{2g}$	19,996	500	20,000	Shoulder on 9.
18.	$\rightarrow {}^2A_{1g}$	20,175	496	20,195	"
19.	$\rightarrow {}^2B_{2g}$	21,808	459	21,780	"
20.	$\rightarrow {}^2A_{2g}$	22,531	444	22,500	"
21.	$\rightarrow {}^2E_g$	22,833	438	22,930	"
22.	$\rightarrow {}^2E_g$	24,116	415	24,220	Shoulder on CT
23.	$\rightarrow {}^2B_{1g}$	24,287	412	24,340	"
24.	$\rightarrow {}^2A_{1g}$	26,308	390	26,200	"
25.	$\rightarrow {}^2B_{2g}$	26,968	371	26,990	"
26.	$\rightarrow {}^2E_g$	27,608	362	27,670	"
27.	$\rightarrow {}^2A_{2g}$	28,356	353	28,410	"
		IV. β-$Co(NH_3)_2Cl_2$			
1.	$^4A_{2g} \rightarrow {}^4E_g(1)$	30			
2.	$\rightarrow {}^4E_g(3)$	1,187			Not in region investigated
3.	$\rightarrow {}^4E_g(1)$	6,902	1448	6,826	Mixed with NH_3 overtones
4.	$\rightarrow {}^4E_g(3)$	7,101	1401	7,040	"
5.	$\rightarrow {}^4B_{2g}$	8,795	1137	8,800	M-Broad
6.	$\rightarrow {}^4B_{1g}$	15,514	645	15,504	MS-Broad
7.	$\rightarrow {}^4A_{2g}$	17,422	574	17,390	MS-Broad
8.	$\rightarrow {}^4E_g(1)$	19,054	525	19,050	S-Sharp

TABLE 27 - Continued

	Transition	Calculated cm^{-1}	Calculated mu	Observed cm^{-1}	Peak Description
9.	$^4A_{2g} \rightarrow {}^4E_g(3)$	19,594	510	19,610	S-Sharp
10.	$\rightarrow {}^2B_{1g}$	8,523	1174	8,510	Shoulder on 5.
11.	$\rightarrow {}^2A_{1g}$	9,225	1088	9,174	"
12.	$\rightarrow {}^2B_{2g}$	15,062	664	15,135	Shoulder on 6.
13.	$\rightarrow {}^2A_{2g}$	15,920	625	15,870	"
14.	$\rightarrow {}^2E_g$	15,547	643	15,585	"
15.	$\rightarrow {}^2E_g$	16,246	615	16,250	"
16.	$\rightarrow {}^2E_g$	19,833	504	19,900	Shoulder on 9.
17.	$\rightarrow {}^2A_{2g}$	20,017	500	20,000	"
18.	$\rightarrow {}^2A_{1g}$	21,387	467	21,440	"
19.	$\rightarrow {}^2E_g$	23,557	424	23,625	"
20.	$\rightarrow {}^2B_{2g}$	24,415	410	24,450	"
21.	$\rightarrow {}^2E_g$	24,511	408	24,625	"
22.	$\rightarrow {}^2A_{2g}$	25,705	390	25,640	Shoulder on CT
23.	$\rightarrow {}^2A_{1g}$	26,608	377	26,600	"
24.	$\rightarrow {}^2B_{1g}$	26,724	375	26,800	"
	V. $Co(NH_3)Cl_2$				
1.	$^4E_g(1) \rightarrow {}^4E_g(3)$	927			Not in region investigated
2.	$\rightarrow {}^4A_{2g}$	1,185			
3.	$\rightarrow {}^4B_{2g}$	7,590	1318	7,639	Mixed with NH_3 overtones
4.	$\rightarrow {}^4E_g(1)$	8,023	1246	8,000	M-Broad

TABLE 27 - Continued

	Transition	Calculated cm^{-1}	mu	Observed cm^{-1}	Peak Description
5.	$^4E_g(1) \rightarrow {}^4E_g(3)$	8,353	1197	8,333	M-Broad
6.	$\rightarrow {}^4B_{1g}$	16,008	625	16,000	MS-Broad
7.	$\rightarrow {}^4A_{2g}$	17,825	561	17,794	VS-Sharp
8.	$\rightarrow {}^4E_g(1)$	18,683	535	18,657	VS-Sharp
9.	$\rightarrow {}^4E_g(3)$	19,279	519	19,268	VS-Sharp
10.	$\rightarrow {}^2B_{1g}$	7,373	1356	7,408	Shoulder on 3.
11.	$\rightarrow {}^2A_{1g}$	7,807	1281	7,790	Shoulder on 4.
12.	$\rightarrow {}^2E_g$	13,818	724	13,730	Shoulder on 6.
13.	$\rightarrow {}^2E_g$	14,229	703	14,270	"
14.	$\rightarrow {}^2A_{2g}$	14,793	676	17,800	"
15.	$\rightarrow {}^2B_{2g}$	14,925	670	15,100	"
16.	$\rightarrow {}^2E_g$	17,873	560	17,875	Shoulder on 7.
17.	$\rightarrow {}^2A_{2g}$	18,930	528	18,940	"
18.	$\rightarrow {}^2A_{1g}$	20,164	496	20,000	Shoulder on 8.
19.	$\rightarrow {}^2B_{2g}$	21,741	460	21,740	"
20.	$\rightarrow {}^2E_g$	22,159	451	22,220	"
21.	$\rightarrow {}^2A_{2g}$	22,800	439	22,770	"
22.	$\rightarrow {}^2E_g$	23,397	427	23,340	"
23.	$\rightarrow {}^2B_{1g}$	24,355	411	24,310	Shoulder on CT
24.	$\rightarrow {}^2A_{1g}$	25,253	396	25,250	"
25.	$\rightarrow {}^2E_g$	27,517	363	27,450	"
26.	$\rightarrow {}^2B_{2g}$	26,987	371	27,010	"
27.	$\rightarrow {}^2B_{1g}$	29,759	354	29,720	"

TABLE 27 - Continued

	Transition	Calculated cm^{-1}	Calculated mu	Observed cm^{-1}	Peak Description
		VI. $CoCl_2$			
1.	$^4T_{1g}(F) \rightarrow {}^4T_{1g}(F)$	355		Not in region investigated	
		945			
2.	$\rightarrow {}^4T_{2g}(F)$	6,155	1625	6,150	S-Broad
		6,361	1572	6,349	S-Broad
		6,484	1542	6,464	S-Broad
3.	$\rightarrow {}^4A_{2g}(F)$	12,845	779	12,820	M-Broad
4.	$\rightarrow {}^4T_{1g}(P)$	16,711	598	16,750	VS-Sharp
		17,095	585	17,007	VS-Sharp
		17,327	577	17,391	VS-Sharp
5.	$\rightarrow {}^2E_g(G)$	8,904	1123	8,890	Shoulder on 2.
6.	$\rightarrow {}^2T_{1g}(G)$	14,046	712	13,990	Shoulder on 3.
		14,145	707	14,085	"
7.	$\rightarrow {}^2T_{2g}(G)$	14,056	711	14,085	"
		14,529	688	14,500	Shoulder on 4.
8.	$\rightarrow {}^2T_{1g}(H)$	17,817	561	17,830	"
		18,212	549	18,200	"
9.	$\rightarrow {}^2A_{1g}(G)$	18,724	534	18,700	"
10.	$\rightarrow {}^2T_{2g}(H)$	20,761	482	20,650	"
		20,879	479	20,850	"
11.	$\rightarrow {}^2T_{1g}(H)$	21,663	462	21,620	Shoulder on CT
		21,738	460	21,740	"

TABLE 27 - Continued

	Transition	Calculated cm^{-1}	Calculated mu	Observed cm^{-1}	Peak Description
12.	$^4T_{1g}(F) \rightarrow {}^2E_g(H)$	23,250	430	23,250	Shoulder on CT
13.	$\rightarrow {}^2T_{2g}(D)$	25,662	390	25,660	"
		25,534	392	25,580	"
14.	$\rightarrow {}^2T_{1g}(P)$	26,368	379	26,340	"
		26,521	377	26,430	"
15.	$\rightarrow {}^2E_g(D)$	27,002	370	26,910	"

TABLE 28

SPECTRAL FITTING PARAMETERS

Compound	Dq	B'	C'/B'	Ds	Dt	λ'	B'/B	λ'/λ
$Co(NH_3)_6Cl_2$	1030	822	4.78	0.0	0.0	-160	0.85	0.90
$Co(NH_3)_4Cl_2$	931	740	4.46	-648	355	-170	0.76	0.95
α-$Co(NH_3)_2Cl_2$	901	790	4.12	-230	205	-130	0.81	0.73
β-$Co(NH_3)_2Cl_2$	717	770	4.21	-340	-200	-150	0.78	0.84
$Co(NH_3)Cl_2$	850	770	4.00	-222	- 74	-165	0.78	0.93
$CoCl_2$	657	770	4.06	0.0	0.0	-165	0.78	0.93

FIGURE 19

Solution Spectrum of $Co(NH_3)_6^{++}$

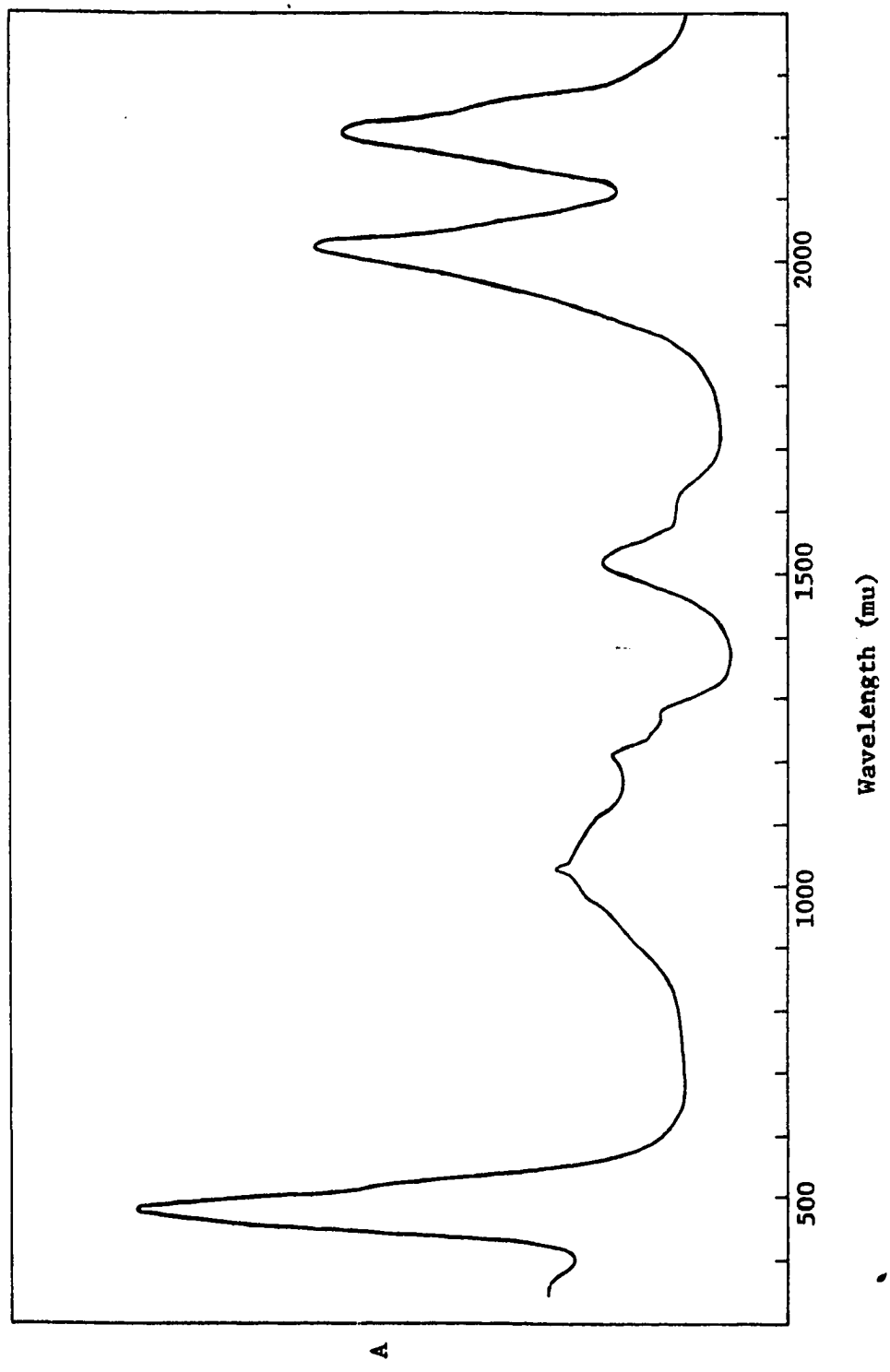

FIGURE 20

$Co(NH_3)_6Cl_2$ Spectrum

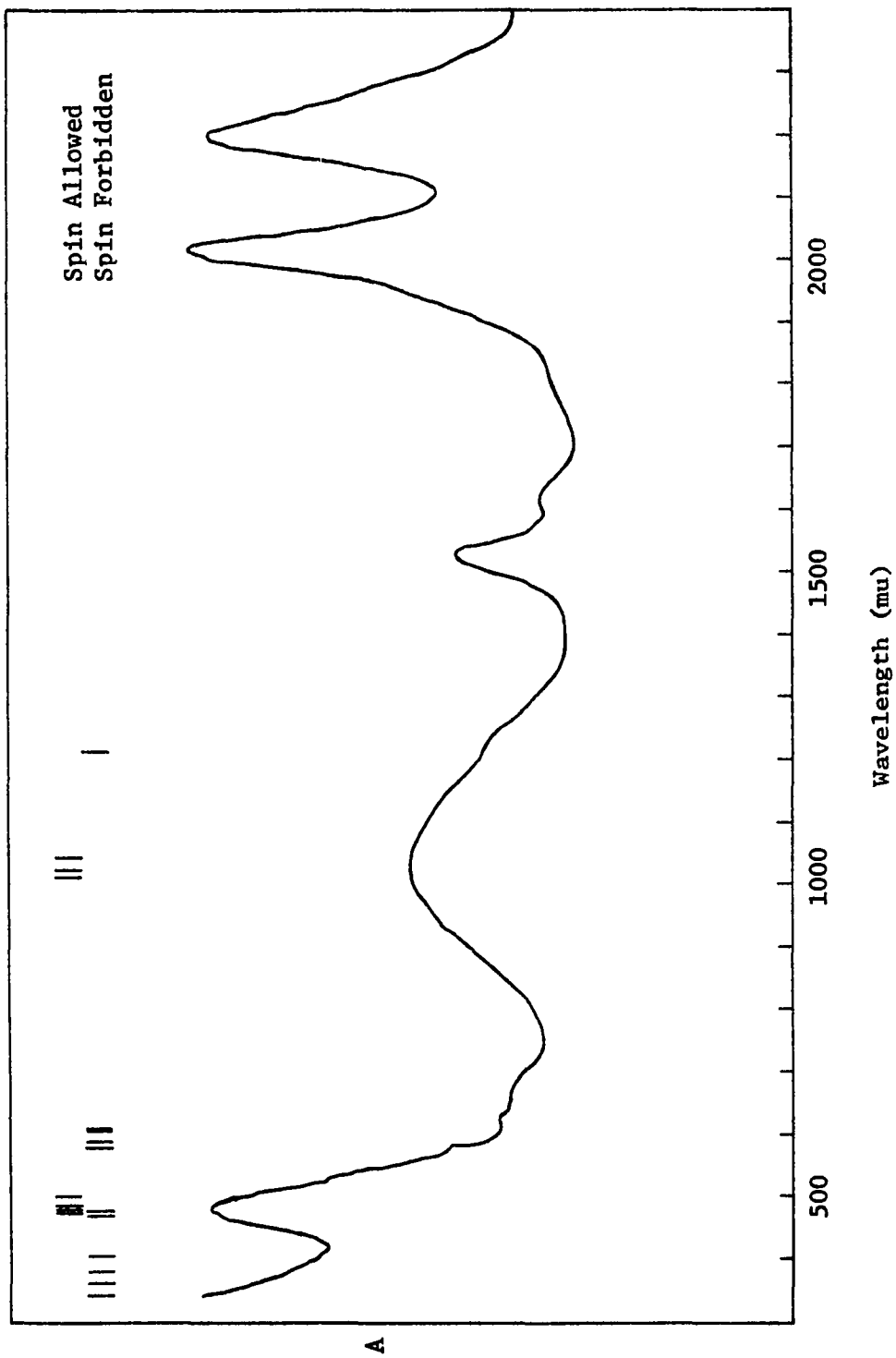

FIGURE 21

$Co(NH_3)_4Cl_2$ Spectrum

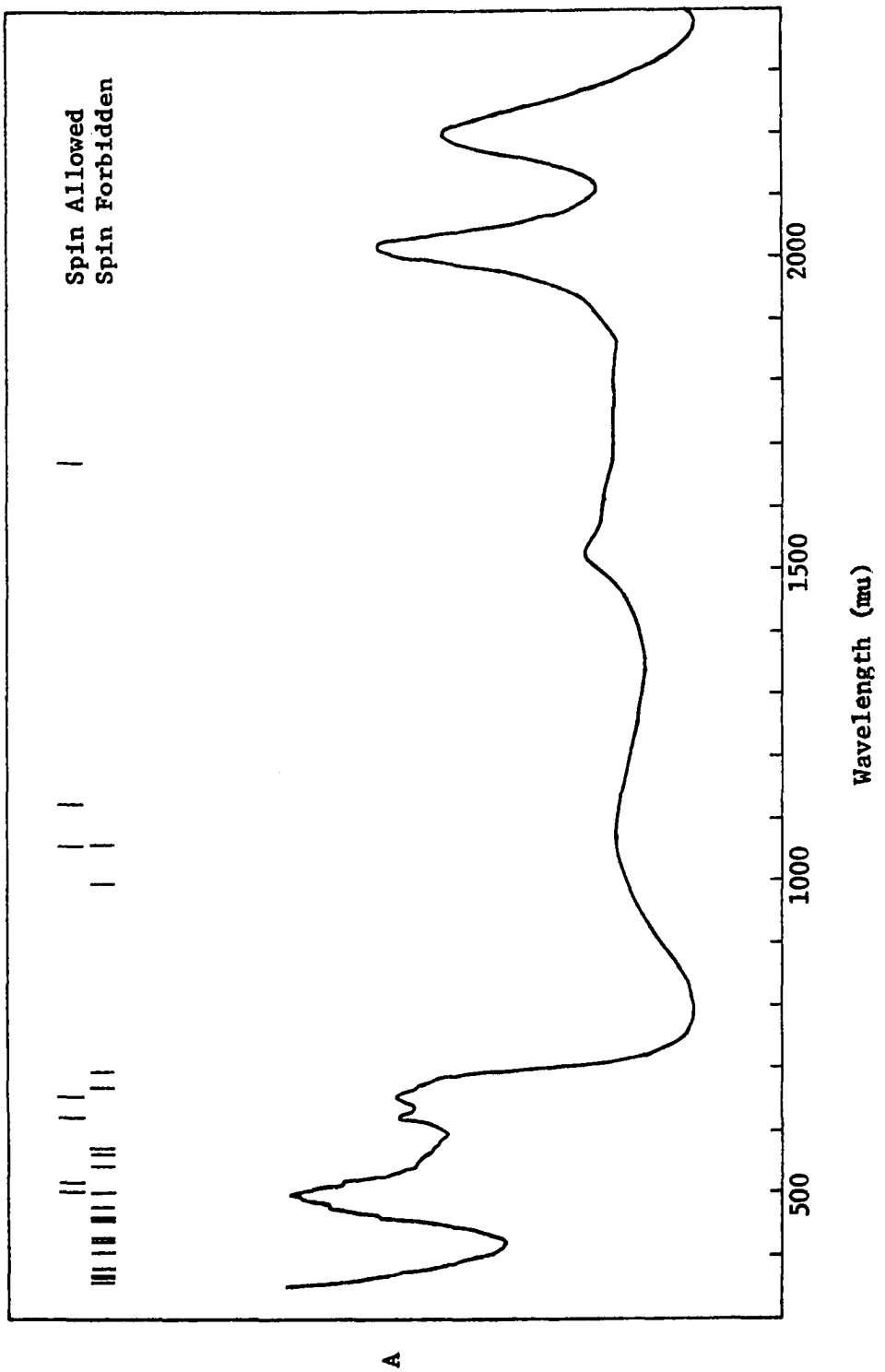

FIGURE 22

β-$Co(NH_3)_2Cl_2$ Spectrum

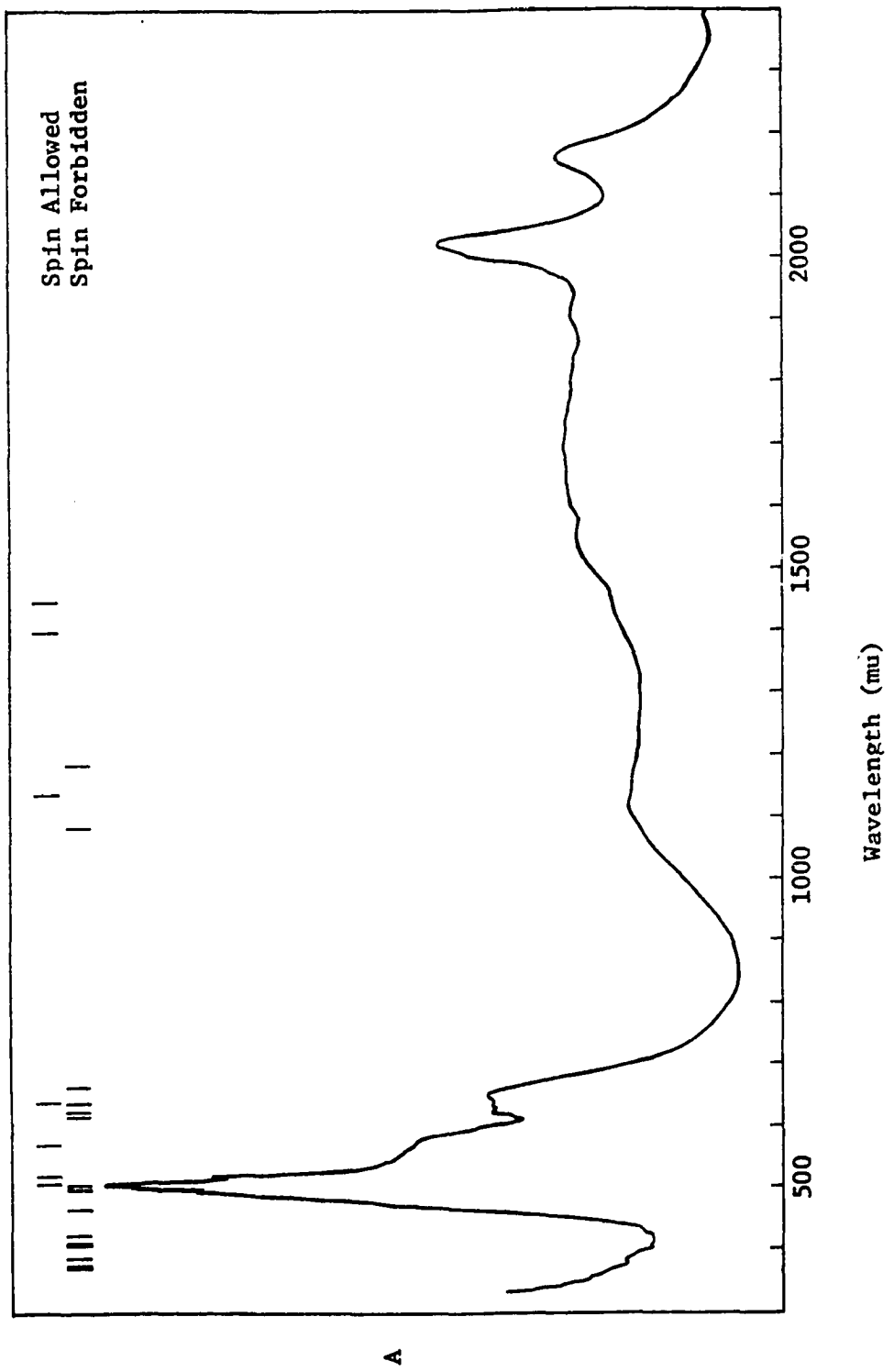

FIGURE 23

α-$Co(NH_3)_2Cl_2$ Spectrum

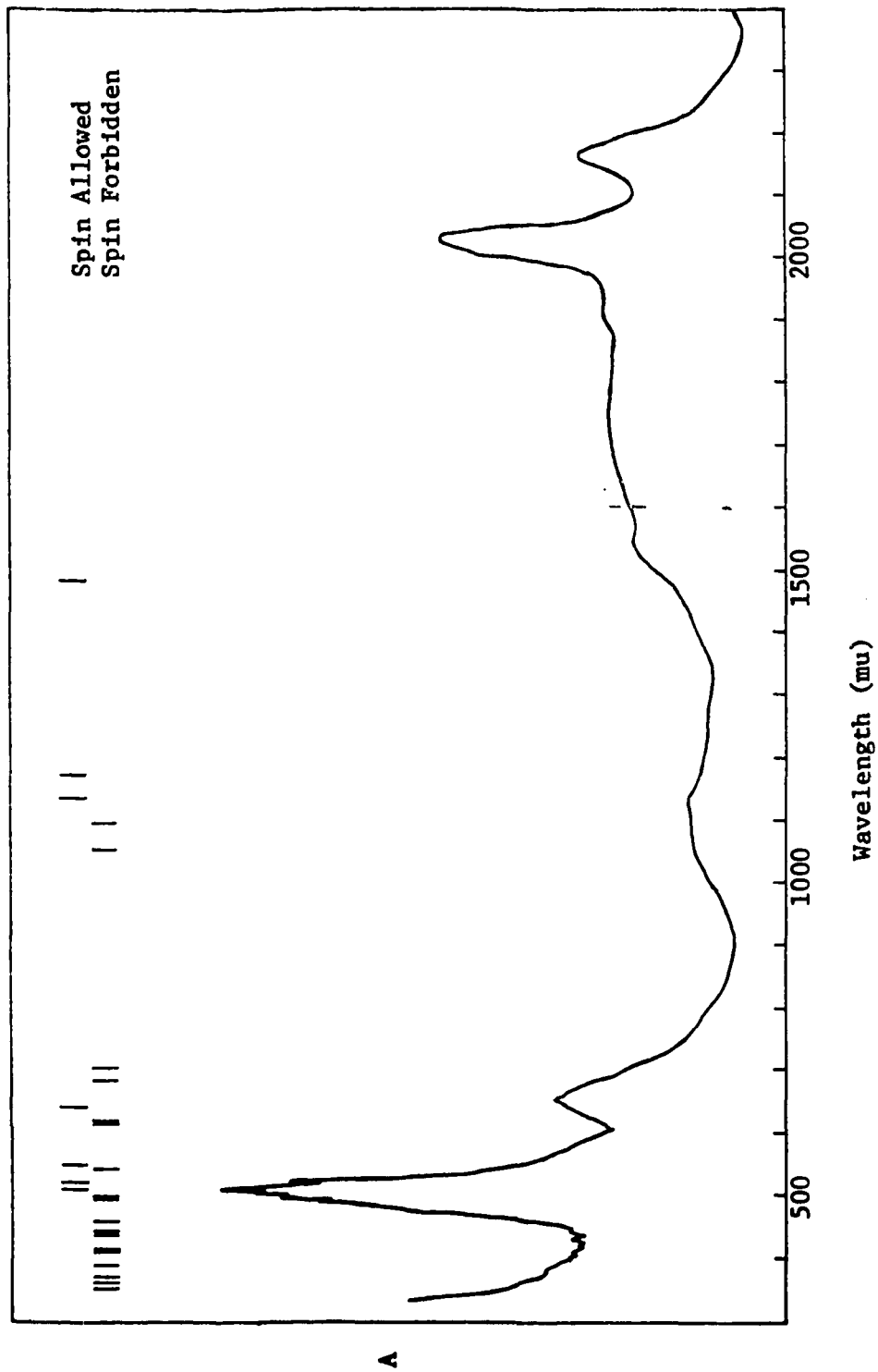

FIGURE 24

$Co(NH_3)Cl_2$ Spectrum

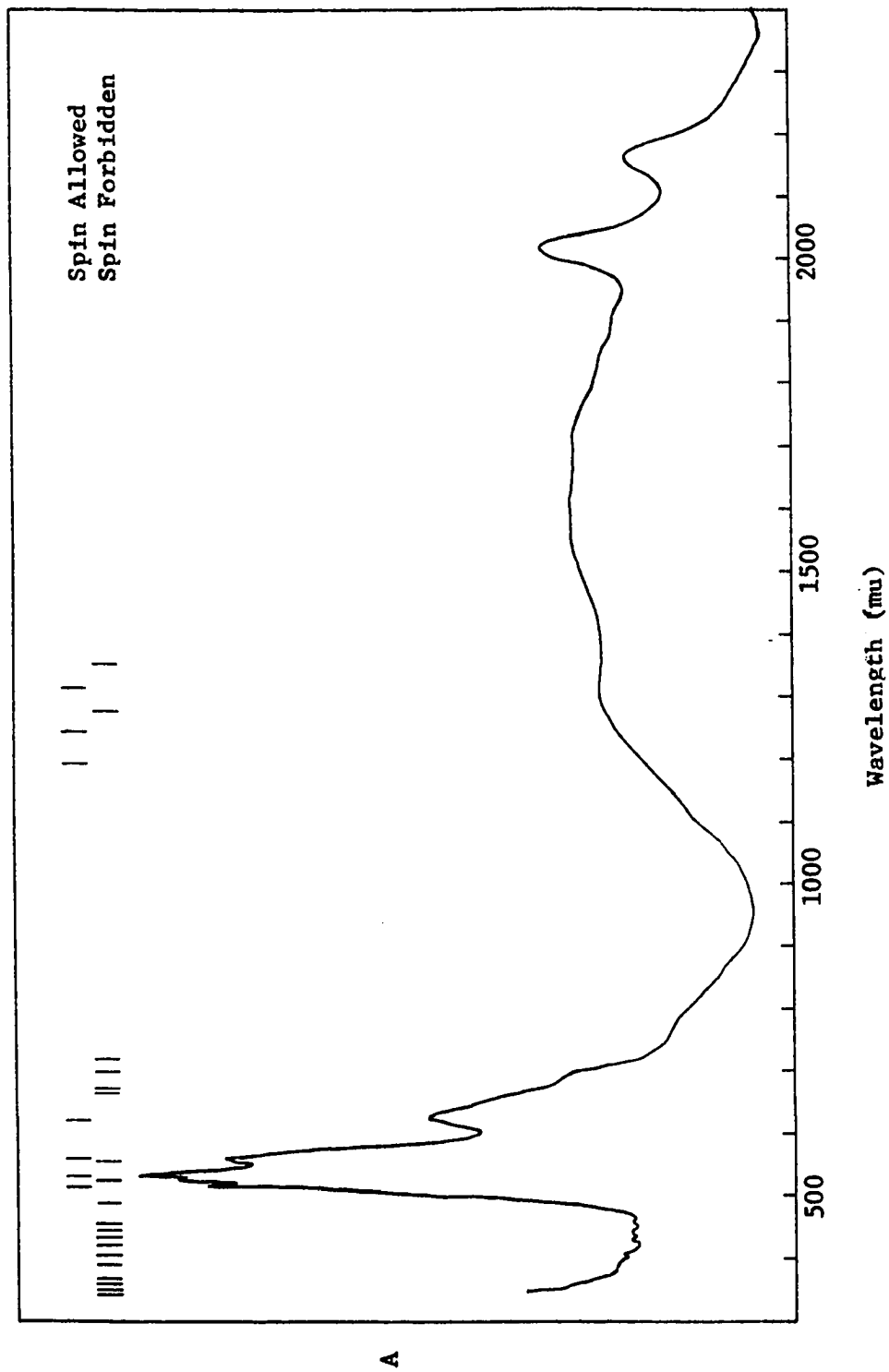

FIGURE 25

$CoCl_2$ Spectrum

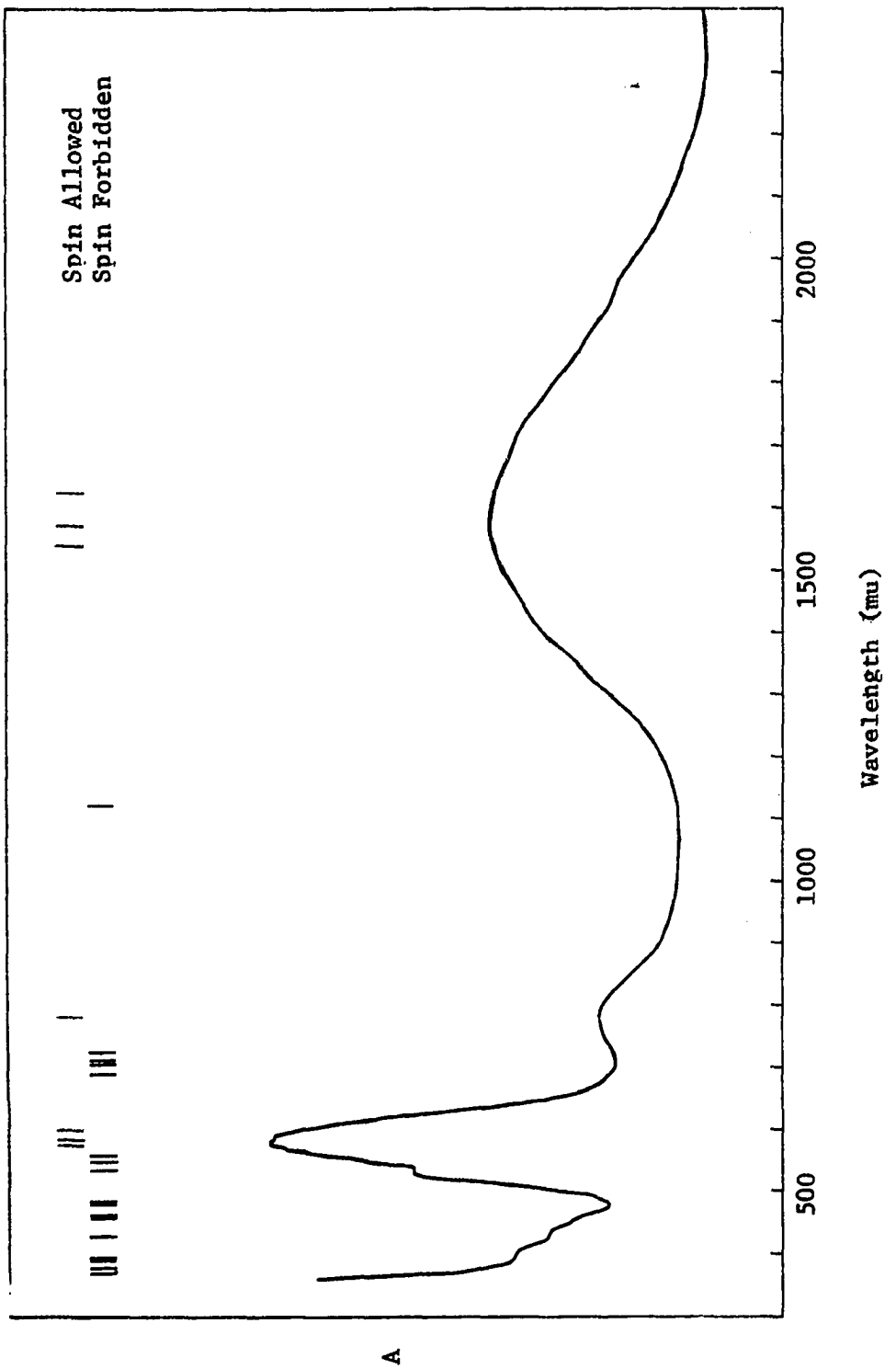

CHAPTER 5

MAGNETIC MOMENTS

Preliminary Discussion

The magnitude of the measured magnetic moments can be very useful in determining the ligand symmetry of the complex compounds. As mentioned in Chapter 4 there are two possibilities for the ground state of d^7 octahedral complexes, i.e., ^2E_g or $^4T_{1g}$. There is also a possibility that the complexes have tetrahedral symmetry with a $^4A_2$ ground state.

For octahedral cobalt(II) complexes the number of unpaired electrons in a ^2E_g ground state (the strong field case) is one, i.e., a "d" orbital configuration, "t_{2g}^6, e_g^1". For the $^4T_{1g}$ ground state, the ligand field splitting is less than the pairing energy and there are three unpaired electrons (the weak field case), i.e., a "d" orbital configuration, "t_{2g}^5, e_g^2".

The number of unpaired electrons is the same in both octahedral and tetrahedral environments for the weak field cases. However, the total magnetic susceptibility is influenced by factors other than the number of unpaired electrons. There is a contribution from excited states which have the same multiplicity as the ground

state. This contribution is brought about by the mixing of these states through spin-orbit coupling. For cobalt(II) this contribution is positive.[73]

There is another possible contribution from the orbital angular momentum of the electrons. For the octahedral weak field case, the "t_{2g}" level contains five electrons, and as a consequence of the lack of symmetry, a net magnetic moment contribution due to the orbital angular momentum results. For the strong field case the "e_g" level contains one electron, but no contribution results since the "d_z2" and the "$d_{x^2-y^2}$" orbitals cannot be transformed into one another. However, for the tetrahedral configuration, both weak and strong field, the arrangement of the electrons is symmetric, i.e., a filled "e" level and a half filled "t_2" level, and as a result would contribute no additional moment from movement about the z axis.

It can be shown that an orbital moment contribution from the ground state exists only when the ground state is a threefold orbitally degenerate term, i.e., "T".[57]

Thus the magnitude of the magnetic moment should indicate whether the complex is octahedral or tetrahedral, weak or strong field, and also yield some knowledge as to the amount of distortion present in the complex.

It can easily be shown how the relative distortion can be obtained from magnetic data. Assuming a complex of octahedral symmetry with the z axis as a basis, a rotation of 90° about this

axis transforms the "d_{xz}" orbital into the equivalent "d_{yz}" orbital. This leads to an orbital momentum contribution. A like rotation of 45° transforms the "$d_{x^2-y^2}$" into the "d_{xy}" orbital, but these orbitals are no longer equivalent due to ligand field splitting. In this manner it can be seen that when a symmetry is low enough so that the "d_{xz}" and "d_{yz}" orbitals likewise have different energies that the orbital moment contribution can be partially or completely suppressed. Thus the more symmetrical octahedral complexes should possess the higher magnetic moments, with the magnetic moments becoming smaller as the amount of distortion increases.

Experimental

Cobalt(II) chloride hexahydrate was further purified by removing the iron and nickel impurities on a cation exchange column of Dowex 50W x 8.50-100 mesh. The middle portion of the solution was recrystalized. The powdered cobalt(II) chloride-ammine complexes were prepared from this purified sample by the method discussed in Chapter 4.

The magnetic susceptibility data were measured on a Faraday type balance which is shown in Figure 26.

The powdered sample was placed in a small quartz bucket (A) which is attached to a quartz spring (B) (Worden Labs) by a long, rigid quartz fibre (C).

The quartz spring is attached to the top of the cylindrical vacuum chamber (D) by means of hooks. The bottom section of the chamber is reduced in size so that it can be encased by a Dewar

FIGURE 26. SCHEMATIC OF FARADAY MAGNETIC BALANCE

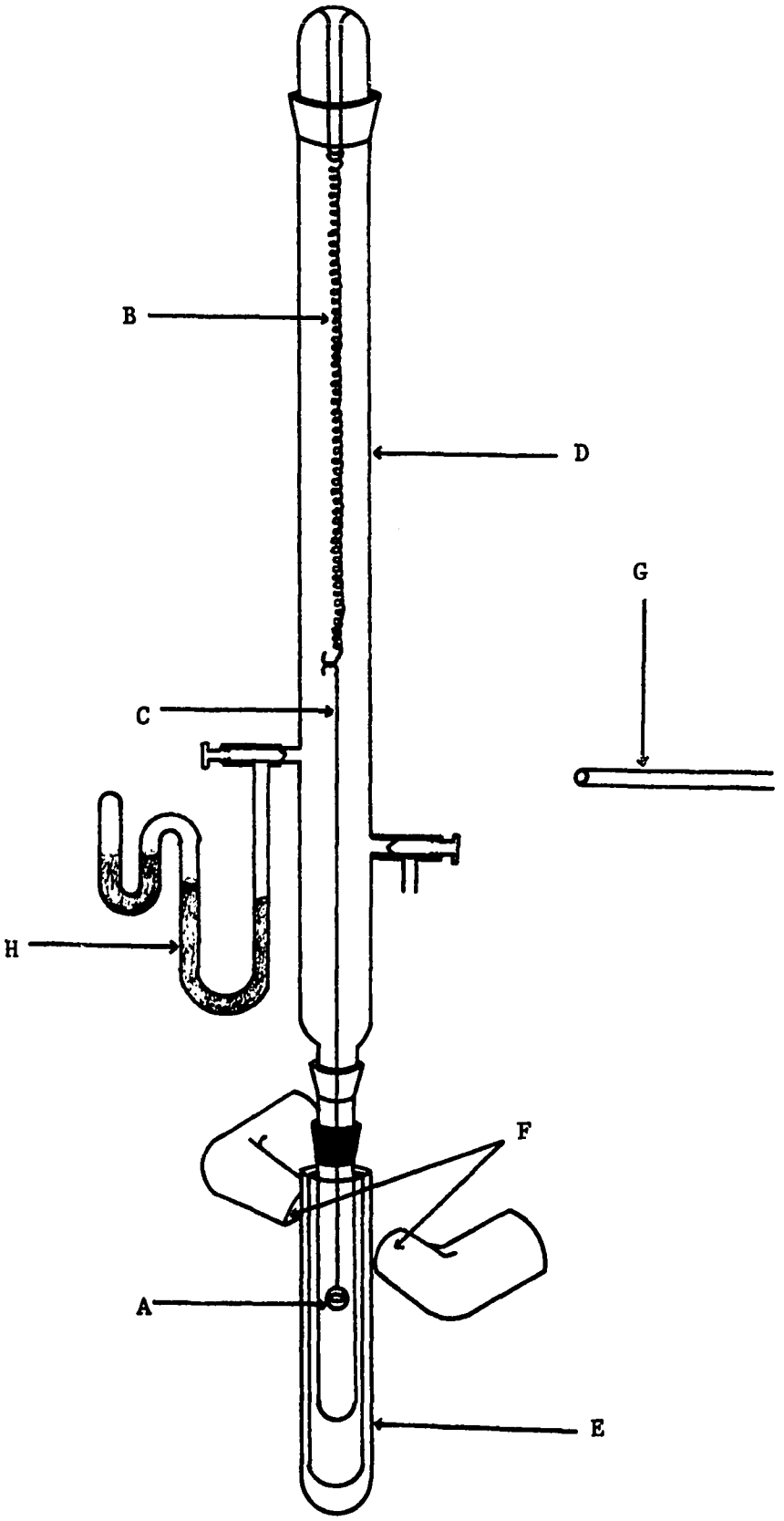

flask (E) in order to control the temperature.

Susceptibility measurements are made by passing a double pole magnet (F) upwards past the sample at a controlled velocity and measuring the total deflection of a crosshair, both up and down, as the sample enters and leaves the magnetic field. A cathetometer (G) is used to measure the deflections. The pole faces of the magnets measure 4.5 cm. in diameter with a pole separation of 5.5 cm. The large pole separation was necessary since the cobalt(II) complexes exhibit a large susceptibility. For a smaller pole separation the mass of the sample was necessarily less than 0.01 grams since a large sample caused the sample bucket to pull into the sides of the tube. This is a definite disadvantage in using this type of balance.

The magnet is moved up or down by use of a reversing switch which operates a screw drive attached to the base of the magnet.

A manometer (H) was attached to the vacuum chamber to allow a measurement of the pressure of the nitrogen gas which was placed in the chamber to insure thermal contact between the sample and walls of the chamber. The manometer is separated from the vacuum chamber by a stopcock.

Two spring constants were determined. One of the constants was employed to measure the mass of the sample in the absence of a magnetic field, and the other was used to determine the susceptibility under the influence of the field.

To determine the spring constant for mass determination,

N.B.S. calibrated weights were used. A spring constant of 5.0768 x 10^{-3} grams/cm. was obtained with an error of ±0.00002 grams within a 99% confidence limit.

The spring constant for determining the magnetic susceptibility was obtained using a substance of known susceptibility. $HgCo(SCN)_4$ was chosen as the standard since it can be prepared to a high grade of purity and has a known molar susceptibility of 16.44 x 10^{-6} c.g.s. units at 20°C with a temperature dependence of -0.05 c.g.s units per degree.[74]

The spring was calibrated magnetically by applying the equations,

$$X_g = Kd/m$$

and

$$X_m = X_g M,$$

where X_g is the gram susceptibility of a compound with a mass of m grams, X_m is the molar susceptibility of a compound with a molecular weight of M, and d is the total deflection of the spring when the magnetic field is passed by the sample, i.e., the deflection due to the paramagnetism of the sample (d_p) and the deflection due to the diamagnetism of the glass bucket (d_d).

From the equations it can be seen that a plot of m versus d will yield a slope of K/X_g and an intercept of d_d on the d axis. This plot is shown in Figure 27. The value of K and d_d were determined to be 8.476 x 10^{-6} and 0.0043 respectively. Thus the gram susceptibility can be calculated by the following equation:

FIGURE 27

d vs. m for $HgCo(SCN)_4$

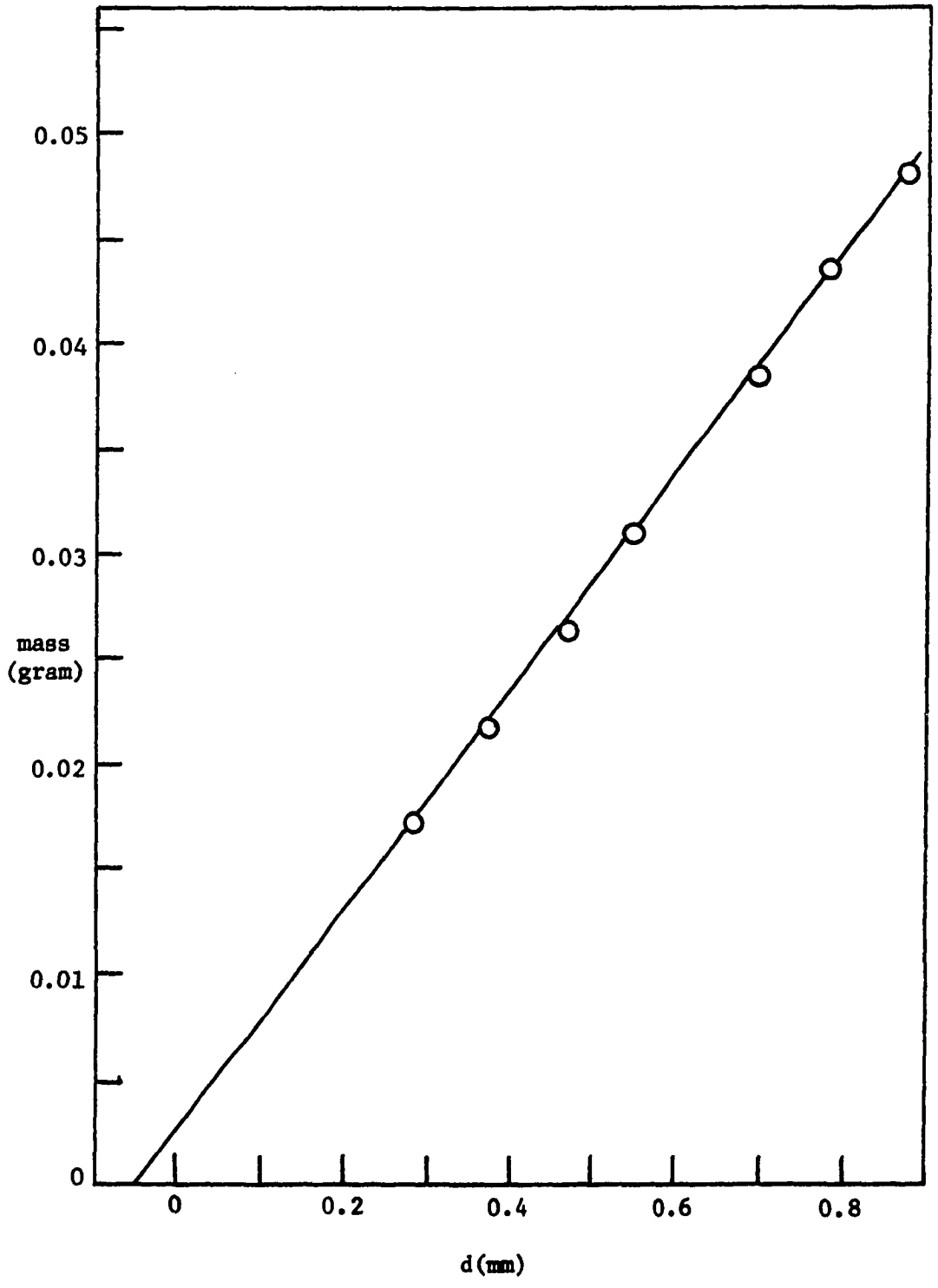

$$X_g = \frac{8.476 \times 10^{-6}}{m} (d + 0.0043).$$

Difficulty was encountered in determining the magnetic constant of the spring due to the accumulation of an electrostatic charge inside the sample chamber and on the quartz bucket. This caused an extraneous deflection to be observed since the bucket was weakly attracted to the walls of the sample chamber. By applying a very thin coat of polyoxyethylene sorbitan monolaurate, Tween 20, (Atlas Powder Co.) to the tube, all observable electrostatic charge was eliminated.

The susceptibility of the cobalt(II) ammine chloride complexes were determined as a function of temperature by the use of temperature baths. The temperatures chosen were: liquid nitrogen (77°A), dry ice-acetone (195°A), ice-water (273°A), room temperature (296°A), and steam-water (373°A).

The temperature at the walls of the sample chamber was measured using a calibrated NBS certified platinum resistance thermometer. The resistance was measured with a Leeds & Northrup resistance bridge and a Honeywell galvanometer. The temperature could not be determined at the same time that the susceptibility measurements were being obtained, but was determined under the same conditions immediately afterward.

Thermal equilibrium of the sample was obtained by placing approximately 3 cm. pressure of nitrogen or ammonia gas into the evacuated chamber and waiting for 3-6 hours depending upon the type

of bath being used. Thermal equilibrium was assumed when the amount of deflection of the sample did not change for at least one hour.

Susceptibility measurements of $Co(NH_3)_6Cl_2$ and $Co(NH_3)_4Cl_2$ were not obtained at steam temperature due to the rapid rate of deammination at this temperature. The measurement of the susceptibility of the hexammine complex at room temperature was accomplished by using ammonia as the thermal equilibrium gas instead of nitrogen. The magnetic susceptibility measured at the steam-water temperature of β-$Co(NH_3)_2Cl_2$ was in error since the conversion temperature of the β to the α isomer was found to be 67°C. The measured susceptibility corresponds to what would be expected from a mixture of the two isomers. Also the measured susceptibility of α-$Co(NH_3)_2Cl_2$ corresponds to that of the β isomer at liquid nitrogen temperature since rapid conversion to the β form occurs at this temperature.

A correction must be made to the molar susceptibility due to the diamagnetism of the cobalt ion and its ligands. This is accomplished by adding the diamagnetic contributions to the experimentally determined X_m. The Pascal[75] constants of interest are: cobalt(II), 13×10^{-6} c.g.s.; chloride, 23×10^{-6} c.g.s.; ammonia, 37×10^{-6} c.g.s. This corrected molar magnetic susceptibility is designated by X_m^c. The data obtained in this manner is shown in Table 29.

Calculations and Evaluations

A law developed by vanVleck[76]:

$$X_m^c = N_o\mu^2/(3kT)$$

where N_o and k have their usual meanings and μ is the moment in Bohr magnetons is the basis for determing the magnetic moment from the susceptibility. It is assumed that the separation between ground state and excited state energy levels is large compared to kT and that the separation of the energy levels within the ground state is small compared to kT.

A similar empirical equation derived by Curie is used to determine the experimentally observed magnetic moment with

$$X_m^c = C_m/T$$

where C_m is the Curie constant.

From the above equation a plot of T versus $1/X_m^c$, Figure 28-33, should yield a straight line with an intercept of zero and a slope of C_m. However, most compounds have magnetic susceptibilities which do not obey the Curie law due to a non-zero intercept. This deviation is considered to be caused by the interaction between neighboring molecular dipoles. For complexes having a non-zero intercept on the T axis X_m^c is represented by the Curie-Weiss law,

$$X_m^c = C_m/(T - \theta),$$

where θ is known as the Weiss constant.

From the above equation it can be seen that a plot of X_m^c versus $1/(T - \theta)$ should yield a straight line with an intercept of zero and a slope of C_m. However, deviations from a zero intercept are often observed. The non-zero intercept is due to temperature independent paramagnetism (T.I.P.). T.I.P. is considered to arise from excited state contributions to the magnetic susceptibility.

TABLE 29

MAGNETIC SUSCEPTIBILITY DATA

Compound	T(°A)	$X_g \times 10^6$ (c.g.s)	$X_m^c \times 10^6$ (c.g.s.)	$1/X_m^c$	$(1/T-\theta)\times 10^3$
$CoCl_2$	372.9	76.45	9,985	100.2	2.820
	296.2	97.02	12,656	79.01	3.604
	273.7	106.53	13,891	71.99	3.922
	198.3	152.66	19,880	50.30	5.568
	77.3	457.59	59,472	16.82	17.065
$Co(NH_3)Cl_2$	372.1	64.66	9,570	104.5	2.715
	294.8	81.45	12,068	83.08	3.436
	271.0	89.11	13,161	75.98	3.742
	195.0	125.7	18,535	53.95	5.230
	77.3	323.4	47,571	21.02	13.610
α-$Co(NH_3)_2Cl_2$	371.9	56.70	9,380	106.6	2.658
	294.9	71.71	11,840	84.45	3.343
	270.8	77.81	12,840	77.88	3.636
	195.0	107.5	17,701	56.49	5.020
β-$Co(NH_3)_2Cl_2$	296.7	65.79	10,791	92.00	3.280
	268.2	72.11	11,910	84.06	3.621
	195.0	98.75	16,187	61.46	4.923
	77.3	234.2	38,493	25.99	11.70

TABLE 29 - Continued

Compound	T(°A)	$X_g \times 10^6$ (c.g.s.)	$X_m^c \times 10^6$ (c.g.s.)	$1/X_m^c$	$(1/T-\theta)\times 10^3$
$Co(NH_3)_4Cl_2$	295.7	52.80	10.569	94.62	3.159
	270.5	57.51	11,401	87.71	3.432
	195.0	78.41	15,639	63.94	4.632
	77.3	170.0	33,749	29.63	10.18
$Co(NH_3)_6Cl_2$	296.5	45.04	10,595	94.48	2.946
	271.1	49.15	11,549	86.59	3.184
	195.0	65.14	15,259	65.54	4.202
	77.3	128.0	29,832	33.52	8.313

FIGURE 28. T°A vs. $1/X_m^c$ for $CoCl_2$

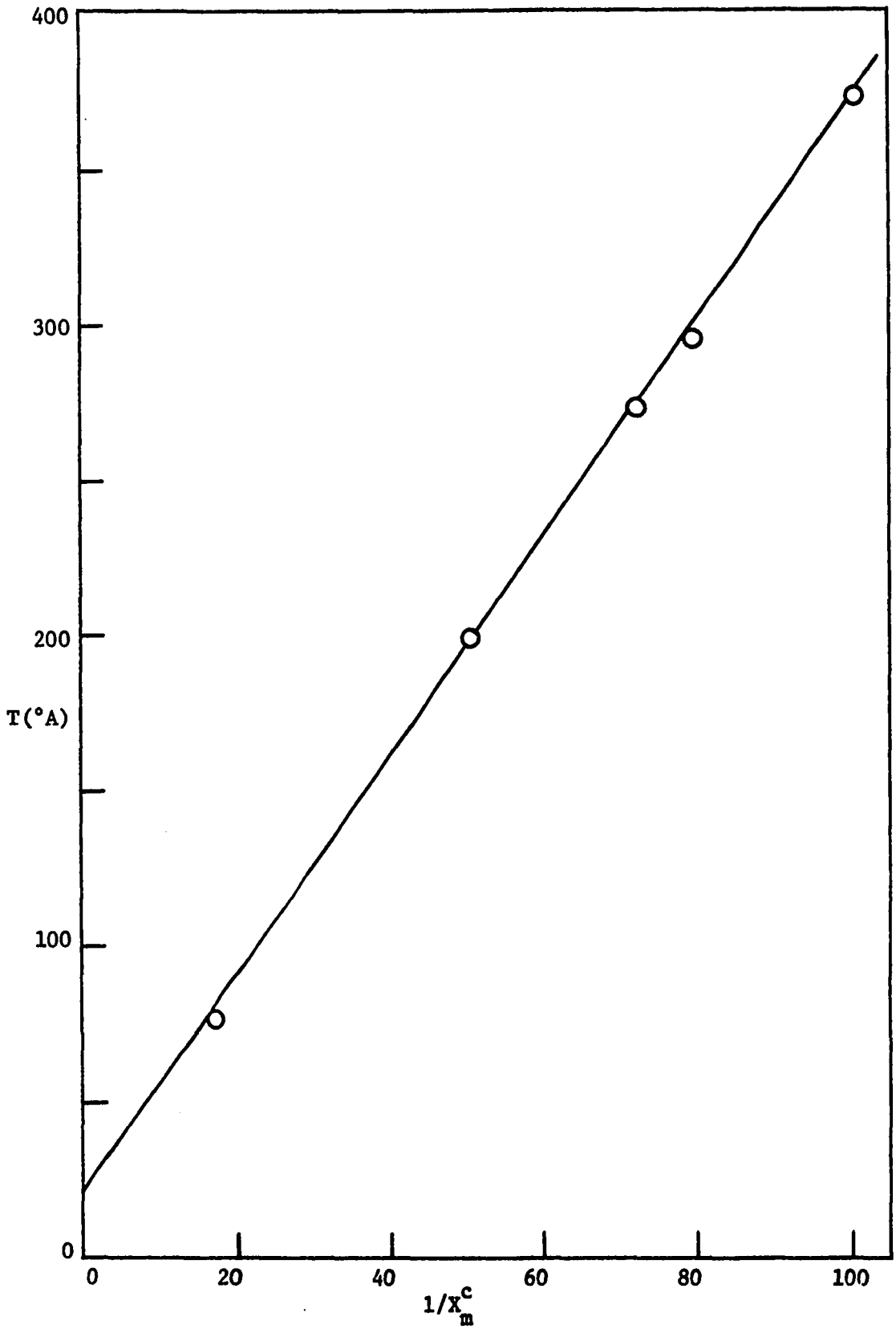

FIGURE 29. T°A vs. $1/X_m^c$ for $Co(NH_3)Cl_2$

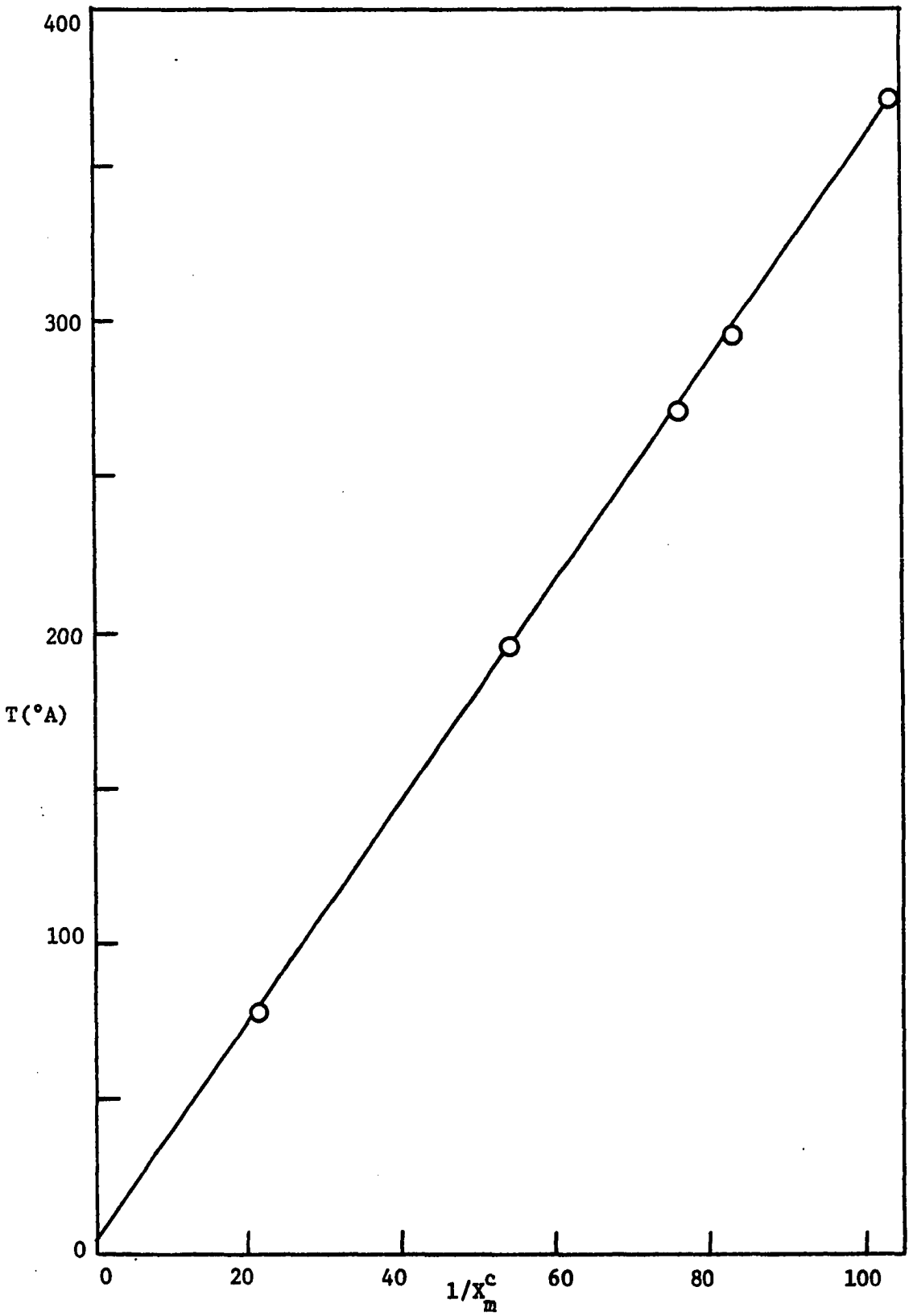

FIGURE 30. T°A vs. $1/X_m^c$ for α-$Co(NH_3)_2Cl_2$

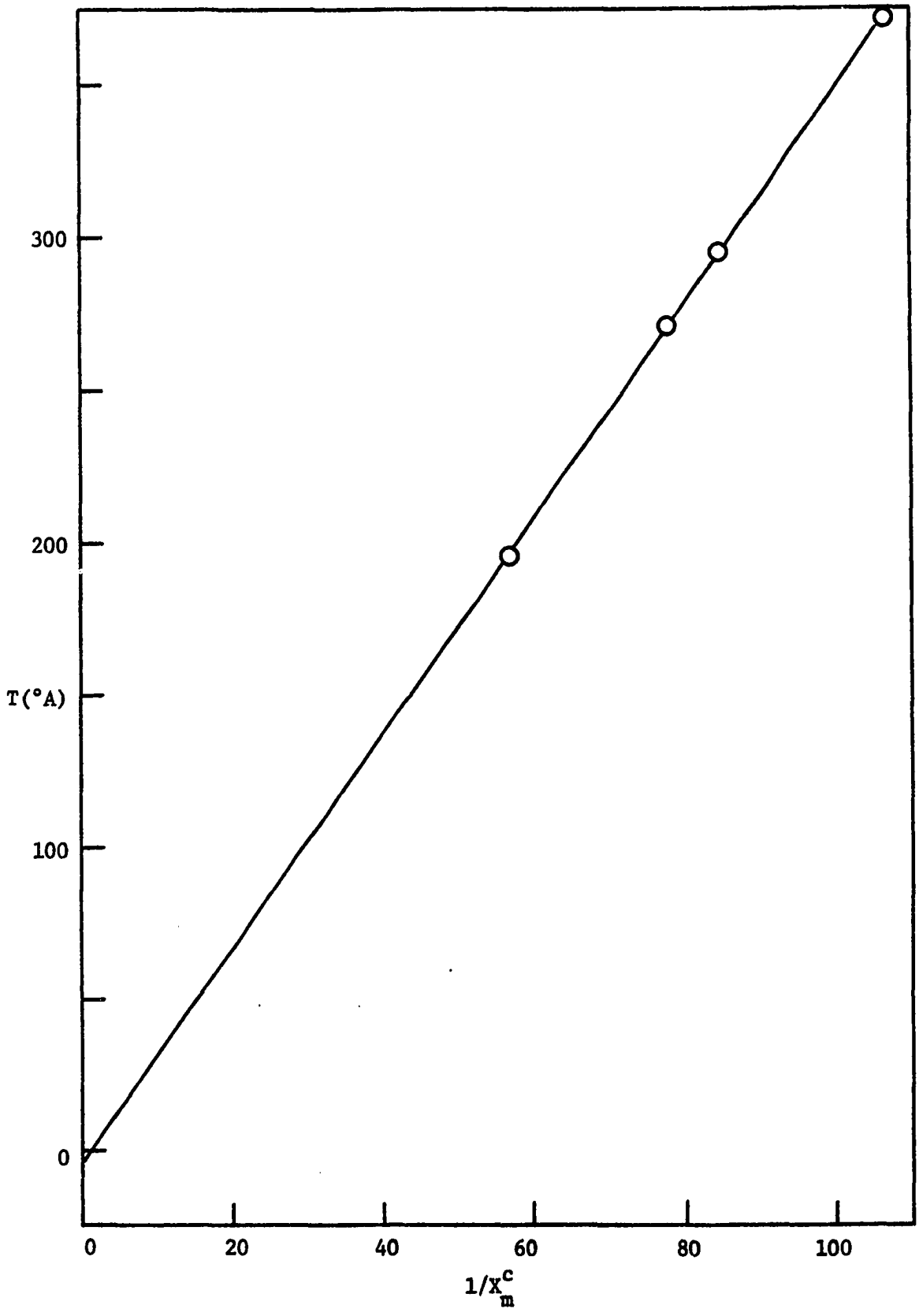

FIGURE 31. T°A vs. $1/X_m^c$ for β-$Co(NH_3)_2Cl_2$

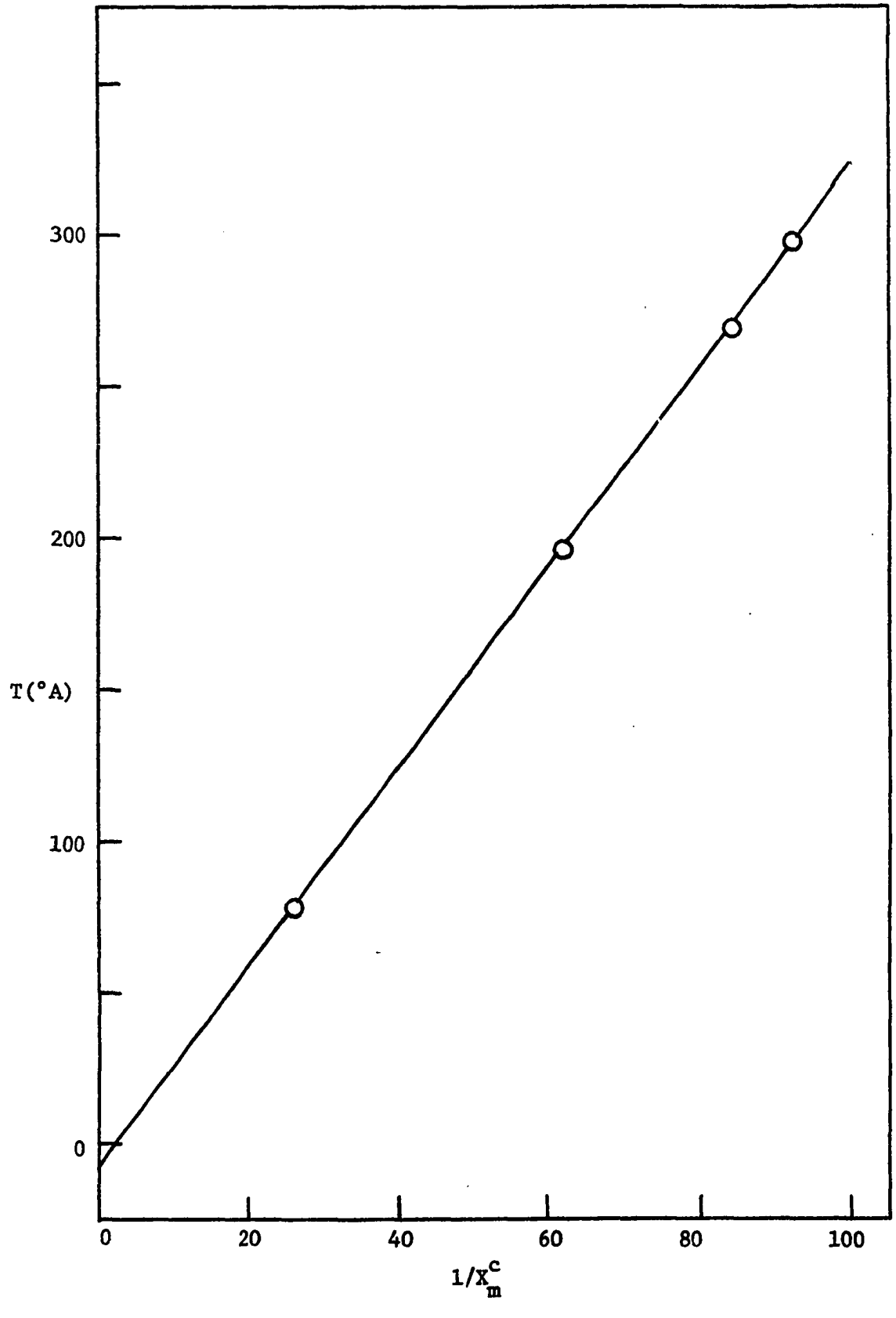

FIGURE 32. T°A vs. $1/X_m^c$ for $Co(NH_3)_4Cl_2$

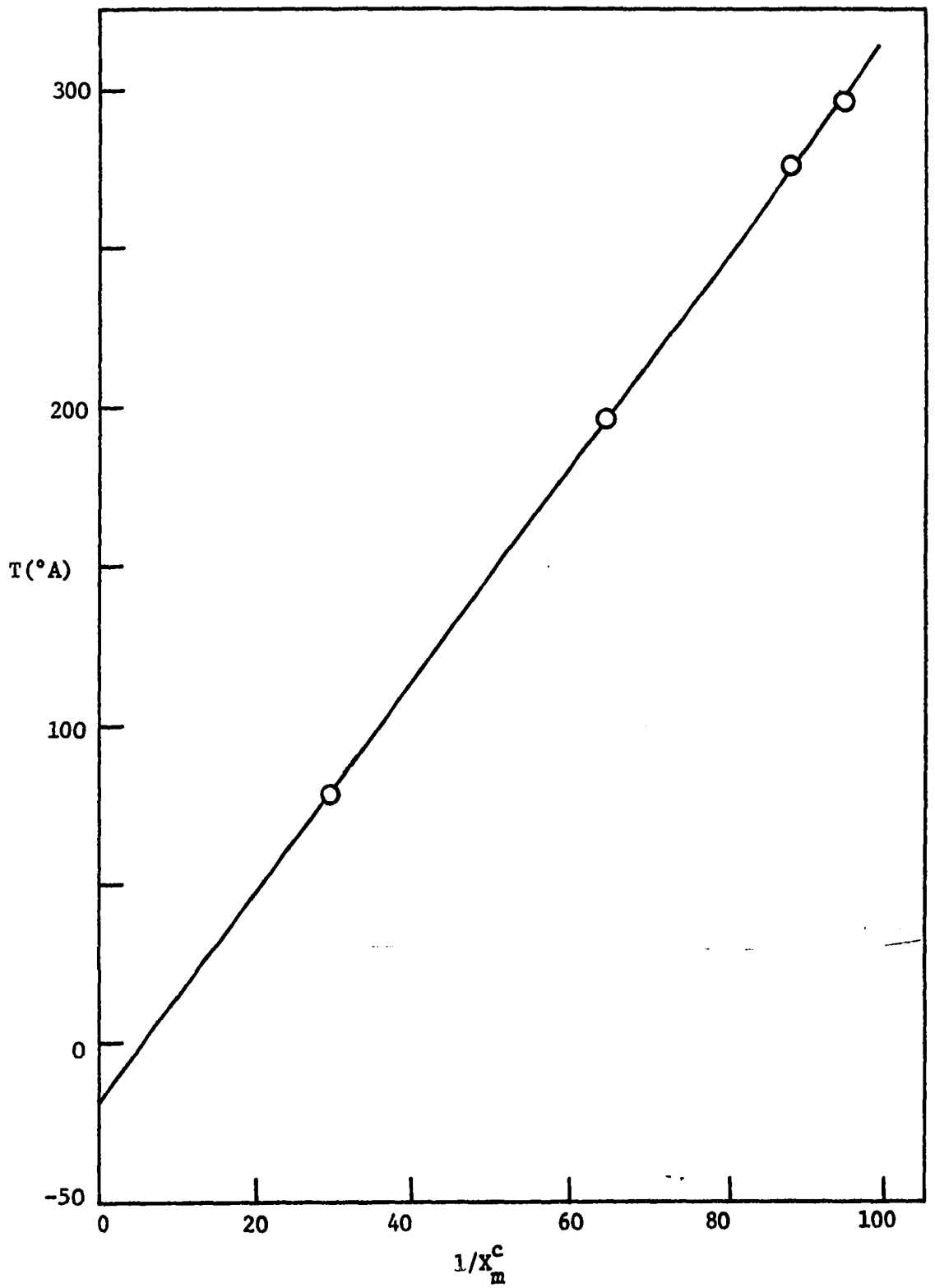

FIGURE 33. T°A vs. $1/X_m^c$ for $Co(NH_3)_6Cl_2$

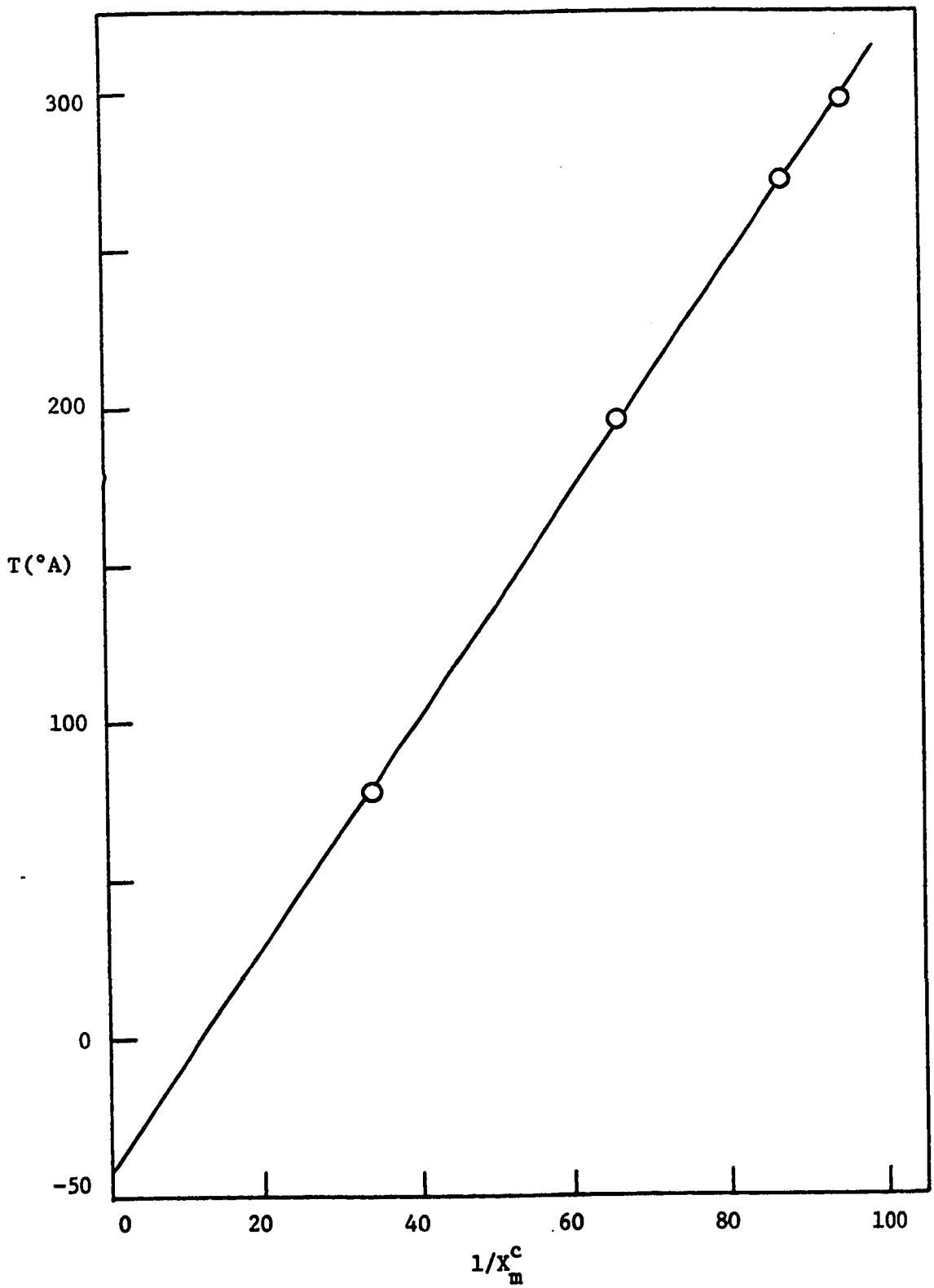

These plots are presented in Figures 34-39. The equation representative of these curves is

$$X_m^c = C_m/(T - \theta) + T.I.P.$$

By setting

$$X_m^c = N_o u^2/3k(T - \theta),$$

combining the two equations and solving for u by substituting for the constants N_o and k the equation becomes:

$$u = 2.84 \sqrt{C_m} \text{ B.M.}$$

The data analyzed in the above manner gave the values of u, θ, and T.I.P. shown in Table 30. All of the straight line plots were analyzed with a least squares program.

The magnetic moment determined for $CoCl_2$ agrees with the value reported by Cotton.[18] This further indicates that the standardization of the balance is correct.

The magnetic moments of $Co(NH_3)Cl_2$ and α-$Co(NH_3)_2Cl_2$ indicate highly symmetric complexes since they are of the same magnitude as the moment of $CoCl_2$. The value of 5.37 determined for $Co(NH_3)_6Cl_2$ indicates that the species is even more symmetric than cobalt(II) chloride.

The magnetic moments of β-$Co(NH_3)_2Cl_2$ and $Co(NH_3)_4Cl_2$ are lower than the others. This indicates a lower symmetry than D_{4h}.

FIGURE 34. X_m^c vs. 1/T-θ for $CoCl_2$

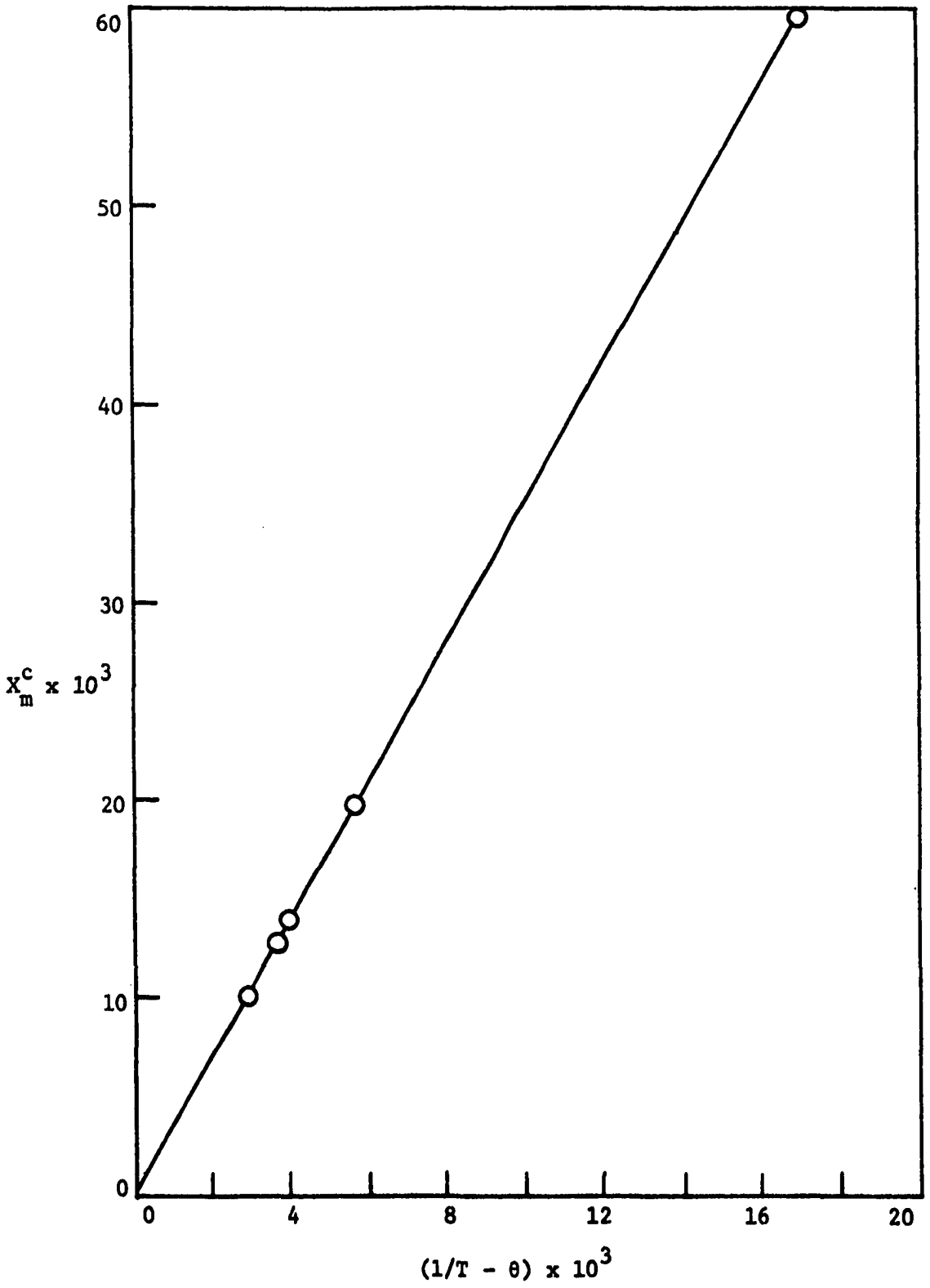

FIGURE 35. X_m^c vs. $1/T-\theta$ for $Co(NH_3)Cl_2$

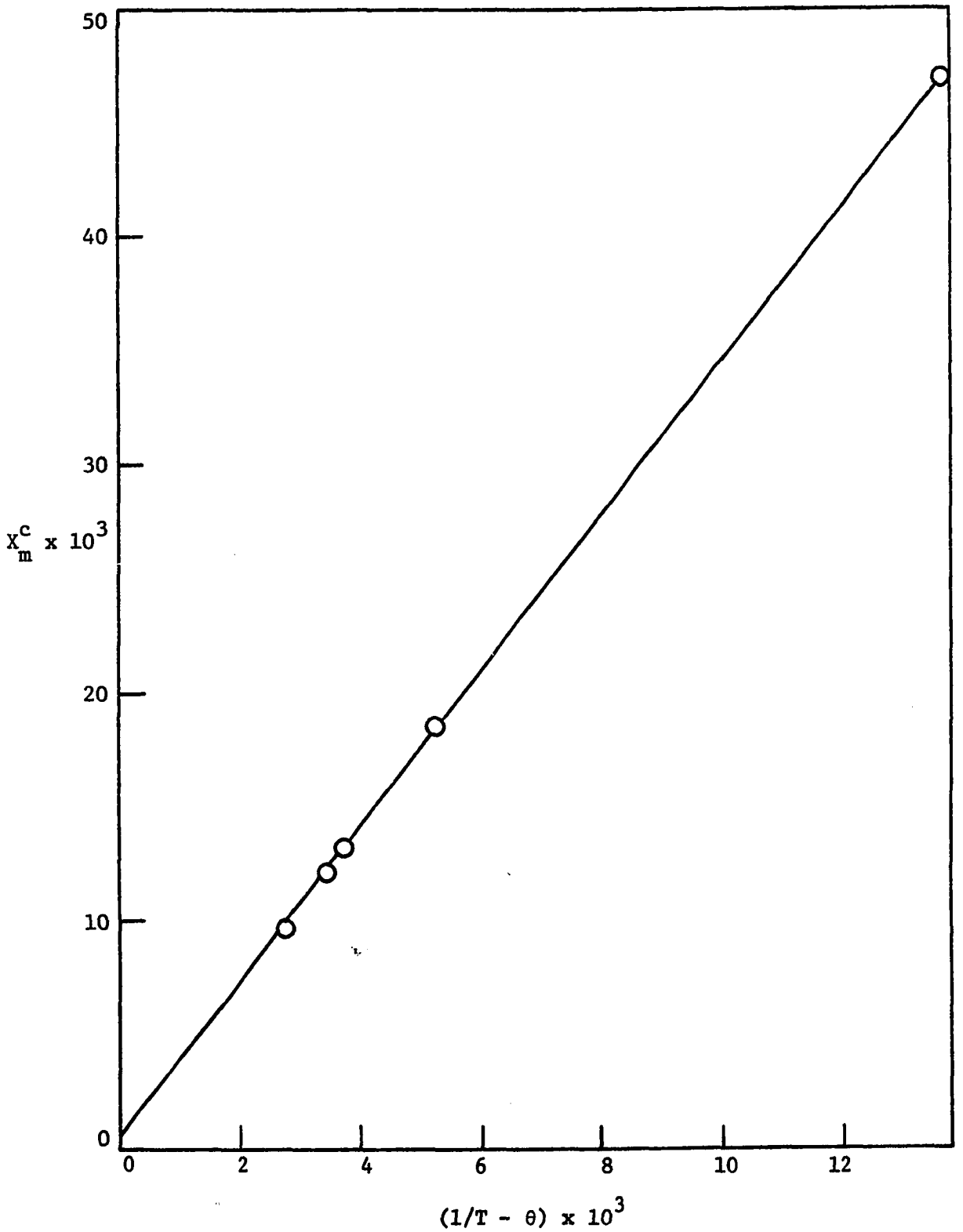

FIGURE 36. X_m^c vs. 1/T-θ for α-$Co(NH_3)_2Cl_2$

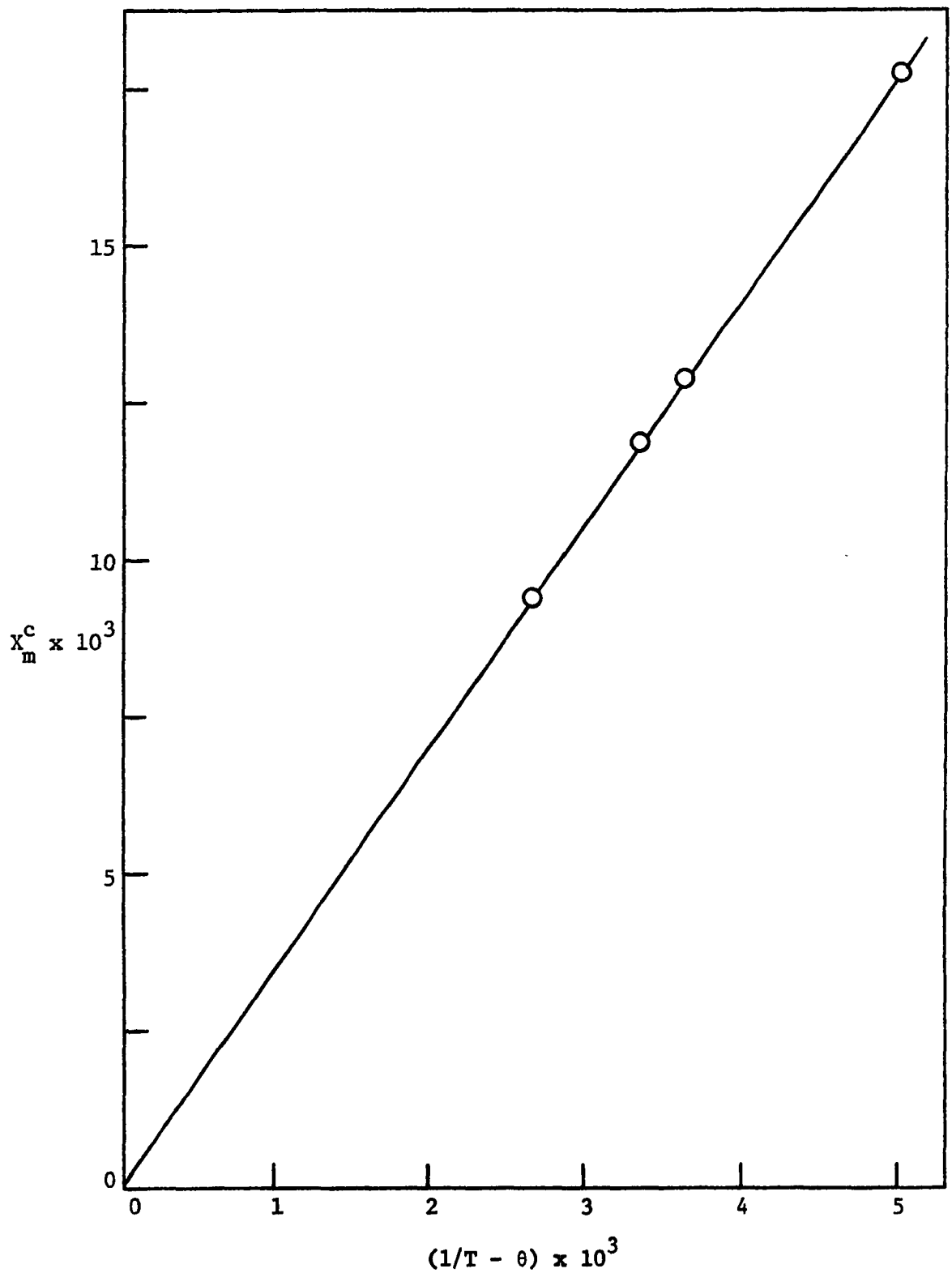

FIGURE 37. X_m^c vs. 1/T-θ for β-$Co(NH_3)_2Cl_2$

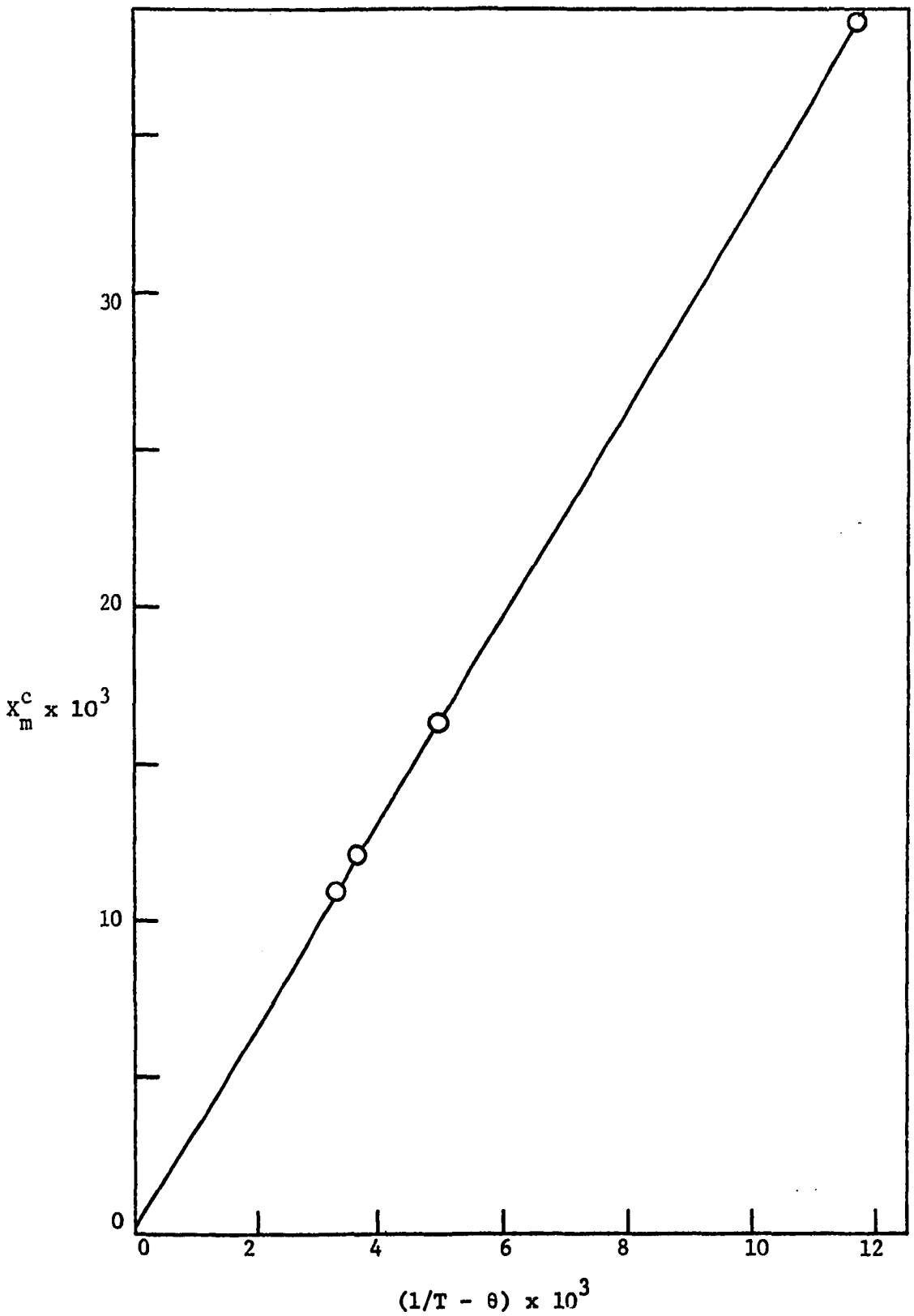

FIGURE 38. X_m^c vs. 1/T-θ for $Co(NH_3)_4Cl_2$

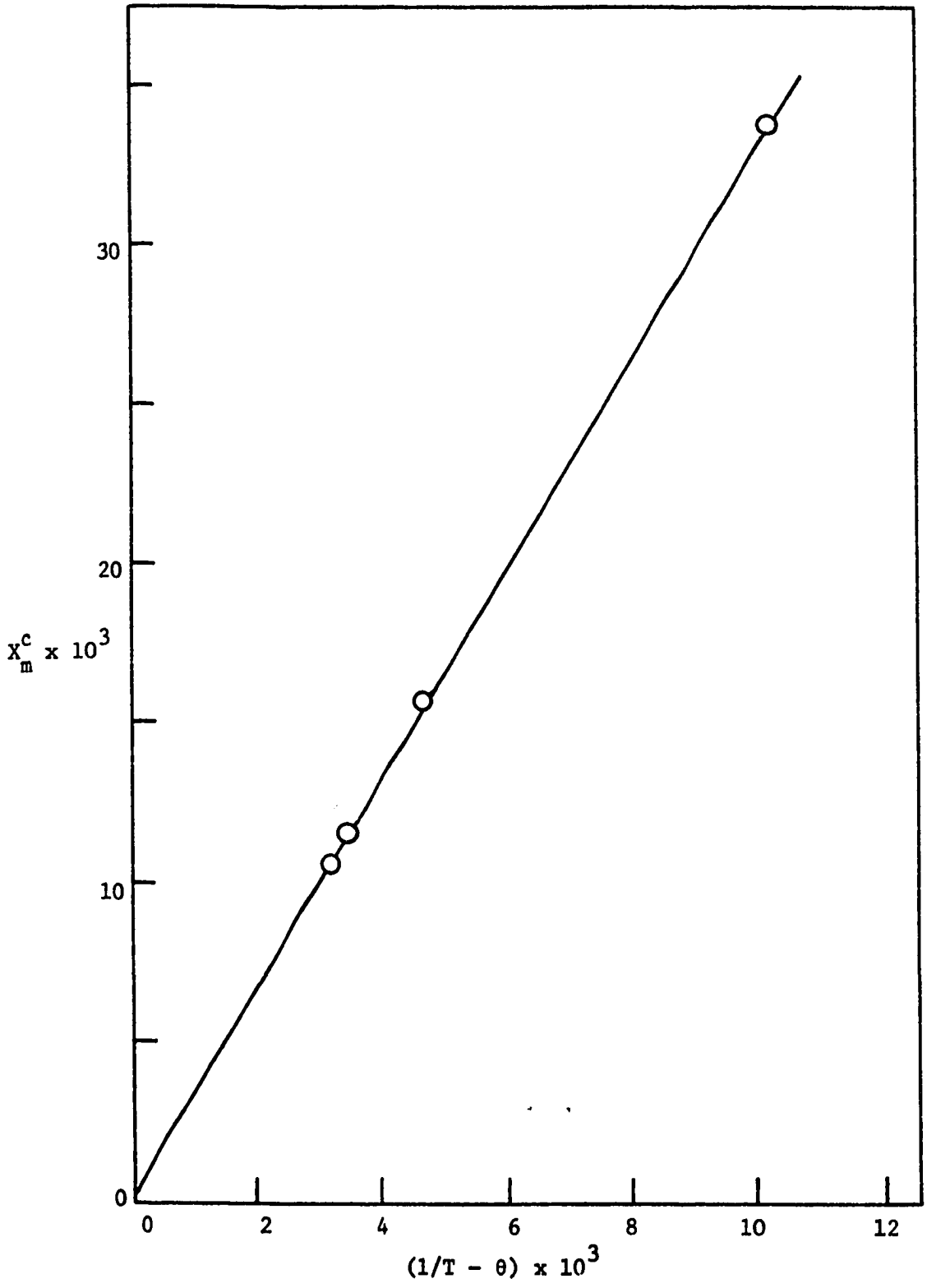

FIGURE 39. X_m^c vs. 1/T-θ for $Co(NH_3)_6Cl_2$

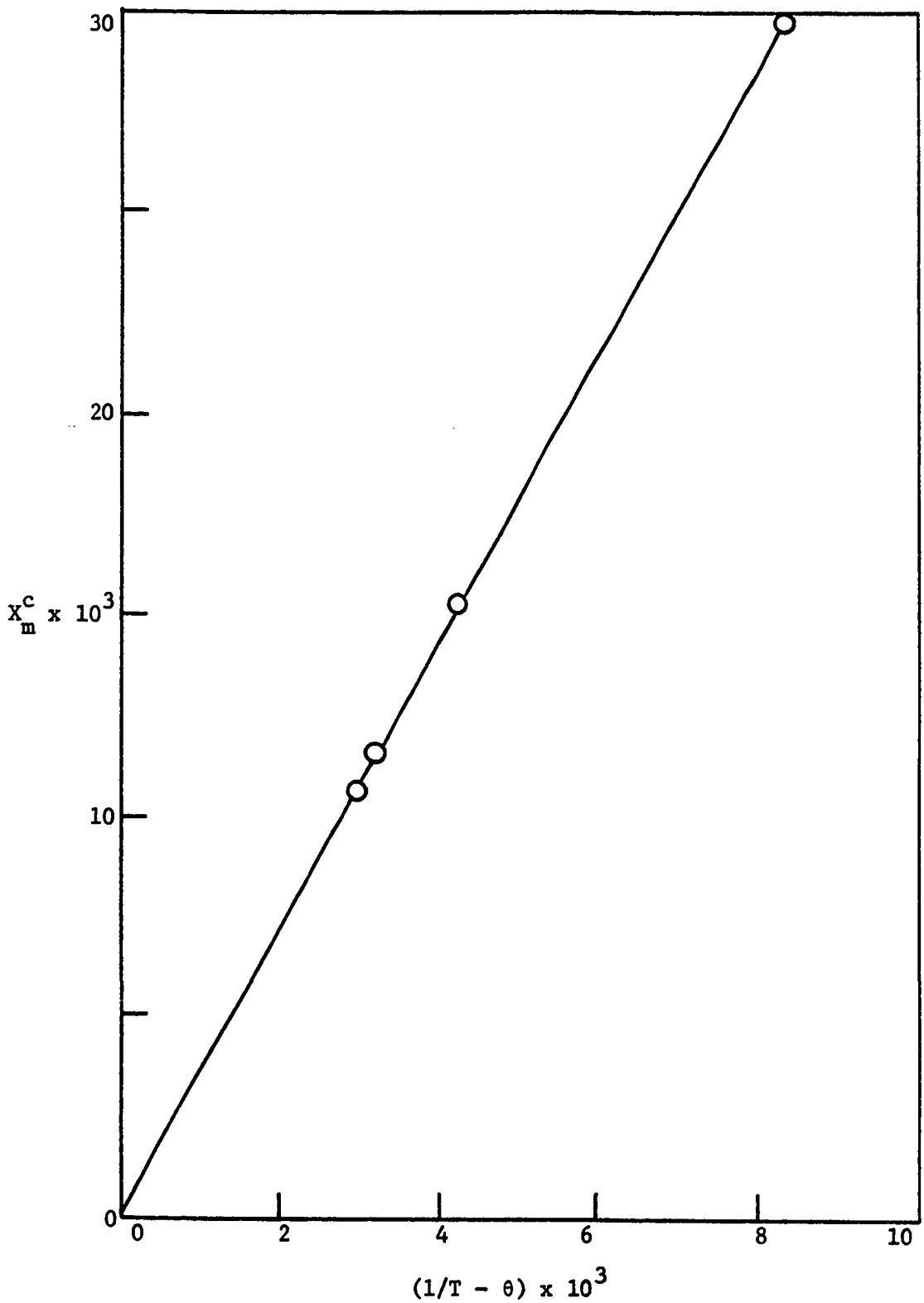

TABLE 30

MAGNETIC DATA SUMMARY

Compound	μ(B.M.) Exp.	μ(B.M.) Lit.*	θ(°A) Exp.	θ(°A) Lit.	T.I.P. x 10^6 (c.g.s)
$CoCl_2$	5.29	5.29(18) 5.38(78)	18.7	38(18) -10(78)	282
$Co(NH_3)Cl_2$	5.30		3.8		143
α-$Co(NH_3)_2Cl_2$	5.31	5.50(20) 5.50(79)	-11.5		51
β-$Co(NH_3)_2Cl_2$	5.14	5.41(20)	- 8.2		45
$Co(NH_3)_4Cl_2$	5.16		-20.9		182
$Co(NH_3)_6Cl_2$	5.37	4.96(20) 5.25(79) 5.29(80)	-43.0		157

* These values obtained from the literature are for the most part room temperature determinations.

CHAPTER 6

CONCLUSIONS AND DISCUSSIONS

The crystal structures of $Co(NH_3)_6Cl_2$ and $CoCl_2$ have been determined by x-ray analysis, thus the symmetry of these compounds is known. From this information and the experimental evidence in the preceeding chapters, the unknown symmetry of the intermediate ammine complexes can be deduced. A correlation between the spectral, magnetic, and thermodynamic properties of the cobalt(II) chloride ammine complexes is also obtained.

From the x-ray analysis it is known that the hexammine complex of highest stability has a regular octahedral (O_h) symmetry with six ammonia molecules in the inner coordination sphere. Spectral evidence supports this structure since no splitting is observed in the absorption bands. The high magnetic moment of 5.37 B.M. further substantiates this symmetric structure.

Two values of ΔH_f, 22.95 Kcal/mole and 8.69 Kcal/mole, were obtained for the reaction, $CoCl_2 \cdot 6NH_3 = CoCl_2 \cdot 4NH_3 + 2NH_3$. The small value of ΔH_f is consistent with the conversion of the hexammine to an equilibrium mixture of $[Co(NH_3)_4Cl_2](NH_3)_2$ (A) and $Co(NH_3)_4Cl_2$. Complex (A) has four ammonia molecules and two chloride

ions in the inner coordination sphere. The formation of a species of this structure is not surprising since both water[4] and pyridine[5] form stable complexes of this type with cobalt(II) chloride.

Spectral and magnetic data could not be obtained to substantiate the existence of compound (A) due to its instability.

Two molecular symmetries are possible for octahedral $Co(NH_3)_4Cl_2$. This could be the reason for the difference in color found for this blue complex and the dirty-white color found by Clark, et al.[9] With two chlorides located trans to one another on the z axis and four ammonia molecules in the xy plane, the coordination sphere would possess D_{4h} symmetry, or D_{2h} if a rhombic distortion of the ammonia molecules exists. If instead the two chlorides are located cis to one another, the symmetry will be C_{2v} or lower.

For the reasons stated below, it is suggested that the tetrammine complex is of lower symmetry than D_{4h}, and thus the cis configuration is indicated.

The spectra of $Co(NH_3)_4Cl_2$ indicates a species of low symmetry and/or a large distortion when compared to the spectra of the hexammine.

If the compound is the trans isomer, under D_{4h} symmetry, a ground state of $^4A_{2g}$ is expected. From the spectrochemical series, ammonia is a stronger ligand than chloride, therefore, creating a stronger crystal field in the xy plane than along the z axis. The best fit for the spectra assuming this ground state was obtained with Dq = 700 cm^{-1} and B = 590 cm^{-1}. This value of B is smaller than the

values ordinarily obtained for cobalt(II) compounds.

The correlation between D_{4h} and D_{2h} is given in Table 20. The Fortran program for D_{4h} can be used to fit the spectra for D_{2h} symmetry by using an additional splitting parameter for the loss of degeneracy of the E_g state. The spectra of the tetrammine could not be fit assuming this symmetry.

Assuming a ^4E_g ground state, the fit presented in Table 27 was obtained with Dq = 930 cm^{-1} and B = 730 cm^{-1}. These values are in the region expected for this complex. There exists two explanations for fitting the spectra with a ^4E_g ground state.

If the compound is the cis isomer, a pseudo D_{4h} symmetry is assumed and the ground state is ^4E_g. The basis of assuming D_{4h} symmetry for a cis complex which actually possesses C_{2v} symmetry or less is that the field in the xy plane is averaged. This is discussed by Ballhausen.[6] From Table 20 it is seen that the overall effect in going from D_{4h} to C_{2v} symmetry is the loss of degeneracy of the E state. Spin-orbit coupling also accounts for a splitting of the ^4E_g states, therefore, unless the spectra is fit using the actual symmetry of the complex the value obtained for the spin-orbit coupling parameter is meaningless, and no faith can be placed in the parameter except for fitting purposes.

The other explanation for $Co(NH_3)_4Cl_2$ possessing a ^4E_g ground state is to assume that the complex is trans with D_{4h} symmetry, but the crystal field created by the chlorides on the z axis is increased due to π bonding with the cobalt. Interactions of this nature have been used by Fogel, et al.,[4] and Yatsumirskii[8] to explain the spectra of $Co(H_2O)_4Cl_2$ and $Co(NH_3)_4(H_2O)_2Cl_2$ respectively.

The thermodynamic data does not determine which of the two isomers is obtained, however, the magnetic moment of 5.16 B.M. for the tetrammine is significantly lower than the 5.37 B.M. obtained for the hexammine.

A complex of lower symmetry than D_{4h} removes the degeneracy of the d_{xz} and d_{yz} orbitals thus reducing the orbital contribution. The lower magnetic moment supports the cis configuration for the tetrammine.

Two isomeric forms of the diammine complex were isolated. The low temperature, β, species is blue, and the high temperature, α, complex is red. The enthalpy of transition was obtained from vapor pressure data and was found to be 11.6 Kcal/mole.

Magnetic moments of the complexes and the spectra prove that both of the isomers are octahedral. Two different configurations are possible, one cis, the other trans. Thermodynamic data does not allow one to assign a structure to either of the isomers. Likewise the spectra of both complexes can be fit assuming D_{4h} symmetry with either a $^4A_{2g}$ or ^4E_g ground state. The trans complex is expected to possess D_{4h} symmetry with z axis compression, and the cis isomer should possess C_{2v} symmetry or pseudo D_{4h} symmetry with z axis elongation.

The magnetic moments of the two isomers differ by 0.17 B.M. The blue species has a magnetic moment very nearly the same as the tetrammine indicating that they are similar in structure. The red complex has a moment similar to the monoammine and cobalt(II) chloride also indicating species of like structure. Also since the degeneracy of the d_{xz} and d_{yz} orbitals is removed for C_{2v} symmetry, therefore,

reducing the orbital angular momentum contribution, the cis configuration is assigned to the blue complex which has the lower magnetic moment. This assignment is in disagreement with Biltz,[27] however, there are other factors which support the assignment of this complex as the cis isomer.

Assuming a pseudo D_{4h} symmetry for the cis complex, the distortion obtained in fitting the spectra should be lower for the cis complex than the trans complex. This effect is discussed by Ballhausen.[6] This is indeed the case for the above assignment as can be seen from Table 27.

The relative spectral intensity of a cis complex should be higher than a trans complex due to a loss of the center of symmetry under C_{2v}. Since the intensity of a reflectance spectra is dependent upon the particle size and packing of the sample, the intensities of the crystal field bands cannot be related unless an absorption band exists in both spectra which is independent of the structure of the two isomers. The intensity of the ammonia overtone bands in the near IR should be equivalent in the two species since both contain the same number of ammonia molecules per complex.

Equating the respective overtone bands in the two spectra one is able to obtain a relative intensity correlation between the spectra of the two complexes. From the spectra of Figure 22 and 23, the bands of the red isomer are noticeably more intense, thus further supporting this as the cis complex.

The monoammine species was fitted assuming a D_{4h} symmetry

and a ^4E_g ground state, and averaging the field strength along the z axis. The distortion obtained for this fitting is essentially one-half that obtained for the fitting of the trans-diammine complex. This is to be expected since the monoammine complex has one ammonia ligand and one chloride on the z axis while the trans-diammine possesses two ammonia ligands on the z axis, and both have four chloride ligands in the xy plane.

The magnetic moments of trans-diamminecobalt(II) chloride, and cobalt(II) chloride are very nearly the same indicating species of like structure.

The spectra obtained for $CoCl_2$ was similar to that reported by Ferguson.[31] The fit obtained yields a somewhat different evaluation of the fitting parameters. This can be attributed to the fact that he assumed fixed B and C/B values.

The magnetic moment (5.29 B.M.) is the same as that reported by Cotton.[18]

The exact crystal structure of the intermediate ammines cannot be determined and a question still exists as to the actual site symmetry of $Co(NH_3)_4Cl_2$.

A more exact fitting of the spectra would require crystal spectra which would show more detail and yield information concerning the polarization and vibronic states. Until crystals of the complexes can be grown, this fitting must suffice.

All of the spectra could be fitted without considering π bonding between the metal and the chloride ligands. Using similar

techniques Fogel[4] has been unable to fit the spectra of some of the corresponding aquo complexes assuming the expected ground state under D_{4h} symmetry. However, by inverting the states arising from the octahedral $^4T_{1g}(F)$ ground state a good fit is obtained. This inversion is explained by π bonding between the metal and water ligand. Since the spectra of the ammine complexes can be fitted without inversion of the ground state, π bonding in the aquo complex is supported.

PART II

CRYSTAL FIELD TREATMENT OF COPPER(I) CHLORIDE

CHAPTER 1

CRYSTAL FIELD TREATMENT OF COPPER(I) CHLORIDE

Introduction

No reference could be found in the literature where the absorption spectra of a central metal ion possessing a completely filled "d" subshell is treated using crystal field methods. However, charge transfer spectra have been used to determine the crystal field splitting of the "d" orbitals for ions containing no "d" electrons.[84,85]

Crystal field absorption bands arise when a set of degenerate orbitals splits into two or more nondegenerate levels under the influence of a system of ligands, thus allowing electronic transitions from a lower energy orbital to an unfilled higher orbital of the same subshell.

For a "d" subshell containing ten electrons, even though the orbitals are split under the influence of a ligand field, no d→d transitions are possible because all of the "d" orbitals are filled. However, transitions to unfilled subshells of higher energy are possible, which would leave the "d" shell partially filled.

From the free ion spectra for copper(I)[81], one finds that

the energy difference between the ground state, ^1S, and the first two excited states, ^1D and ^3D, is in the high energy visible and near ultraviolet region of the spectrum. Thus one should observe absorption bands in this region which could be assigned to these transitions.

Preparation

Copper(I) chloride was prepared from copper(II) chloride by the method of Keller and Wycoff[82] with a few modifications.

An aqueous solution of copper(II) chloride was reacted with sufficient sodium sulfite to reduce the copper(II) to copper(I). The white precipitate was transferred to the apparatus shown in Figure 40. The apparatus (A) was previously flushed with dry nitrogen which was passed from (B) to (C) while transferring the precipitate. The flow of nitrogen was reversed and the precipitate was washed successively with glacial acetic acid, absolute ethanol, and finally with anhydrous ether by way of dropping funnel (D). The cuprous chloride was collected on the fritted glass disc (E) and the wash solutions stopped in trap (F). The nitrogen flow was again reversed and the flow was continued for 30 minutes while the cuprous chloride was heated in a water bath. The product was transferred from the apparatus to an air tight storage bottle in a dry bag flushed with dry nitrogen.

This method of preparation yielded a very fine white powder which showed no traces of color due to copper(II).

FIGURE 40

APPARATUS FOR PREPARATION OF CuCl

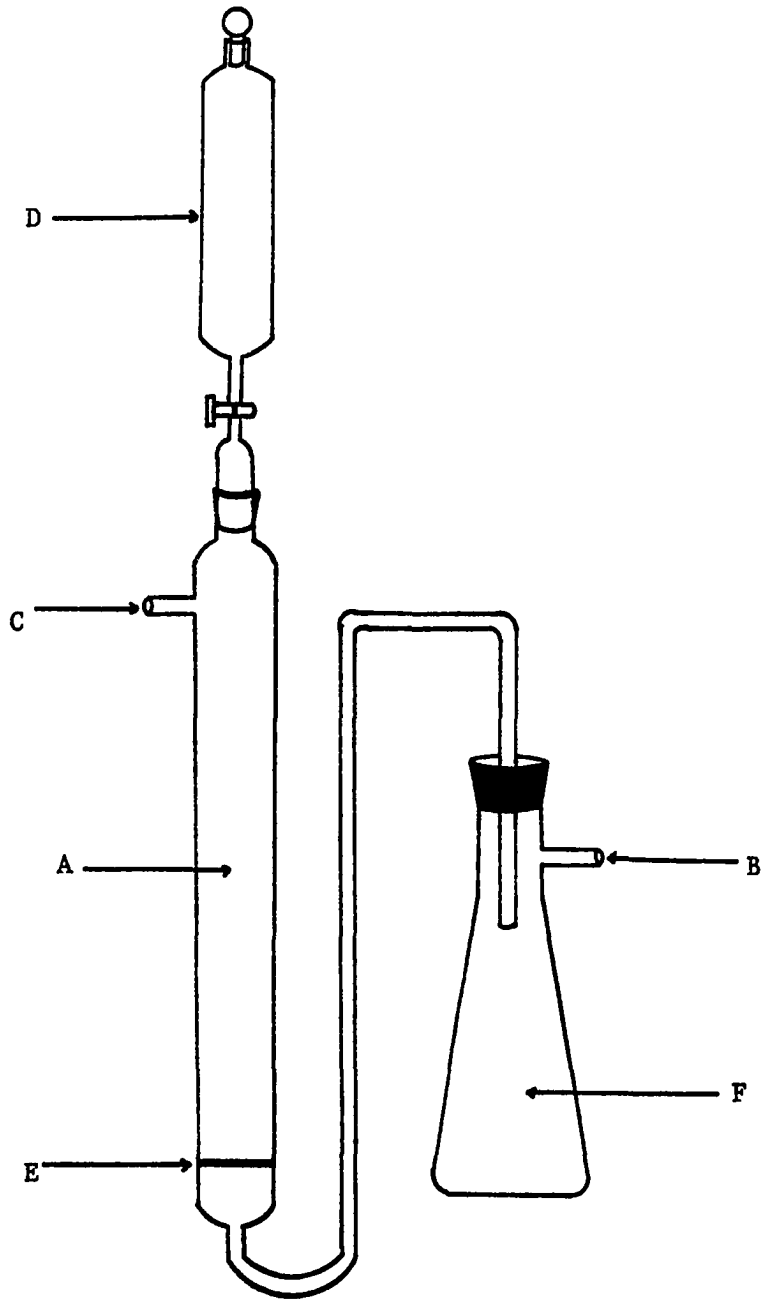

Experimental

The spectra of cuprous chloride was obtained by reflectance methods on a Beckman DK-1 Spectrophotometer in the same manner as discussed in Section 1, Chapter 4 of this dissertation. The measured cuprous chloride spectra is presented in Figure 41. No absorbance was found at energies lower than 600 mu., therefore, this lower energy portion of the spectra is omitted.

Theory

Copper(I) chloride is known to have tetrahedral symmetry[34]. There is a slight tetragonal distortion corresponding to a compression along the z-axis.[87]

Under the influence of the tetrahedral field the 3d orbitals of the copper(I) ion split into two levels, a two fold degenerate "e" level lying lowest in energy, and a three fold degenerate "t_2" level at higher energy.

The electron transmitted from the "d" orbitals can be excited from either of the two levels, thus producing four absorption bands. Two of these transitions are spin allowed being from the ^1S ground state to the ^1D excited state, and the other two are spin forbidden transitions with the electron changing spin in going from the ground state to the ^3D excited state. A transition from the "t_2" level yields both a $^1T_2$ and a $^3T_2$ state, and a transition from the "e" level produces a ^1E and a ^3E state with the T_2 states lying lowest in energy. Thus the D states will each split into a T_2 and an E state. This same splitting can also be derived from group theory.

FIGURE 41. VISIBLE AND NEAR U-V SPECTRA OF CuCl

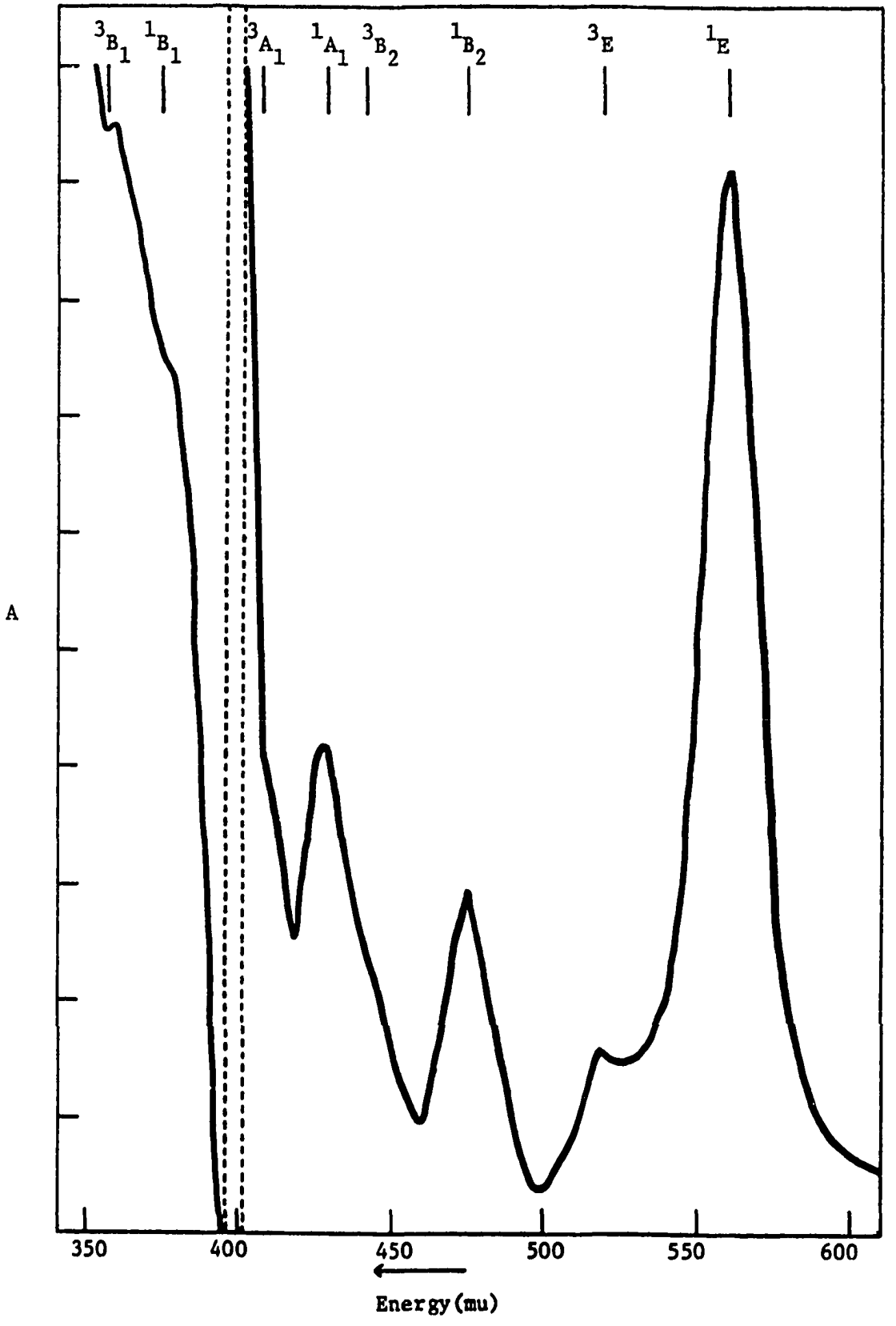

The energy difference between the $^1T_2$ and ^1E states is the same as the splitting of the "d" orbitals due to the tetrahedral field, or 10 Dq. Likewise the energy difference between the two triplet states should also be 10 Dq.

Under tetragonal distortion the T_2 states will split into an E and a B_2 state, and the E states will split into an A_1 and a B_1 state, with the E and the A_1 states lying the lowest in energy of the two pairs.[83]

The energy level diagram showing the successive splitting of the free ion states by the crystal field and tetragonal distortion is given in Figure 42.

Spectra Fitting and Calculations

From the spectra in Figure 41 the more intense bands are assigned to the four spin allowed transitions, and the much lower intense bands which occur as shoulders are assigned to the spin forbidden bands.

By making these assignments and considering the splitting due to tetragonal distortion as given by Ballhausen,[6] the values of Ds, Dt, and Dq can be calculated. The energy of each of the states in terms of these parameters is given in Table 31.

The energy of the states as a function of the free ion is neglected since the energies under consideration are the splittings of the excited states. Crystal field calculations are usually concerned with the relative position of the excited states with respect to the ground state.

FIGURE 42. ENERGY LEVEL DIAGRAM FOR CuCl

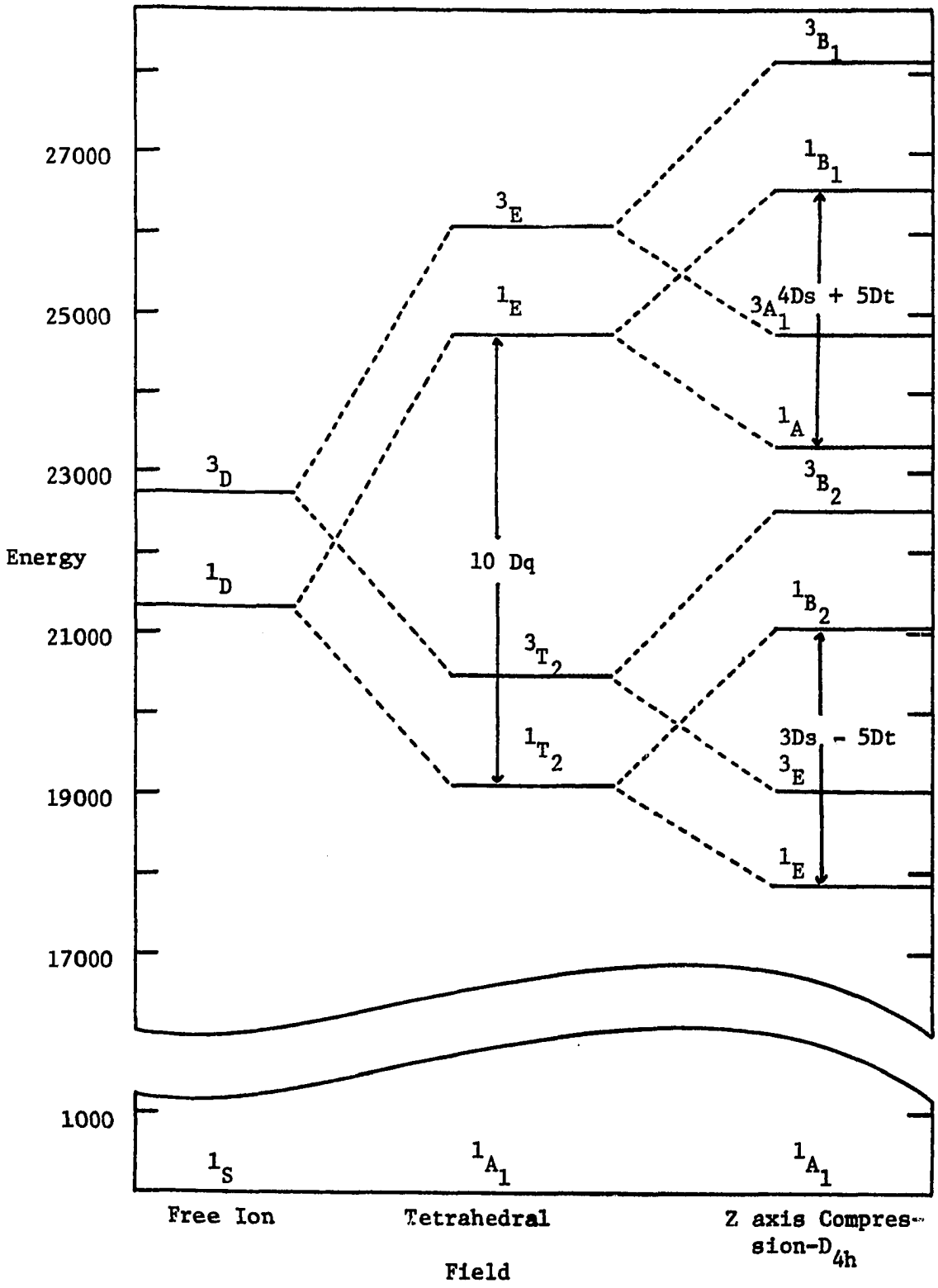

TABLE 31

STATE ENERGIES IN TERMS OF Dq, Ds, and Dt

Term	Energy
E	- 4Dq - Ds + 4Dt
B_2	- 4Dq + 2Ds - Dt
A_1	6Dq - 2Ds - 6Dt
B_1	6Dq + 2Ds - Dt

The values of Dq, Ds, and Dt are given in Table 32, along with the observed and calculated positions of the assigned bands.

The value of Dq is of the same magnitude as the reported values for copper(II) in a tetrahedral field.[6,71] It was expected that this would be true since the splitting of the D states under consideration is similar to the splitting considered for copper(II) which possesses a ^1D ground state.

Conclusions

From the above results it appears that crystal field calculations are valid in treating the excited state spectra of a compound whose central metal possesses ten "d" electrons in its outer shell.

The very strong charge transfer band is in close proximity to the bands under consideration for copper(I) chloride. This causes an increase in the intensity of the bands since they were able to

gain intensity from it.

TABLE 32

SPECTRAL DATA

Transition	Calculated (cm^{-1})	(mu)	Observed (cm^{-1})	(mu)	Peak Description
Dq = 562 cm^{-1}		Ds = 928 cm^{-1}			Dt = -82 cm^{-1}
$^1A_1 \rightarrow {}^1E$	17,857	560	17,857	560	Strong-Sharp
$\rightarrow {}^1B_2$	21,053	475	21,053	475	Moderate-Sharp
$\rightarrow {}^1A_1$	23,364	428	23,364	428	Moderate-Sharp
$\rightarrow {}^1B_1$	26,666	375	26,666	375	Shoulder-Sharp
$\rightarrow {}^3E$	19,231	520	19,231	520	Shoulder-Weak
$\rightarrow {}^3B_2$	22,425	446	22,624	442	Shoulder-Weak
$\rightarrow {}^3A_1$	24,738	404	24,510	408	Shoulder-Weak
$\rightarrow {}^3B_1$	28,140	355	27,933	358	Shoulder-Weak

The intensity of the bands may be greatly reduced for other metal ions as the position of the bands is removed from the charge transfer band.

Further work in this area could consist of interpretation of the spectra of compounds composed of silver(I), gold(I), zinc(II), cadmium(II), mercury(II), and the metals of groups three, four, and five in their highest oxidation states.

Also since copper(I) chloride forms numerous stable complexes, the effect of changing the ligands would be very interesting.

Gmelins[86] lists four different complexes formed between

copper(I) chloride and ammonia, $CuCl \cdot 3NH_3$, $2CuCl \cdot 3NH_3$, and $2CuCl \cdot NH_3$. In addition a structure has been reported for $CuCl \cdot 2NH_3$.[88]

Cuprous complexes with other non-π-bonding as well as pπ and dπ bonding ligands are well known.[34] Four coordinate species are the most common complexes, however, a three coordinate cyanide complex $K[Cu(CN)_2]$ has been formed.[34]

A correlation between the known crystal structures and ligand symmetries with the crystal field spectra of the complexes of unknown structure and symmetry should make a very interesting and informative study.

REFERENCES

1. Joy, H. Computer Program for Diagonalization of Secular Determinant (unpublished), Oak Ridge National Laboratories, 1966.

2. Grindstaff, W. K., Ph.D. Dissertation, University of Oklahoma, 1966.

3. Lewis, L. C., Ph.D. Dissertation, University of Oklahoma, 1967.

4. Grindstaff, W. K., Joy, H. W., and Fogel, N. L., Unpublished, Submitted for Publication.

5. Lewis, L. C. and Fogel, N. L. J. Chem. Soc. (1970), 1141-46.

6. Ballhausen, C. J. Introduction to Ligand Field Theory. New York: McGraw-Hill Book Co. Inc., 1962.

7. Bauman, R. P. Absorption Spectroscopy. John Wiley, New York, 1962.

8. Yatsumirskii, K. B. and Volchenskova, I. I. Teor. Eksp. Khim. 4(6) (1968), 808-15.

9. Clark, L. C., Quick, A. J., and Harkings, W. D. J. Am. Chem. Soc., 42 (1920), 2496.

10. Rose, H. Pogg. Ann. 20 (1830), 157.

11. Bersch, J. Ber. Wien. Akad. 2(56), 729.

12. Ephraim, F. Ber., 45 (1912), 1323.

13. Biltz, W. Z. Anorg. Chem. 148 (1925), 145.

14. Chatelet, M. Compt. rend., 200 (1935), 461.

15. Kauffman, G. Inorg. Syn., 9 (1967), 157.

16. Ibers, J. A., Barnet, M. T., Craven, B. M., Freeman, H. C., and Kime, N. E. Chem. Commun., 10 (1966), 307-8.

17. Roberts, G. L. and Field, F. H. J. Am. Chem. Soc., 72 (1950), 4232-5.

18. Cotton, F. A. and Haas, T. E. Inorg. Chem., 3(7) (1964), 1004-7.

19. Jorgensen, C. K. and Ballhausen, C. J. Acta. Chem. Scand., 9 (1955), 116-21, 397-404.

20. Mellor, D. P. and Goldacre, R. J. J. Proc. Roy. Soc. N. S. Wales, 73 (1940), 233.

21. Biltz, W. and Huttig, G. F. Z. Anorg. Chem., 109 (1920), 141.

22. Mellor, D. P. and Goldacre, R. J. J. Proc. Roy. Soc. N. S. Wales, 72 (1939), 39.

23. German, W. L. and Jamsett, R. A. J. Chem. Soc. (1940), 1360-2.

24. German, W. L. and Jamsett, R. A. J. Chem. Soc. (1939), 1337-41.

25. Curtis, M. and Burns, J. J. Am. Chem. Soc., 39 (1917), 33.

26. Rose, F. Untersuchungen, uber ammoniakalische Kobalt-berbindung, Heidelberg (1871), 26.

27. Biltz, W. and Fetkenheuer, B. Z. Anorg. Chem., 89 (1914), 121.

28. Mizuno, J. J. Phys. Soc. Japan, 15 (1960), 1412.

29. Cotton, F. A. and Holm, R. J. Am. Chem. Soc., 82 (1960), 2983.

30. Liehr, A. P. J. Phys. Chem., 67 (1963), 1314.

31. Ferguson, J., Wood, D. L., and Knox, K. J. Chem. Phys., 39(4) (1963), 881-9.

32. Pribylov, K. P. and Barnova, G. S. Rus. J. Inorg. Chem., 15(7) (1970), 895.

33. Lazerko, G. A. Geterogennye Khim. Reaktsii (1961), 162-9.

34. Cotton, F. A. and Wilkinson, G. Advanced Inorganic Chemistry, John Wiley & Sons, New York, (1966).

35. Sadtler Research Laboratories, High Resolution Infrared Spectra of Inorganic Compounds.

36. Ayres, G. H. Quantitative Chemical Analysis, Harper, 1958, 610.

37. Nakamoto, K. IR Spectra of Inorganic and Coordination Compounds, John Wiley, 1963.

38. Wendlandt, W. W. J. Inorg. & Nucl. Chem., 25(8) (1963), 985-93.

39. Tucker, E. Least Squares Program to Find Best Equation of a Plane Curve, University of Oklahoma (unpublished) 1967.

40. Sanden, H. V. Z. Anorg. Chem., 109 (1920), 126.

41. Jacimirskij, T. Thermochemie, 90, 161.

42. NBS. C500, Selected Values of Chemical Thermodynamics Constants, 253, 256.

43. Rossini, F. D. and Bichousky, F. R. The Thermochemistry of the Chemical Substances, New York (1936), 88.

44. Reid, A. F. Aust. J. Chem. 19(10) (1966), 1785-99.

45. Bethe, H. Ann. Physik, (5), 3 (1929), 133.

46. Lever, A. B. P. Advan. Chem. Ser. No. 62 (1967), 430-51.

47. Griffith, J. S. Trans. Faraday Soc., 54 (1958), 1109.

48. Mulliken, R. S. J. Chem. Phys., 3 (1935), 375.

49. Slater, J. C. Phys. Rev., 34 (1929), 1293.

50. Racah, G. Phys. Rev., 62 (1942), 438.

51. Dunn, T. M., McClure, D. S., and Pearson, R. G. Some Aspects of Crystal Field Theory, Harper & Row, New York, 1965.

52. Cotton, F. A. Chemical Applications of Group Theory, John Wiley, New York, 1966.

53. Fieschi, R. and Lowdin, P. O. Tech. Note 4, Quant. Chem. Group Uppsala, 1957.

54. Jahn, H. A. and Teller, E. Proc. Roy. Soc. A161, (1937), 220.

55. Wilson, E. B., Declus, J. C., and Cross, P. C. Molecular Vibrations, McGraw-Hill, New York, 1955.

56. Stevens, K. W. H. Proc. Roy. Phys. Soc., A65 (1952), 209.

57. Schlafer, H. L. and Gliemann, G. Ligand Field Theory, Wiley Interscience, New York, 1969.

58. Abragam, A. and Pryce, M. H. L. Proc. Roy. Soc. (London), A205 (1951), 135.

59. Abragam, A. and Pryce, M. H. L. Proc. Roy. Soc. (London), A206 (1951), 173.

60. Low, W. Phys. Rev., 109 (1958), 256.

61. Reid, A. F. Aust. J. Chem., 19(10), (1966), 1785-99.

62. Sacconi, L., Sabatini, A., and Gans, P. Inorg. Chem. 3(12), (1964), 1772-4.

63. Takehiko, S. Inorg. Chem., 3(12), (1964), 1908-9.

64. Tanabe, Y. and Sugano, S. J. Phys. Soc. Japan, 9 (1954), 753.

65. Moffitt, W. J. Chem. Phys., 25 (1956), 1189.

66. Yamada, S. Bull. Chem. Soc. Japan, 25 (1952), 127.

67. Piper, T. S. and Calin, R. L. J. Chem. Phys., 35 (1961), 1809.

68. Koide, S. Phil. Mag., 4 (1959), 243.

69. Schaffer, C. E. and Jorgensen, C. K. J. Inorg. & Nuc. Chem., 8 (1958), 143.

70. Ballhausen, C. J. and Moffitt, W. J. Inorg. & Nucl. Chem., 3 (1956), 178.

71. Sutton, D. Electronic Spectra of Transition Metal Complexes, McGraw-Hill, London, 1968.

72. Dunn, T. M. Modern Coordination Chemistry, Interscience, New York, 1960.

73. Figgis, B. N. and Lewis, J. Modern Coordination Chemistry, New York, 1960.

74. Adams, D. M. and Raynor, J. B. Advanced Practical Inorganic Chemistry, John Wiley, New York, 1965.

75. Lewis, J. and Wilkens, R. G. Modern Coordination Chemistry, Interscience, New York, 1960.

76. Van Vleck, J. H. Electric and Magnetic Susceptibilities, London: Oxford University Press, 1952.

77. Selwood, P. W. Magnetochemistry, Interscience, New York, 1943.

78. Elliot, N. J. Chem. Phys., 21 (1953), 890.

79. Klemm, W. and Schuth, W. Z. Anorg. Chem., 210 (1933), 33.

80. Bose, D. M. Z. Phys., 65 (1930), 677.

81. Moore, C. E. Atomic Energy Levels, NBS, C467, 1958.

82. Keller, R. N. and Wycoff, J. D. Inorg. Syn., 2.

83. Liehr, A. D. J. Phys. Chem., 64 (1960), 43.

84. Gray, H. B. Coord. Chem. Rev., 1(2) (1966).

85. Gray, H. B. Inorg. Chem., 3 (1964), 1113.

86. Gmelins Handbuch Der Anorganischen Chemie, 60B1 (1958), 237-51.

87. Structure Reports, 20, 237.

88. Structure Reports, 22, 262.